Title
Neural Regulatory Mechanisms that Link Metabolism and Behavior in Caenorhabditis elegans

Author
Bouagnon, Aude

Publication Date
2019

Peer reviewed|Thesis/dissertation

Neural Regulatory Mechanisms that Link Metabolism and Behavior in Caenorhabditis elegans

by
Aude Bouagnon

DISSERTATION
Submitted in partial satisfaction of the requirements for degree of
DOCTOR OF PHILOSOPHY

in

Biomedical Sciences

in the

GRADUATE DIVISION
of the
UNIVERSITY OF CALIFORNIA, SAN FRANCISCO

Approved:

DocuSigned by:
Todd Nystul
B55FB5CFA606452...

Todd Nystul
Chair

DocuSigned by:
Kaveh Ashrafi

Kaveh Ashrafi

DocuSigned by:
Aimee Kao

Aimee Kao

DocuSigned by:
Dengke Ma
0A5FF211220849A...

Dengke Ma

Committee Members

DEDICATION

The good life is one inspired by love and guided by knowledge. Neither love without knowledge, nor knowledge without love can produce a good life.
-Bertrand Russell

This thesis is dedicated to those who have supported, mentored, encouraged, challenged and nurtured me all of these years. This accomplishment is as much a testament to the love and good fortune I have received in life than my own merits. I'd specifically like to thank Kaveh, my advisor, for seeing and cultivating my potential and bearing witness to my development as a scientist. Thank you for your unwavering support, particularly during the times when I doubted myself the most time. I am so lucky to have been placed in your lab nine summers ago. My 6th Grade teacher May Remsing, who planted so many seeds in my young mind, many of which are just now starting to bloom. Thank you for teaching me that learning, at its finest, is a form of playing. My older brother Paul, who has been my best friend and rock from the very beginning. Thank you for always illuminating my blind spots and pushing me to be my very best. My baby brother, Joel, for teaching me the power of big dreams. Your determination, resilience and work ethic were inspirations to me throughout my PhD. Finally, my parents Valerie and Desire, whose sacrifice, generosity and endless encouragement are the reasons I am who I am. Thank you for teaching me to engage with the world with both curiosity and care. Most of all, thank you for being my biggest sources of support, celebration and love. Je vous aime de tout mon cœur ♥.

Contributions

Chapter 1 was published as:

Cunningham KA, **Bouagnon AD**, Barros AG, Lin L, Malard L, Romano-Silva MA, et al. Loss of a neural AMP-activated kinase mimics the effects of elevated serotonin on fat, movement, and hormonal secretions. PLoS Genet. 2014;10(6):e1004394. Epub 2014/06/13. pmid:24921650; PubMed Central PMCID: PMCPMC4055570.

Portions of Chapter 2 were submitted as:

Bouagnon A, Srivastava S, Panda O, Schroeder F, Srinivasan S, Ashrafi K. Intestinal peroxisomal fatty acid β-oxidation regulates neural serotonin signaling through a feedback mechanism. PLos Biology, submitted April 2019.

Neural Regulatory Mechanisms that Link Metabolism and Behavior in Caenorhabditis *elegans*
Aude Bouagnon

Abstract

The neurotransmitter 5-hydroxytryptamine or serotonin, functions as an indicator of food availability and is an ancient mechanism by which invertebrate and vertebrate species translate sensory information about food availability and quality to distinct nutrient-related behaviors and physiologies. Serotonin signaling is influenced by internal and environmental signals and coordinates a wide range of behaviors related to nutrient-status including appetite, reproduction, growth, learning, memory and mood. Despite these fundamental roles, the precise mechanisms that link neural serotonin to physiologies occurring in distant peripheral tissues remain poorly understood. Moreover, little is known about the mechanisms that link internal metabolic signals from peripheral tissues to neural serotonin circuits to regulate behavior. In this work, we leverage the experimental advantages of *C. elegans* to investigate these two distinct yet coordinated aspects of serotonin signaling. In chapter I, we examine how neuronal serotonin signaling communicates to distant tissues to regulate behaviors like movement, development and fat metabolism. In chapter II,III and IV, we identify the metabolic, molecular, and cellular components of a novel gut-to-brain regulatory axis that links peripheral metabolic signals to serotoninergic circuits that regulate behavior. Together, this work highlights the influence that peripheral metabolic signals exert on neuroendocrine signaling cascades and offers mechanistic insights into how nutrient cues modulate a neuromodulatory mechanism implicated in the control of mood, cognition and behavior.

TABLE OF CONTENTS

LIST OF FIGURES

Chapter I: Loss of a Neural AMP-Activated Kinase Mimics the Effects of Elevated Serotonin on Fat, Movement, and Hormonal Secretions

Abstract

AMP-activated protein kinase (AMPK) is an evolutionarily conserved master regulator of metabolism and a therapeutic target in type 2 diabetes. As an energy sensor, AMPK activity is responsive to both metabolic inputs, for instance the ratio of AMP to ATP, and numerous hormonal cues. As in mammals, each of two genes, aak-1 and *aak-2*, encode for the catalytic subunit of AMPK in C. elegans. Here we show that in C. elegans loss of *aak-2* mimics the effects of elevated serotonin signaling on fat reduction, slowed movement, and promoting exit from dauer arrest. Reconstitution of *aak-2* in only the nervous system restored wild type fat levels and movement rate to *aak-2* mutants and reconstitution in only the ASI neurons was sufficient to significantly restore dauer maintenance to the mutant animals. As in elevated serotonin signaling, inactivation of AAK-2 in the ASI neurons caused enhanced secretion of dense core vesicles from these neurons. The ASI neurons are the site of production of the DAF-7 TGF-b ligand and the DAF-28 insulin, both of which are secreted by dense core vesicles and play critical roles in whether animals stay in dauer or undergo reproductive development. These findings show that elevated levels of serotonin promote enhanced secretions of systemic regulators of pro-growth and differentiation pathways through inactivation of AAK-2. As such, AMPK is not only a recipient of hormonal signals but can also be an upstream regulator. Our data suggest that some of the physiological phenotypes previously attributed to peripheral AAK-2 activity on metabolic targets may instead be due to the role of this kinase in neural serotonin signaling.

Introduction

AMP-activated protein kinase (AMPK) is a sensor of energy status that is conserved from single celled yeasts to humans [1]. At the cellular level, it becomes activated in response to deficits in energy availability, such as a rise in the ratio of AMP to ATP, to inhibit energy utilizing pathways while activating energy generating pathways [1]. AMPK is also a recipient of many hormonal signals and links organism-wide signals of energy balance with myriad cellular mechanisms that are differentially regulated based on energy availability [2]. While many of the consequences of AMPK activity are due to its regulation of substrates in peripheral tissues, activity of hypothalamic AMPK in mammals is also thought to contribute to energy balance through modulation of feeding behavior [3]. Given its broad effects on energy balance, AMPK is a therapeutic target for type 2 diabetes as well as certain cancers [4,5]. Despite the key role of this kinase complex in energy balance and its therapeutic relevance, many of the physiological consequences of AMPK activity and its upstream inputs and downstream effectors still remain poorly understood.

C. elegans provides a genetically tractable system for studying the physiological roles of AMPK in the context of whole animals. In C. elegans as in mammals, AMPK is a kinase complex with catalytic a and regulatory b and c subunits [1,6]. Similar to mammals, two genes, aak-1 and *aak-2*, separately encode AMPK's catalytic a subunit [6]. Thus far, roles for *aak-2* have been reported in several facets of C. elegans biology including the regulation of feeding [7], fat [1,8,9], L1 diapause and nutrient deprivation [1,10], dauer maintenance [2,9,11,12], and longevity [3,6,13,14]. In most of these processes, the requirement for *aak-2* has been attributed to its roles in peripheral tissues.

As in mammals, 5- hydroxytryptamine (5-HT), serotonin, signaling in C. elegans serves as an indicator of food availability [4,5,15,16]. Animals deficient in 5-HT signaling due to inactivation of tryptophan hydroxylase, *tph-1*, the rate limiting enzyme in serotonin biosynthesis, exhibit many of the phenotypes seen when animals are removed from food [1,6,15]. In turn, treatment of animals with exogenous serotonin elicits many of the phenotypes seen when food deprived animals are re-exposed to food [6,17– 20]. Beyond simply an indication of food availability, serotonin signaling informs on a number of other inputs, including food quality [7,21,22], pathogenicity [22,23], and the experience of starvation prior to re-feeding [18,19,24]. For instance, when taken off food, C. elegans quickly reduce their feeding, as measured by the pharyngeal pumping rate [18], and once again elevate it as they are reintroduced to food. If animals experience a period of fasting, they display an even greater increase in feeding rate upon re-encountering food [18]. This increased feeding rate can also be induced if well-fed animals, which already have elevated levels of serotonin signaling relative to food deprived animals, are treated with serotonin or fluoxetine, a serotonin uptake inhibitor [25]. In another example, as animals deplete their food stores, they move more rapidly, presumably to forage for new food resources, and slow their movement once they find such resources [17]. If animals are fooddeprived for a period of time before they re-encounter food, they exhibit a more significant slowing of movement known as enhanced slowing. This enhanced slowing is dependent on serotonin signaling since animals deficient in serotonin production only partially exhibit the enhanced slowing response and addition of serotonin to well-fed animals reduces movement rate [17,26]. Thus, serotonin is not simply a binary, on/off indicator of food availability but levels of

serotonin signaling allow animals to tune their behavioral and physiological responses to food related cues and experiences.

We previously found that 5-HT secreted from the ADF neurons, a pair of ciliated sensory neurons that are known to be responsive to the environment [27], acts on the SER-5 serotonergic receptor on the AVJ pair of interneurons to modulate food intake rate [7]. Our studies suggested that signaling through SER5, a Gas coupled receptor, leads to activation of protein kinase A (PKA) and subsequent PKA-mediated phosphorylation of AAK-2 at residue S244 causing inhibition of AAK-2 activity, likely through inhibition of phosphorylation at the adjacent T243 residue, equivalent of T172 in mammalian AMPK catalytic subunit [7,28]. Thus, loss of AAK-2 activity mimicked the very high levels of feeding seen food deprived animals encounter food or well-fed animals are treated with additional doses of serotonin.

Here, we demonstrate that loss of *aak-2* mimics the effects of elevated serotonin signaling on enhanced fat metabolism, reduced movement, and exit from the dauer state. In the context of dauer maintenance, we show that inactivation of *aak-2* links serotonin signaling to the release of DAF-7, a TGF-b family ligand, and DAF-28, encoding an insulin family member, from the ciliated ASI neurons in a cell autonomous fashion. While AMPK is often considered a downstream effector of hormonal signaling, our results show that AAK-2 containing AMPK complexes are also upstream regulators. Importantly, by revealing that serotonin signaling exerts many of its effects on animal behavior and physiology by inactivation of AAK-2 containing AMPK complexes in the nervous system, our data suggest a need for reinterpretation of some of the findings in

which the requirement for *aak-2* had only been attributed to its peripheral, metabolic roles.

Results

Loss of *aak-2* mimics effects of elevated serotonin signaling on movement and fat

Given that serotonin exerted its effects on feeding in part through inactivation of AAK-2 containing AMPK complexes, we asked whether *aak-2* mutants exhibit any other phenotypic consequences of elevated serotonin signaling. Consistent with the enhanced slowing response, *aak-2* deficient animals had reduced movement rate off-food (Figure 1A; [28]). The rate of movement of *aak-2* mutant animals was similar to wild type animals exposed to the serotonin reuptake inhibitor, fluoxetine, and the already slowed off-food movement of *aak-2* mutants was not further reduced by fluoxetine treatment (Figure 1A).

To determine the relationship between exogenous serotonin treatment and the effects of endogenous serotonin increase by fluoxetine treatment, we conducted dose response studies. As previously reported [26], we noted that transient treatment of wild type animals off of food with increasing doses of exogenous 5-HT causes a progressive slowing of movement culminating in sickness and paralysis (Figure S1A-B). Based on the dose-response studies and consistent with previous similar studies [20,29,30], we chose the 5 mM exogenous 5-HT concentration as one that mimics the movement phenotypes of wild type animals treated with high doses of fluoxetine (Figure S1A). While both wild type and *aak-2* deficient animals became paralyzed with increasing doses of exogenous serotonin, *aak-2* mutants were more sensitive to paralyzing effects of high doses of serotonin, consistent with the notion that these mutants already

experience elevated serotonin signaling (Figure S1B). Using pharyngeal pumping rate as another read-out, we found that treatment of wild type animals with 5 mM 5-HT caused elevated feeding rate similar to fluoxetine treatment and increasing the dose of serotonin to 10 mM did not cause further feeding elevation (Figure S1C). The already elevated feeding rate of *aak-2* deficient animals was unchanged with increasing doses of exogenous serotonin levels up 10 mM. However, as in the case of movement, *aak-2* mutants were more sensitive to deleterious effects of elevated 5-HT, such that elevating the dose of exogenous 5-HT beyond 10 mM had a feeding reducing effect accompanied by other signs of sickness (Figure S1C).

As in mammals, enhanced serotonergic signaling in C. elegans causes fat reduction [19]. While in mammals, the fat reducing effects of serotonin have been attributed to its anorectic effects, in C. elegans serotonergic regulation of feeding behavior is through a cellular circuit that is distinct from serotonergic regulation of fat metabolism [7,19]. The fat reducing effects of elevated serotonin in C. elegans are due to enhancement of fat utilization in peripheral tissues. Recent studies have suggested that a complex regulatory loop between serotonin and octopamine signaling cascades in the nervous system ultimately leads to transcriptional upregulation of various components of fat mobilization and oxidation machineries in the periphery [19,31].

To determine whether loss of *aak-2* mimics the effects of elevated serotonin on fat, we assessed fat content using the fluorescent BODIPY-labeled fatty acids and biochemical measurement of triacylglycerides, both of which indicated that *aak-2* mutants had reduced fat compared to wild type (Figure 1B-C). The reduced fat phenotype of *aak-2* mutants was similar in magnitude to wild type animals subjected to

5 mM exogenous 5- HT and not further diminished upon 5-HT treatment (Figure 1CE; [19]). To verify these results, we used Coherent anti-Stokes Raman Scattering, CARS, a label free microscopic method for the assessment of fat levels [32–34]. The CARS results corroborated the noted fat reduction upon *aak-2* inactivation and 5 mM serotonin treatment (Figure 1D-E; [19]). Moreover, the notion that *aak-2* mutants have particularly low fat levels in their skin-like hypodermal tissues, a result readily suggested by treatment of these mutants with BODIPY-labeled fatty acids (Figure 1B), was corroborated by CARS (Figure 1E).

Fat reducing effects of serotonin elevation are associated with increased total oxygen consumption [19]. Accordingly, *aak-2* mutants exhibited elevated rates of oxygen consumption relative to wild type animals (Figure 1F). We next examined transcriptional expression patterns of nearly a hundred fat and sugar metabolic genes [35,36] by RT-PCR. Although the precise magnitude of changes were not identical and there were genes that were differentially regulated in *aak-2* mutants and serotonin treated wild type animals (Figure S1D, Table S1), we noted a significant overlap between those that were upregulated, downregulated, or unchanged in *aak-2* mutants and wild type animals treated with 5 mM 5-HT compared to untreated wild type animals (Figure S1D, Table S1). Genes that were significantly upregulated by both elevated serotonin and *aak-2* inactivations included homologs of an acyl-CoA synthase, required for activation of fatty acids, a carnitine palmitoyl transferase, which can shuttle fatty acids across the mitochondrial membranes for fat oxidation, and a mitochondrial acyl-CoA dehydrogenase, an enzymatic component of fat oxidation. The similarities in the patterns of transcriptional changes in various metabolic genes supported the notion that

elevated serotonin and loss of *aak-2* affect fat metabolism through a common pathway. Finally, we examined the effects of inactivations of W01A11.5, encoding a putative carnitine palmitoyl transferase, cpt-1a, and F08A8.4, encoding a putative acyl-CoA oxidase, on fat content of *aak-2* mutants. This is because we had previously shown that these gene inactivations partially block the fat reducing effects of elevated serotonin signaling [19]. These gene inactivations also partially blocked the fat reducing effects of *aak-2* deficiency (Figure 1G-H, Figure S2A-C).

These results combined with our previous findings suggested that loss of *aak-2* mimics the effects of elevated serotonin signaling on food intake behavior, fat, and movement.

Effects of losses of aak-1 and *tph-1* on *aak-2* mutant phenotypes

As both aak-1 and *aak-2* separately encode for the catalytic subunits of AMPK. We considered the possibility that the phenotypes caused by loss of *aak-2* may in fact be due to aberrant activation of aak-1. However, none of the phenotypes of *aak-2* mutants were altered in aak-1; *aak-2* double mutants (Figure 2A-C). Additionally, aak-1 transcript levels were unchanged in *aak-2* mutants (Figure S3). Thus, the phenotypes caused by loss of *aak-2* were not simply compensatory responses of AAK-1 activation.

To decipher the relationship between serotonin production and *aak-2*, we next examined *tph-1*; *aak-2* double mutants. The feeding, fat, and movement phenotypes of the double mutants were either the same as those of *aak-2* mutants or intermediate between those of *tph-1* and *aak-2* single mutants (Figure 2D-F). One interpretation of these results is that *aak-2* functions, at least in part, upstream of *tph-1*. For instance, loss of *aak-2* could promote production of serotonin by elevating *tph-1* expression.

However, expression of *tph-1* was unchanged in *aak-2* mutants relative to wild type animals (Figure S3). A second interpretation is that *aak-2* functions downstream of *tph-1* but only mediates some of the effects of serotonin on fat, feeding, and movement. Since we previously found that in the context of feeding regulation, elevated serotonin acts through the SER-5 receptor to cause inhibition of AAK-2 in interneurons that are not known to produce serotonin, we favor the second interpretation. This interpretation is consistent with the notion that loss of *aak-2* mimics phenotypes seen when serotonin signaling is elevated beyond that of steady state well-fed animals.

Reconstitution of *aak-2* in the nervous system rescues the fat and movement defects of *aak-2* mutants

In C. elegans, *aak-2* is broadly expressed in both neural and peripheral tissues [9,28]. To determine whether loss of *aak-2* in specific tissues could account for its movement and fat phenotypes, we reconstituted wild type *aak-2* in select tissues of the mutant animals. Reconstitution of *aak-2* throughout the nervous system restored wild type movement rate (Figure 1A) and fat levels to aak2 mutants (Figure 1B) while reconstitutions within body wall muscle, intestine, pharyngeal muscle, and hypodermis failed to do so (Figure S4 and data not shown).

We previously reported that normalized feeding rate is restored when *aak-2* is reconstituted within only the AVJ pair of interneurons as well as the pharynx of *aak-2* mutants [7]. These transgenic animals, however, still exhibited reduced fat levels that were indistinguishable from those of *aak-2* mutants (Figure S4). These data suggested that elevated serotonin signaling elicits feeding and fat phenotypes through inhibition of AAK-2 containing complexes in distinct regions of the nervous system.

Loss of *aak-2* causes fat reduction independent of the dauer state

The observations that loss of neural *aak-2* mimics the effects of serotonin signaling forced us to re-evaluate previously published claims where requirements for *aak-2* in various physiological processes have been largely attributed to its peripheral, metabolic roles. One such example is the requirement for *aak-2* in fat rationing during the dauer stage [9]. The dauer stage of C. elegans is an altered developmental state that is restricted to an early larval stage [37]. Entry into the dauer state is initiated by lack of nutrients or excessive population density, which lead to reductions in activities of pro-growth and developmental pathways of insulin signaling and TGF-b signaling [37]. Relative to non-dauer early larval animals, dauers contain elevated lipid levels, which presumably acts as an energetic reservoir for these non-feeding animals [37].

A previous study suggested that *aak-2* is required for proper fat rationing during the dauer state [9]. Animals deficient in daf-2, encoding an insulin receptor-like gene, or in daf-7, encoding a neurally expressed TGF-b family ligand that links environmental conditions to growth and development pathways, enter the dauer state constitutively [38,39]. It was previously reported that daf-2; *aak-2* and daf-7; *aak-2* double mutants enter the dauer state with the expected high levels of lipids but then suffer a rapid fat depletion during the dauer state, implicating a specific role for AAK-2 in lipid rationing during the dauer stage [9]. This contrasted with our finding that the low fat phenotype of *aak-2* deficient animals was not restricted to the dauer stage. To explore this potential discrepancy, we re-examined fat contents of daf-7; *aak-2* and daf-2; *aak-2* double mutants [9]. Multiple independent methods of assessing fat levels — vital staining with BODIPYlabeled fatty acids, fixed staining with Sudan Black B, and total lipid extraction followed by thin layer chromatography — all showed significant reductions in lipid levels

in daf-7; *aak-2* and daf2; *aak-2* relative to daf-7 and daf-2 mutants, respectively, both prior to and at the time of dauer entry (Figure 3, S5). We also examined fat levels of daf-2; *aak-2* double mutants with CARS, and consistent with all of other results, noted that these double mutants had low fat levels (Figure S6). Moreover, the CARS experiments indicated that treatment of daf-2 animals with 5 mM exogenous serotonin causes fat reductions to the same extent as that seen in daf-2; *aak-2* mutants and exogenous serotonin treatment did not further reduce the fat content of these double mutants (Figure S6). Thus, the role of *aak-2* in fat regulation is not dauer stage-specific and the low fat phenotype of *aak-2* deficient animals is not dependent on either intact insulin or TGF-b pathways.

aak-2 deficient animals exit dauer even in the absence of food cues

Under normal physiological circumstances, dauers must be able to sense the reappearance of food to resume growth. Serotonin, an indicator of food availability, is known to promote dauer exit [15]. Therefore, we considered the possibility that the noted requirement for *aak-2* in dauer survival may reflect an increased tendency of animals to exit the dauer stage rather than a failure to maintain dauer survival due to rapid exhaustion of lipid stored during this state.

The claim that *aak-2* dauers fail to maintain survival has been based on studies that rely on a ‘‘dauer trap’’ system, where dauers are kept suspended within a sterile water drop and their survival is periodically assessed within the drop [9,11,12]. We noted that at the time of dauer entry nearly 100% of daf-2; *aak-2* and daf-7; *aak-2* double mutants as well as daf-2 or daf-7 single mutants survived 1% SDS treatment, a treatment traditionally used to distinguish dauers from non-dauers [40] (data not

shown). Thus, at least by this criteria *aak-2* deficient animals enter the dauer stage. After a few days in the dauer trap assay, *aak-2* deficient animals exhibited features associated with animals that have exited dauer yet fail to grow due to lack of nutrients. These features included loss of radial constriction and growth of the germ-line as well as behaviors such as pumping that are never seen in dauers (data not shown). These findings suggested that rather than dying as dauers, *aak-2* deficient animals appear to exit the dauer state but then starve to death under the conditions of the dauer trap.

To distinguish the possibility that *aak-2* deficient animals expire as dauers or prematurely exit this stage, we examined daf-2; *aak-2* and daf-7; *aak-2* double mutants when maintained as dauers on plates with food (E. coli) or within the dauer trap assay also supplemented with food. In a timeframe coincident with previously reported loss of viability during the dauer state, the *aak-2* deficient animals exited the dauer state and grew into reproductive adults (Figure 4A-B). We also rarely observed any *aak-2* deficient animals that died as dauers. These findings suggest that the reported requirements for *aak-2* in proper dauer survival actually reflect increased tendency of these animals to exit this stage and are consistent with the notion that loss of *aak-2* elicits a set of phenotypes also seen upon enhanced serotonin signaling.

Loss of *aak-2* mimics 5-HT signaling in promoting neuroendocrine secretions from ASI neurons

Serotonin is thought to promote enhanced signaling through the insulin and TGF-b signaling pathways in C. elegans [16]. Therefore, we asked whether inactivation of AAK-2 links serotonin signaling to these signaling cascades. The ciliated sensory neurons ASI secrete the DAF-7 TGF-b ligand as well as DAF-28, an insulin-like peptide,

both of which are packaged and secreted in dense-core vesicles [41,42]. To assess the effects of serotonin and *aak-2* on dense-core vesicle secretion, we fused full-length DAF-28 to a fluorescent mCherry reporter and expressed the fusion in ASI neurons using the daf-7 promoter [43,44]. Such transgenes have been used to quantitatively assess dense-core vesicle mediated secretions from various C. elegans neurons including the ASI [41,45,46]. Secreted peptides accumulate within coelomocytes, scavenger cells that non-specifically endocytose molecules within the pseudocoelom. This reporter system has been validated by a variety of assays that have functionally probed the consequences of dense core vesicle secretions [45–47]. Treatment of wild type animals with exogenous 5-HT resulted in a ,30% increase of fluorescent signal accumulation in coelomocytes (Figure 5A). Similarly, loss of *aak-2* increased accumulation of the DAF-28 reporter, which was not further enhanced by exogenous serotonin treatment (Figure 5A). Similar results were obtained when examining coelomocyte accumulation of a full length DAF-7 fused to mCherry and expressed in the ASI neurons (Figure S7A).

We next set out to determine whether the enhanced coelomocyte accumulation of DAF-28 and DAF-7 fusion reporters in *aak-2* mutants were due to increased transcriptional activity, enhanced secretion, or both. Transcriptional expression levels of daf-7 and daf-28 were indistinguishable in wild type and *aak-2* mutants as assessed by RT-PCR assays (Figure S7B). To examine whether the enhanced accumulation of the reporter fusions in the coelomocytes depended on dense core vesicle secretions, we generated *aak-2*; unc31 double mutants expressing the DAF-28::mCherry transgenic secretion reporter. unc-31 is a neurally expressed gene that encodes for the C. elegans

homolog of Calcium Activated Protein for Secretion, CAPS, which is critical for fusion of dense core vesicles with plasma membranes [48]. Loss of unc-31 is known to block enhanced secretion of dense core vesicles in C. elegans [41]. Not only was the elevated coelomocyte accumulations of DAF28::mCherry of *aak-2* mutants abrogated by loss of unc-31, the levels were below those seen in wild type animals and similar to the levels of unc-31 mutants (Figure S7C). These findings suggested that the enhanced secretions seen in *aak-2* mutants require the canonical dense core vesicle release machinery.

Within the context of feeding regulation, we previously found that 5-HT acts through the G protein-coupled receptor, SER-5, to ultimately cause inactivation of AAK-2 in the AVJ pair of interneurons [7]. As ser-5 is expressed in the ASI neurons, we tested whether it links serotonin to enhanced secretions from these neurons. Indeed, loss of ser-5 abrogated enhanced accumulation of reporter fusions secreted from the ASI upon serotonin treatment (Figure 5B). In turn, selective reconstitution of ser-5 only in the ASI neurons of ser-5 mutants once again allowed for serotonin induced secretion from these neurons (Figure 5C). Additionally, selective ASI expression of gsa-1(R182C), encoding a gain-of-function mutation in Gas [49], expected to mimic enhanced signaling through the Gas coupled SER-5 receptor [50] and causing inactivation of AAK-2 [7], led to increased dense-core vesicle secretion from the ASI neurons (Figure 5D). Finally, we showed that *aak-2*; ser-5 double mutants had increased ASI secretions similar to those seen in *aak-2* mutants (Figure 5E) and that loss of *aak-2* did not alter ser-5 gene expression (Figure S7B).

The epistasis and cell specific reconstitution studies presented above suggest that serotonin promotes enhanced secretions from the ASI neurons through activation of SER-5 and subsequent inactivation of AAK-2 in the ASI neurons to promote enhanced secretion of DAF-7 TGF-b and the DAF-28, which play critical roles in whether animals stay in dauer or undergo reproductive growth.

Increased neuroendocrine signals contribute to dauer exit of *aak-2* mutants

Elevated secretions of TGF-b like ligand, DAF-7, and insulins, are known to counteract the dauer constitutive phenotypes of daf-2 and daf-7 mutants [38,39]. We reasoned that if enhanced DAF-7 secretion from the ASI neurons accounted, at least in part, for tendency of daf-2; *aak-2* mutant animals to exit the dauer stage, then reconstitution of *aak-2* in ASI neurons should promote maintenance of the dauer state. This was indeed the case. While daf-2 mutants stayed in dauer throughout the course of the experiment, by 8 days, virtually all daf-2; *aak-2* had exited dauer. By contrast, after 8 days, ,60% of transgenic animals in which *aak-2* was only reconstituted in the ASI neurons, were still in the dauer state (Figure 6A). They retained viability as dauers since they remained responsive to a gentle touch (data not shown). All of these animals remained in the dauer state until the experiment was terminated on day 15.

It was previously reported that loss of atgl-1, encoding a lipase required for mobilization of triglycerides [51], allowed dauer survival in *aak-2* deficient animals by preventing fat loss of these mutants [9]. We therefore wondered whether the ability of the subset of daf-2; *aak-2* deficient animals in which *aak-2* was reconstituted in the ASI neurons could be due to restoration of fat levels. This was, however, not the case since

the fat levels of these animals were indistinguishable from that of daf-2; *aak-2* mutants (Figure S4).

Our dauer maintenance assays were done in the presence of food such that we could distinguish animals that exit the dauer stage from those that might expire as dauers. We re-assessed the role atgl-1 loss in preventing dauer exit using our assay conditions. Under these conditions, 100% of daf-2 or daf-7 mutants remained in the dauer state by day 10 post dauer entry, while nearly 100% of daf-7; *aak-2* or daf-2; *aak-2* mutants had exited the dauer and resumed growth. Loss of atgl-1 delayed the rate of dauer exit especially during days 2–7, however, by day 10 still nearly 100% of animals had exited the dauer stage and resumed growth (Figure 6B). To further investigate the contribution of fat levels on dauer maintenance, we screened through a metabolic sub-library of RNAi clones to identify additional genes that are important for fat reduction when *aak-2* is lost. We identified several peroxisomal genes whose inactivation increased BODIPY-labeled fatty acid staining in daf-7; *aak-2* animals: pmp-1, pmp-2, daf-22, and prx-5 (data not shown). Like atgl-1, loss of these peroxisomal genes caused a 2-3 day delay in the time frame of dauer exit but did not change the finding that nearly a 100% of animals existed the dauer stage by day 10 (data not shown). Finally, we examined dauer maintenance of daf-7; mgl-1; mgl-3 triple mutants. This is because losses of the neurally expressed metabotropic glutamate receptors encoded by mgl-1 and mgl-3 significantly reduce fat levels of daf-7 mutants [52]. While daf-7 mutants have nearly 2.5 fold more lipid staining based on Sudan Black B compared daf-7; mgl-1; mgl-3 triple mutants [52], the three triple mutants maintained dauer survival virtually similar to daf-7 mutants (Figure 6C). Thus, increasing lipid reserve causes a modest delay in

dauer exit but does not prevent it. Similarly, reduction of lipid reservoirs is insufficient to promote dauer exit in daf-7 mutants.

Discussion

In C. elegans, serotonin signaling modulates a series of food related behavioral, physiological, and metabolic responses. We previously showed that elevated serotonin signaling leads to an increase in feeding rate through inhibition of AAK-2 containing AMPK complexes in the nervous system. The data presented here demonstrate that inactivation of *aak-2* also mimics the effects of elevated serotonin on fat reduction, reduced movement, and whether animals stay in dauer or undergo reproductive growth and development. In the context of dauer decision, our data are consistent with a model whereby serotonin signaling through the SER-5 receptor leads to inactivation of AAK-2 in the ASI neurons, in turn, promoting enhanced release of the DAF-7 TGFb ligand and insulins from these neurons (Figure S8).

Although reconstitution of *aak-2* in only the nervous system of animals was sufficient to revert many of the phenotypes of *aak-2* animals to nearly wild type levels, the requirement for *aak-2* activity mapped to different regions of the nervous system for various phenotypes of *aak-2* mutants. For instance, reconstitution of *aak-2* in only the hlh-34 expression neurons plus the pharynx of C. elegans was sufficient to restore wild type feeding rates but did not alter the fat, movement, or dauer maintenance phenotypes of *aak-2* mutants. In turn, restoration of *aak-2* to the ASI neurons of C. elegans, the site of production of the TGF-b ligand DAF-7, was sufficient to restore normalized secretion of dense-core vesicles from these neurons and significantly restored dauer maintenance without restoration of wild type feeding, fat, or movement to

the *aak-2* mutants. We do not yet know which subset of serotonin responsive neurons may specifically account for the fat and movement effects caused by loss of *aak-2*. The finding that serotonergic regulation of feeding, fat, movement, and dauer exit through inhibition of AAK-2 occur in different regions of the nervous system indicates that behavioral and physiological processes that broadly regulate energy balance, while coordinated by serotonin signaling, are not simply consequences of one another and can be differentially modulated by the nervous system.

The recognition that loss of *aak-2* mimics the effects of serotonin signaling forced us to re-evaluate some of the interpretations of the physiological roles attributed to AAK-2. Specifically, it had been suggested that *aak-2* deficient dauers fail to inhibit proliferation of their germ-lines and fail to maintain survival during this stage due to i) a failure in rationing of lipid reservoirs, ii) inappropriate osmotic regulation, and iii) lack of a hormesis-like effect caused by inappropriately high catalase activity [11]. In each of these cases, the dauer trap assay was used to monitor survival of dauers [9,11]. We found that this assay makes it difficult to distinguish between animals that exit dauer and succumb to early death due to factors such as starvation and animals that fail to maintain survival while remaining in the dauer stage. This distinction is important for appropriately understanding the role of *aak-2* in dauer physiology. For instance, *aak-2* mutants that have been maintained in the dauer trap assay for several days exhibit lower fat levels, an outcome that has been interpreted as a failure by these animals to ration their lipid reserves during the dauer state [9,11]. However, lower lipid levels would also be expected if *aak-2* deficient dauers exit this stage and resume growth but then starve due to lack of nutrient availability in the dauer trap assay. To differentiate early

dauer exit from death during the dauer state, we added E. coli to the dauer trap assay or kept the *aak-2* dauers on plates with food. Under these circumstances, we did not see *aak-2* mutants that expired as dauers. Rather, we found that virtually all *aak-2* deficient dauers exited this state and resumed normal patterns of growth. Moreover, we found that elevation of serotonin signaling or loss of *aak-2* promoted enhanced release of the DAF-7 TGF-b and the DAF-28 insulin, systemic regulators of animal growth and development. Thus, our data suggest that the noted effects of loss of *aak-2* on dauer survival are due its requirement for preventing early dauer exit. Our results, however, neither rule out a role for AAK-2 in modulating metabolism in the periphery including during periods of nutrient deprivation, nor challenge the notion that AAK-2 may regulate the activity of ATGL-1. In fact, a recent study indicated that fat reduction induced by elevated serotonin signaling in the nervous system, a condition that we suggest is mimicked by loss of *aak-2* from the nervous system, depends on transcriptional upregulation of atgl-1 in the periphery [31].

Our analyses of fat staining in *aak-2* mutants led to different conclusions than those previously reported for these mutants [9]. These discrepant results highlight some of the methodological challenges in assessing C. elegans fat levels. Fixed staining and biochemical methods were previously used to claim that *aak-2* mutants enter dauer with wild type levels of fat [9]. Using the same methodologies, we instead found that *aak-2* mutants have lower levels of fat at all stages including at the time of dauer entry. The results of our fixed dye and biochemical fat measurements were corroborated by vital BODIPY-fatty acid labeling as well as label free CARS. Although fixed staining methods and biochemical methods have in the past few years been touted as the strategies by

which C. elegans fat should be assessed [53,54], in our experience both methods are prone to an enormous amount of variability and can be fairly insensitive when used to gauge total lipid contents of whole animals. Fixed staining methods rely on permeabilization of the cuticle to allow penetrance of dyes, a process that can be difficult to achieve uniformly. The fixed staining methods also rely on alcohol dehydration steps, which if not done properly can dissolve away triglycerides. Similarly, the biochemical measurements of extracted triglycerides are prone to a great deal of experimental variation since they rely on relatively large populations of animals and extraction procedures that can have vastly different efficiencies in different trials. Thus, while each of these methods can provide valid assessments of fat levels, it is important to recognize their limitations and susceptibility to a high level of operator error that can lead to reporting of erroneously high or low levels of C. elegans fat content.

In C. elegans, as in mammals, activation of AMPK causes fat reduction [55]. Thus, it may seem paradoxical that loss of *aak-2* could also result in fat reduction. In analogy to mammalian systems, energy deprivation is expected to lead to AMPK activation in C. elegans and subsequent mobilization of fat reservoirs as an energy generating strategy. In mammals, the fat reducing effects of AMPK are largely attributable to activation of this kinase complex in peripheral tissues [56]. While it has not been formally shown to be the case in C. elegans, we speculate that the noted fat reductions caused by activation of AMPK are similarly dependent on activity of this kinase complex in peripheral tissues. By contrast, our findings indicate that the reduced fat of *aak-2* mutants is due to loss of AAK-2 activity from the nervous system. As in the case of elevated serotonin signaling, inactivation of neural AAK-2 is expected to occur

under conditions of plentiful food supplies. In mammals, actions of hormonal cues of food availability on the nervous system are similarly associated with enhanced rates of fat oxidation [57]. For example, increased T3 thyroid hormone, in cases of hyperthyroidism, inactivates hypothalamic AMPK leading to increased brown adipose tissue thermogenesis and weight loss without inducing changes in food intake [58]. Additionally, it has been suggested that hypothalamic inhibition of AMPK may stimulate the sympathetic nervous system that innervates peripheral tissues leading to activation of AMPK in these tissues and stimulation of peripheral fatty acid oxidation [58,59]. Finally, enhanced serotonin signaling in mammals also promotes enhanced fat oxidation, although it is unknown whether this enhancement is dependent on neural AMPK inhibition [60–63]. Thus, in both C. elegans and mammals, inhibition of neural AMPK is associated with enhanced peripheral fat oxidation. An area of divergence between C. elegans and mammals are the effects of elevated serotonin signaling or inactivation of hypothalamic AMPK on feeding behavior. While elevation of serotonin signaling causes feeding increase through inhibition of AAK-2 in specific neurons of C. elegans, elevated serotonin signaling or inhibition of hypothalamic AMPK are thought to cause satiety in mammals [3,57,59].

There is ample evidence to assume that rather than simply a binary on/off indicator of food availability, serotonin-signaling functions along a continuum of levels. The available data support the existence of at least three states: a level of serotonin signaling seen in well-fed animals, which is lowered as animals are removed from food, and a highly elevated level that drives transient behaviors such as the enhanced slowing response. One appealing aspect of the regulatory link between serotonin

signaling and AAK-2 containing AMPK complexes is that the known features of AMPK regulation could also account for a variety of regulatory states. For instance, AMPK can be in an activated state during periods of nutrient deprivation, in an intermediate state (a nonactivated, non-inhibited state) during a well-fed state, or in a fully inhibited state as that mimicked by loss of *aak-2* or elevation of serotonin levels beyond those of well-fed animals. Under standard laboratory conditions, the behavioral phenotypes of *aak-2* mutants, highly elevated feeding rate and dramatically reduced movement rate, are seen transiently when food deprived wild type animals reencounter food. Therefore, we speculate that the burst of serotonin signaling upon re-encountering food leads to inhibition of neural AAK-2 containing complexes and subsequent behavioral and physiological outcomes seen under these conditions. As serotonin levels return to the level of well-fed animals, neural AAK-2 complexes are likely to be in an intermediate state, neither activated nor fully inhibited.

In numerous organisms, AMPK has been extensively studied as a master regulator of energy balance. In most of these cases, AMPK is considered to function in the context of peripheral tissues and as a downstream effector of hormonal signals [1,2]. Our findings here demonstrate that the AAK-2 containing AMPK complexes can also act as an upstream regulator of hormonal pathways by modulating their neural secretions. The molecular mechanisms that promote enhanced DCV secretions from the ASI neurons upon AAK-2 inactivation remain to be identified. Whether promotion of DCV secretion is a general feature of AAK-2 inhibition or if it is dependent on particular neural contexts also remains to be seen.

Materials and Methods

Strains

Standard C. elegans methods were used for strain construction [64]. N2 Bristol was used as the wild type control and the following mutant alleles were analyzed: ser-5(tm2654)I, aak-1(tm1944)III, tph1(mg280)III, daf-2(e1370)III, daf-7(e1372)III, unc-31(ft1)IV, *aak-2* (ok524)X, *tph-1*(mg280)III; *aak-2*(ok524), aak-1(tm1944); aak2(ok524), daf-2(e1370)III; *aak-2*(ok524), daf-7(e1372)III; aak2(ok524), unc-31(ft1)IV; *aak-2*(ok524). Transgenic animals were generated by injecting plasmids and the unc-122::gfp or myo-3::gfp co-injection marker at a concentration of 50 ng/ml. For secretion assays, animals carrying full length DAF-28::mCherry and DAF7::mCherry driven by a daf-7 promoter were used. Previously described [41] wild type animals carrying integrated copies of these transgenes were crossed into indicated mutant backgrounds to allow for direct comparisons. Dauer constitutive strains were maintained at 15uC, except when testing dauer entry and maintenance, which were conducted at 25uC.

Plasmid construction

Plasmids were constructed using Gateway Technology. pmyo-2 and pmyo-3 entry vectors were constructed as described [47]. punc119::*aak-2*a, punc-119::*aak-2*c, pgrl-21::*aak-2*a, pgrl-21::*aak-2*c, pdaf7::*aak-2*a, pdaf-7::*aak-2*c were generated by Gateway cloning. For the unc-119 promoter, 2000 bp including the ATG was amplified by PCR from genomic DNA and sub-cloned into Gateway entry vector pDONR-P4-P1R. For the daf-7 promoter, 2800 bp including the ATG was amplified by PCR from genomic DNA and sub-cloned into Gateway entry vector pDONR-P4-P1R. For the grl-21 promoter, 745 bp including the ATG was amplified by PCR from genomic DNA and sub-cloned

into Gateway entry vector pDONR-P4-P1R. Rescue constructs were generated using the pKA453 plasmid to obtain promoter::orf::intercistronic::GFP polycistronic fusions. This resulted in the expression of GFP from the same transcript as the ORF without modification. pdaf-7::daf-7::mCherry and pdaf-7::daf-28::mCherry, integrated lines were generated as described in [41]. To generate pdaf-7::ser-5::gfp, and pdaf7::gsa-1(R182C)::gfp, ser-5 or gsa-1 cDNA, was amplified and cloned according to the procedure outlined in [7], and recombined using Gateway cloning methodology. The R182C mutation was inserted into the gsa-1 sequence by oligo-mediated sitedirected mutagenesis and the desired mutation was confirmed by sequencing the resulting plasmid.

Lipid analysis

Extended methods for BODIPY staining, triglyceride measurements, and Sudan Black B staining are provided in reference [65]. Sudan Black B assays were performed at room temperature (22uC) [38] with the following modification to minimize staining variability, which allowed for quantitative comparisons between various genotypes: animals from one genotype were labeled with fluorescein isothiocyanate (FITC) and then fixed and stained in the same tube as unlabeled animals from another genotype. For quantitation, Sudan Black images were collected on a Zeiss Axioplan 2 microscope fitted with a Hamamatsu ORCA-AG camera. Staining intensities were quantitated using Improvision Openlab software. Mean pixel intensity was calculated for staining in the region from the first intestinal cells adjacent to the pharynx midway through the animal to the vulva. Background was determined based on pixel intensity of nonspecific staining in the pharynx. Values are reported as mean pixel intensity minus background

for at least ten randomly selected animals per genotype. In each case, test and control animals were fixed and stained in the same tube.

Biochemical determination of extracted triglycerides: synchronized nematodes from a liquid culture of approximately 5000 animals were washed three times by centrifugation and resuspension in 10 ml S-basal medium supplemented with 0.1% PEG8000. After the washes, the nematode population pellet was finally suspended in approximately 200 ml of S-basal +0.1% PEG-8000. 50 ml of this suspension was reserved for protein determination (see below) and 100 ml of suspension was diluted with 59 ml of water for lipid determination. To extract triglycerides, chloroform (0.2 ml) and methanol (0.4 ml) was added to the 0.159 ml aqueous suspension of nematodes and mixed by periodic vigorous vortexing over 20 min. An additional 0.2 ml of chloroform and 0.2 ml of 0.2 N HCl were then added. The mixture was mixed by vigorous vortexing over 20 min, then centrifuged at 2,500 g for 5 min to separate the phases. The lower phase was washed once with 0.75 ml of the aqueous phase derived from a mixture of chloroform, methanol, 0.1 N HCl (1:1:1), then concentrated by vacuum centrifugation. The residue was dissolved in 25 ml of chloroform:methanol (1:1), 10 ml of which was applied to a thin layer chromatography plate (Merck silica gel-60), along with triglyceride standards (0.5–10 mg). The samples and standards were eluted using a hexanes-ether-acetic acid mixture (70:30:1) and the plate was developed by spraying with phosphomolybdic acid stain (Sigma) and heating in a 125uC oven for 10 min. An image of the plate was acquired using a flat bed scanner (Epson) and the integrated density of the bands that exhibited the same elution profile as the triglyceride standards was quantified. The optical densities were then converted to TAG mass by comparison

to a TAG standard curve. The mass of lipids obtained from each extraction was normalized to the total protein extractable for 3-4 independent nematode cultures per experimental condition. To determine total protein levels for normalization, 250 ml of extraction buffer (7 M urea, 2 M thiourea, 4% CHAPS, 50 mM tris-HCl pH 7.4, 5 mM TCEP, 1 mM EDTA) was added to the 50 ml suspension of nematodes from the same suspension that was used for TAG extraction. The sample was rotated end-over-end and periodically vortexed for 1 hr at 37uC. The sample was centrifuged (10 min at 16,500 g) and the amount of protein in the supernatant was determined by Bradford assay (Bio-Rad).

For BODIPY staining a 1 mg/ml stock of C1-BODIPY 500/ 512 C12 (Invitrogen) was added to NGM plates seeded with OP50 at a final dilution of 1:50,000. Synchronized L1 animals were added to plates and imaged as Day-1 adults after growth at 20uC. Fluorescent images were acquired on a Zeiss Axioplan II microscope outfitted with a digital CCD camera using the same sub-saturating exposure settings. Using ImageJ, the area surrounding the head of the animal (starting just above the intestinal cells) was selected from which total integrated intensity was derived. At least 10 animals were imaged for each treatment and experiments were repeated a minimum of 2 times. Significance was determined using a student's t-test.

For the coherent anti-stokes Raman scattering, CARS, imaging [32], a picosecond optical parametric oscillator (picoEmerald - APE) with the stokes tuned at 1064 nm and pump at 817 nm in order to match the lipid CH2 stretching mode at 2845 cm21 [33,34] was used. Both laser pulses are synchronized in time and space and directed to a galvanometric mirror imaging microscope (Nikon Ti-U inverted microscope

coupled to a TriM Scope II - LaVision BioTec system) and focused onto the sample by a 60X Nikon objective. The backscattered signal is then directed to a set of dichroic and band pass filters in order to remove the pump and stokes lasers and to detect only the anti-stokes signal in a photomultiplier (Hamamatsu H7422-40). To quantitate the CARS signal for each animal, all of the Z-slices were combined, and background and maximal values were calculated from these combined slices. Regions of interest (head hypodermal region or intestinal areas) were selected and quantitated for each animal and integrated intensity densities are reported for each region. For each genotype and/or serotonin treatment, average data from at least five separate animals are reported.

Dauer entry and dauer exit

To assess dauer entry, we used 1% SDS treatment as previously describe [40]. Post treatment, animals were gently tapped to monitor movement to determine viability. At least 70 animals per conditions were tested. For dauer exit, 100 animals were plated on each of 5 plates—seeded with OP50 (or HT115 in the case of RNAi bacteria) and rimmed with 40% glycerol—and incubated at the restrictive temperature (25uC). After 48 h, virtually all daf-c animals were in dauer. Plates were kept at 25uC and once per day, animals that had exited dauer were picked off the plates and counted. Graphed data reflects the averages of 5 plates of 100 animals.

Movement

Well-fed, synchronized young adult animals were washed twice with S-basal and plated on unseeded NGM plates. Movement was assayed 5 min after plating by counting the number of body bends per 20 s. Ten animals were counted per strain.

Secretion

Strains were synchronized by hypochlorite treatment and the synchronized L1s were plated onto 6 cm NGM plates seeded with OP50. Animals were grown at 20 uC for 2 days until they reached L4 stage. Sub-saturating fluorescence images of the first pair of coelomocytes from 20–30 transgenic animals were recorded at 166magnification using a Zeiss Axioplan 2 microscope fitted with a Hamamatsu Orca II camera. Fluorescence intensities were quantified using ImageJ software. The outline of each coelomocyte was traced using the image from the punc-122::GFP coelomocyte marker. The fluorescence of DAF-28::mCherry or DAF7::mCherry within that area was then measured. The mean fluorescence for each cell was subtracted from the minimum fluorescence (background) within that cell. Fluorescence intensities were normalized to the wild type, sham treated control.

RNAi

HT115 bacteria containing each RNAi vector were tested as previously described. Briefly, bacteria were grown overnight. The following day, bacteria were pelleted and resuspended to 2x concentration prior to plating on NGM agar containing 6 mM IPTG and 25 mg/ml ampicillin. Animals were added to plates (BODIPY staining) or liquid cultures (TLC) as L1s and grown until the L4 stage. Animals were imaged as L4 (BODIPY) or subjected to total lipid extraction followed by thin layer chromatography (TLC).

Oxygen consumption

Oxygen consumption was measured in synchronized L4 animals that were washed twice with S-basal. Per genotype, 200 animals were placed in a plate with biosensor film used to gauge oxygen consumption (BD Biosciences, Cat# 353830). We previously determined that a three-hour period allows for biosensor film to reach equilibrium. The data are end-point measurements, which reflect oxygen consumption rather than biosensor equilibrium. Per genotype, the measurements were done in quadruplicate, and each experiment repeated 3 times. Measurement of fluorescence was by a Molecular Devices FlexStation.

Statistical analysis

For pair-wise comparisons, student's t-test was used. For multiple comparisons, one-way ANOVA with Bonferroni correction was used. Error bars represent +/-SEM. *represents statistical difference relative to wild type unless otherwise indicated. P-values are indicated in figure legends.

Figures

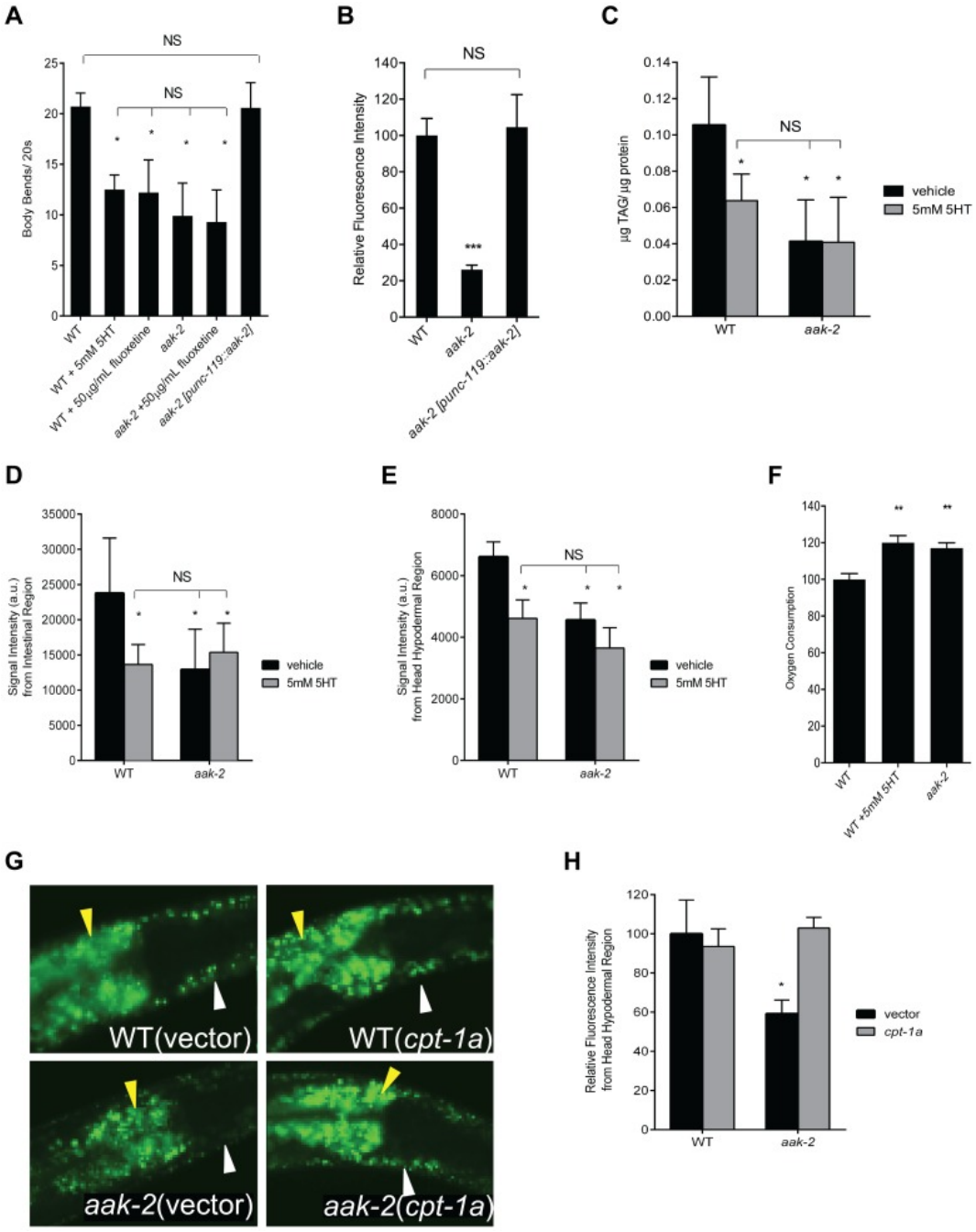
A
B
C
D
E
F
G
H
Body Bends/ 20s
Relative Fluorescence Intensity
µg TAG/ µg protein
Signal Intensity (a.u.) from Intestinal Region
Signal Intensity (a.u.) from Head Hypodermal Region
Oxygen Consumption
Relative Fluorescence Intensity from Head Hypodermal Region
NS
WT
WT + 5mM 5HT
WT + 50µg/mL fluoxetine
aak-2
aak-2 +50µg/mL fluoxetine
aak-2 [punc-119::aak-2]
vehicle
5mM 5HT
WT +5mM 5HT
vector
cpt-1a
WT(vector)
WT(cpt-1a)
aak-2(vector)
aak-2(cpt-1a)

Figure 1.1 Loss of aak-2 mimics increase serotonin signaling

A. *aak-2* mutants and wild type animals (WT) treated with exogenous serotonin (5 mM) or fluoxetine (50 μg/mL) have fewer body bends when removed from food. Pan-neuronal reconstitution of *aak-2* (p*unc-119*) restores wild type body bends to *aak-2* mutants. n=10, *p<0.05, one-way ANOVA with Bonferroni correction for multiple comparisons. B. *aak-2* deficient animals have reduced hypodermal BODIPY fluorescence relative to WT. Wild type BODIPY staining is restored to *aak-2* mutants when *aak-2* is reconstituted in the nervous system (p*unc-119*). n=10, ***p<0.001, one-way ANOVA with Bonferroni correction for multiple comparisons. C. Wild type animals treated with 5mM 5-HT have significantly lower triglycerides per protein (TAG/protein) compared to sham treatment as determined by total lipid extraction followed by Thin Layer Chromatography. Sham treated *aak-2* mutants already have significantly lower TAG/protein compared to WT and 5mM 5-HT treatment does not result in further reduction. TAG/protein levels of 5-HT treated WT are not significantly different than those of *aak-2* +/- 5-HT. n=3, *p<0.05, Student's t-test. D-E. Quantitation of signal intensities of Coherent anti-Stokes Raman Scattering, CARS, of WT and *aak-2* mutants +/- 5mM 5-HT treatment. 5-HT treatment lowered the CARS signal intensities from the intestinal (D) and head hypodermal (E) regions of WT animals. *aak-2* mutants had lower signal intensities relative to WT, which was not further reduced by 5 mM 5-HT treatment. Signal intensities of 5-HT treated WT were not significantly different than those of *aak-2* +/- 5-HT. n=5, *p<0.01, Student's t-test. F. Loss of *aak-2* or 5mM 5-HT treatment caused elevated oxygen consumption. WT and *aak-2* mutants (n=800 per genotype) were sham treated. Data are expressed as a percentage of WT. Error bars represented +/- SEM. **p < 0.01 versus sham treated WT, one-way ANOVA with Bonferroni correction for multiple comparisons G-H. Loss of *cpt-1a* via RNAi restores wild type BODIPY staining to hypodermis (white arrow) and intestine (yellow arrow) of *aak-2* mutants. Representative BODIPY staining images (G) and corresponding quantitations (H) are shown. n=5, *p<0.05, Student's t-test.

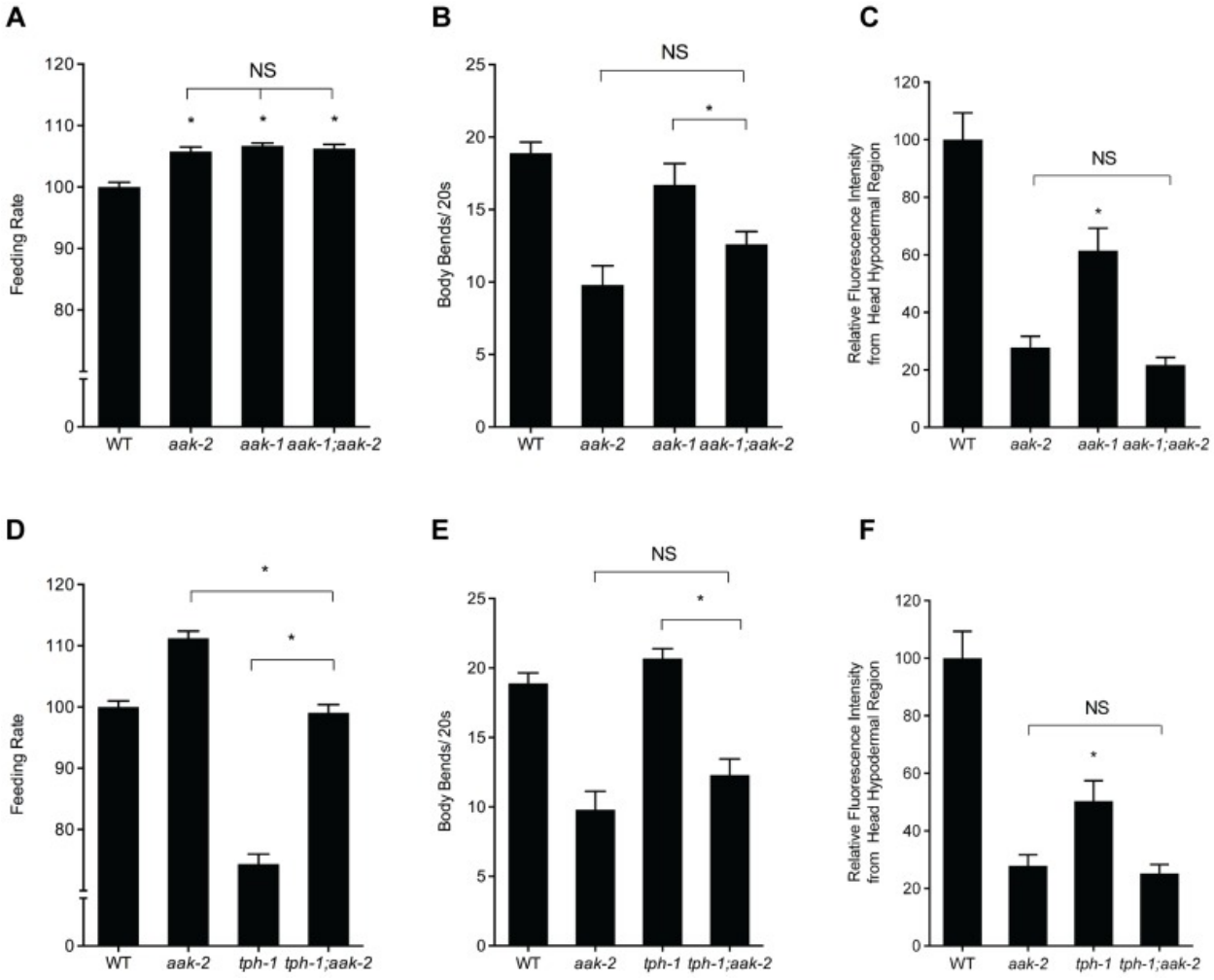
A
B
C
D
E
F
Feeding Rate
Body Bends/ 20s
Relative Fluorescence Intensity from Head Hypodermal Region
NS
*
WT
aak-2
aak-1
aak-1;aak-2
tph-1
tph-1;aak-2

Figure 2. Effects of losses of *aak-1* and *tph-1* on *aak-2* mutant phenotypes
A-C. Phenotypes of *aak-2* loss of function are not dependent on *aak-1*. Feeding (A), movement (B), and hypodermal BODIPY staining levels (C) of *aak-1; aak-2* double mutants are not significantly different than those of *aak-2* mutants. For feeding, movement and BODIPY measurements, n=10, *p<0.05, Student's t-test. Error bars represent +/- SEM. **D-F.** Loss of *aak-2* elicits feeding (D), movement (E), and fat phenotypes (**F**) even in serotonin deficient *tph-1* mutants. The feeding rate of *tph-1; aak-2* mutants was significantly different than both *tph-1* and *aak-2* single mutants (D). *tph-1; aak-2* double mutants moved significantly more slowly than *tph-1* or WT but statistically indistinguishable than *aak-2* mutants off of food (E) For BODIPY staining in the hypodermal head region, loss *aak-2* further reduced the already low hypodermal head staining of *tph-1* mutants (F). For feeding, movement and BODIPY measurements, n=10, *p<0.05, Student's t-test. Error bars represent +/-SEM. Please note that the BODIPY quantitations are of the head hypodermal region only. While *tph-1* mutants have been reported to have elevated intestinal fat levels, their head hypodermal region actually has less staining relative to WT animals. To be consistent with our various other BODIPY measurements, we have concentrated on the same head hypodermal region when comparing *tph-1* with *tph-1; aak-2.*

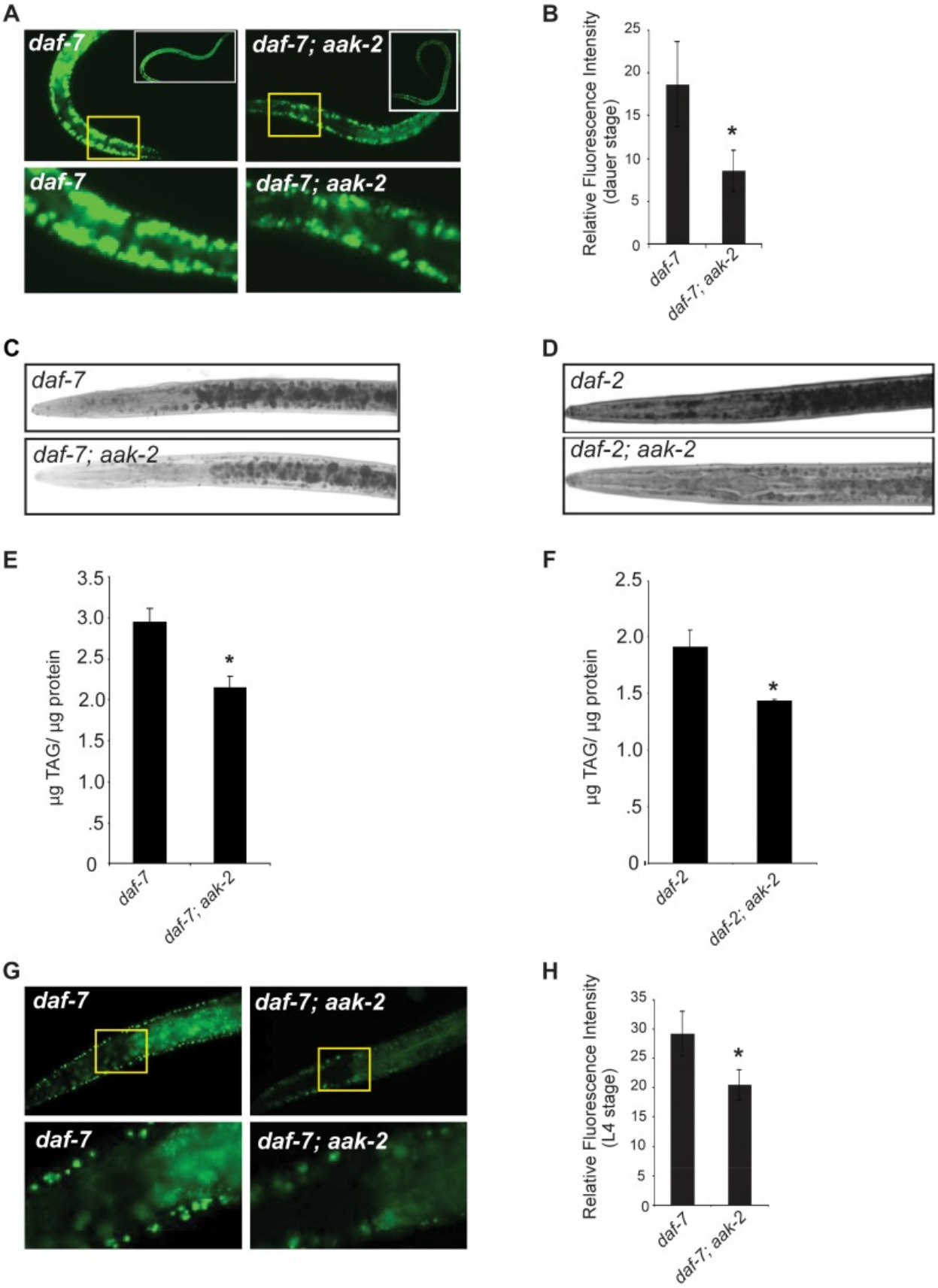
A
daf-7
daf-7; aak-2
daf-7
daf-7; aak-2
B
Relative Fluorescence Intensity (dauer stage)
25
20
15
10
5
0
*
daf-7
daf-7; aak-2
C
daf-7
daf-7; aak-2
D
daf-2
daf-2; aak-2
E
µg TAG/ µg protein
3.5
3.0
2.5
2.0
1.5
1.0
.5
0
*
daf-7
daf-7; aak-2
F
µg TAG/ µg protein
2.5
2.0
1.5
1.0
.5
0
*
daf-2
daf-2; aak-2
G
daf-7
daf-7; aak-2
daf-7
daf-7; aak-2
H
Relative Fluorescence Intensity (L4 stage)
35
30
25
20
15
10
5
0
*
daf-7
daf-7; aak-2

Figure 3. *daf-7; aak-2* and *daf-2; aak-2* have reduced fat relative to *daf-7* and *daf-2* at all stages of development. A. *daf-7; aak-2* dauers have significantly reduced BODIPY fluorescence relative to *daf-7* on the first day after the dauer molt. Insets show entire animals and the bottom panel shows a zoomed-in selection, denoted by the yellow box, from the top panel. **B.** Quantification of anterior hypodermal BODIPY fluorescence for *daf-7* and *daf-7; aak-2* animals on the first day after the dauer molt. n=8. * $p<0.05$, Student's t-test. **C.** Representative Sudan Black B staining of *daf-7* (top) or *daf-7; aak-2* (bottom) animals on the first day after the dauer molt. **D.** Representative Sudan Black B staining of *daf-2* (top) or *daf-2; aak-2* (bottom) animals on the first day after the dauer molt. **E.** *daf-7; aak-2* animals have significantly lower TAG/protein than *daf-7* animals kept at the restrictive temperature (25 °C) on the first day after the dauer molt as determined by total lipid extraction followed by Thin Layer Chromatography. n=4, * $p< 0.05$, Student's t-test. **F.** *daf-2; aak-2* animals have significantly lower TAG/protein than *daf-2* animals kept at the restrictive temperature (25 °C) on the first day after the dauer molt as determined by total lipid extraction followed by Thin Layer Chromatography. n=4, * $p< 0.05$, Student's t-test. **G.** L4 stage *daf-7; aak-2* animals have significantly reduced BODIPY fluorescence intensity relative to *daf-7* animals. Insets show the anterior portion of the animal and the bottom panel shows a zoomed-in selection from the top panel. **H.** Quantification of anterior hypodermal BODIPY fluorescence for *daf-7* and *daf-7; aak-2* animals as L4 animals. n=10, * $p<0.05$, Student's t-test. Error bars represent +/-SEM.

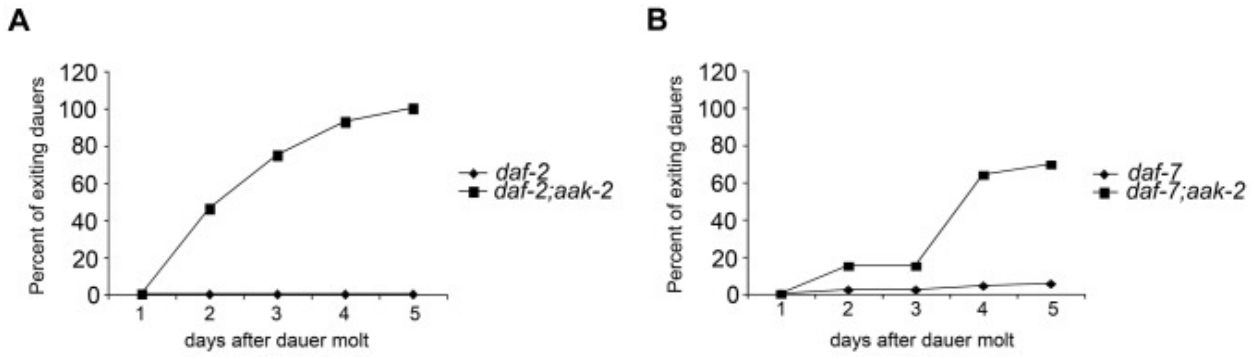

Figure 1.4. *aak-2* deficiency causes dauer exit. A-B. 100% *daf-2; aak-2* (A) and *daf-7; aak-2* (B) animals exit dauer when kept on plates with food (*E. coli* OP50) at the restrictive temperature (25 °C) and resume reproductive, while 100% *daf-2* (A) and *daf*-7(B) mutants animals maintain dauer under similar conditions. A representative comparison is shown. Similar rates of exit and growth were found in at least 5 independent experiments per comparison.

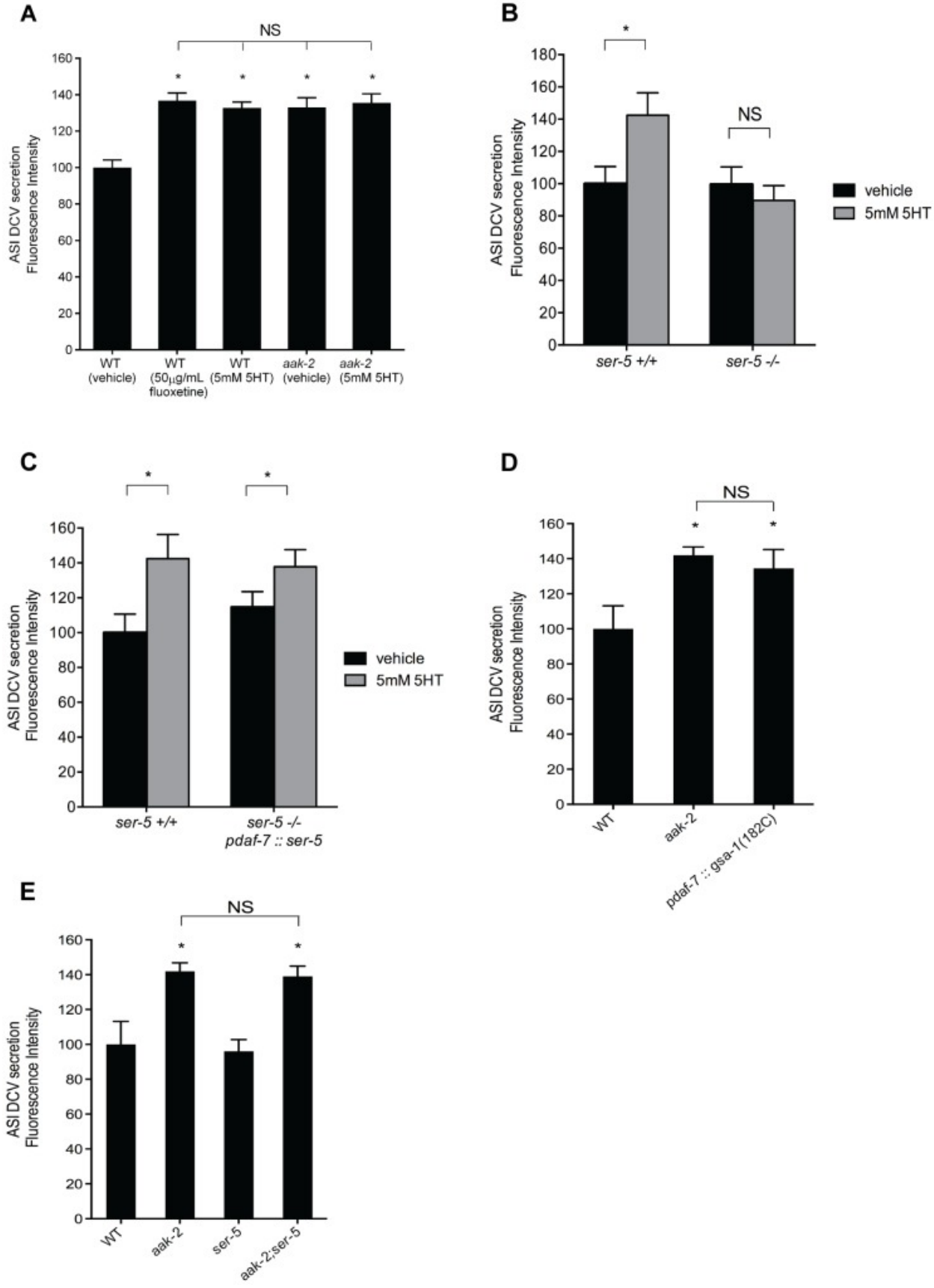
A
NS
ASI DCV secretion Fluorescence Intensity
WT (vehicle)
WT (50μg/mL fluoxetine)
WT (5mM 5HT)
aak-2 (vehicle)
aak-2 (5mM 5HT)
B
NS
ASI DCV secretion Fluorescence Intensity
vehicle
5mM 5HT
ser-5 +/+
ser-5 -/-
C
ASI DCV secretion Fluorescence Intensity
vehicle
5mM 5HT
ser-5 +/+
ser-5 -/-
pdaf-7 :: ser-5
D
NS
ASI DCV secretion Fluorescence Intensity
WT
aak-2
pdaf-7 :: gsa-1(182C)
E
NS
ASI DCV secretion Fluorescence Intensity
WT
aak-2
ser-5
aak-2;ser-5

Figure 1.5. Elevated serotonin or loss of *aak-2* cause increased dense-core vesicle secretion from ASI neurons. A-B. Quantitation of tagged DAF-28::mCherry (A) and DAF-7::mCherry (B) accumulation in coelomocytes. *daf-28::mCherry* and *daf-7::mCherry* were expressed in the ASI neurons using a *daf-7* promoter. Error bars represent standard error. * $p < 0.05$ relative to WT, Student's t-test **C.** Quantitation of tagged DAF-28::mCherry accumulation in coelomocytes when *ser-5* is reconstituted in ASI (p*daf-7*) in otherwise *ser-5* deficient animals. * $p < 0.05$ relative to WT, Student's t-test. **D.** Secretion of DAF-28::mCherry from the ASI neurons is elevated upon ASI specific expression of *gsa-1*(R182C), encoding a gain-of-function version of $G_{\alpha s}$, previously shown to cause inactivation of AAK-2. Error bars represent standard error. * $p < 0.05$, Student's t-test, relative to WT **E.** Elevated secretion of DAF-28::mCherry form ASI in *aak-2* mutants is not dependent on *ser-5.* Error bars represent standard error. * $p < .05$ relative to WT, Student's t-test. In A-E, p*unc-122*::*GFP* was used to mark coelomocytes. Each bar represents examination of 20–30 transgenic animals. For each comparison, the transgene of interest was introduced into indicated backgrounds by crossing.

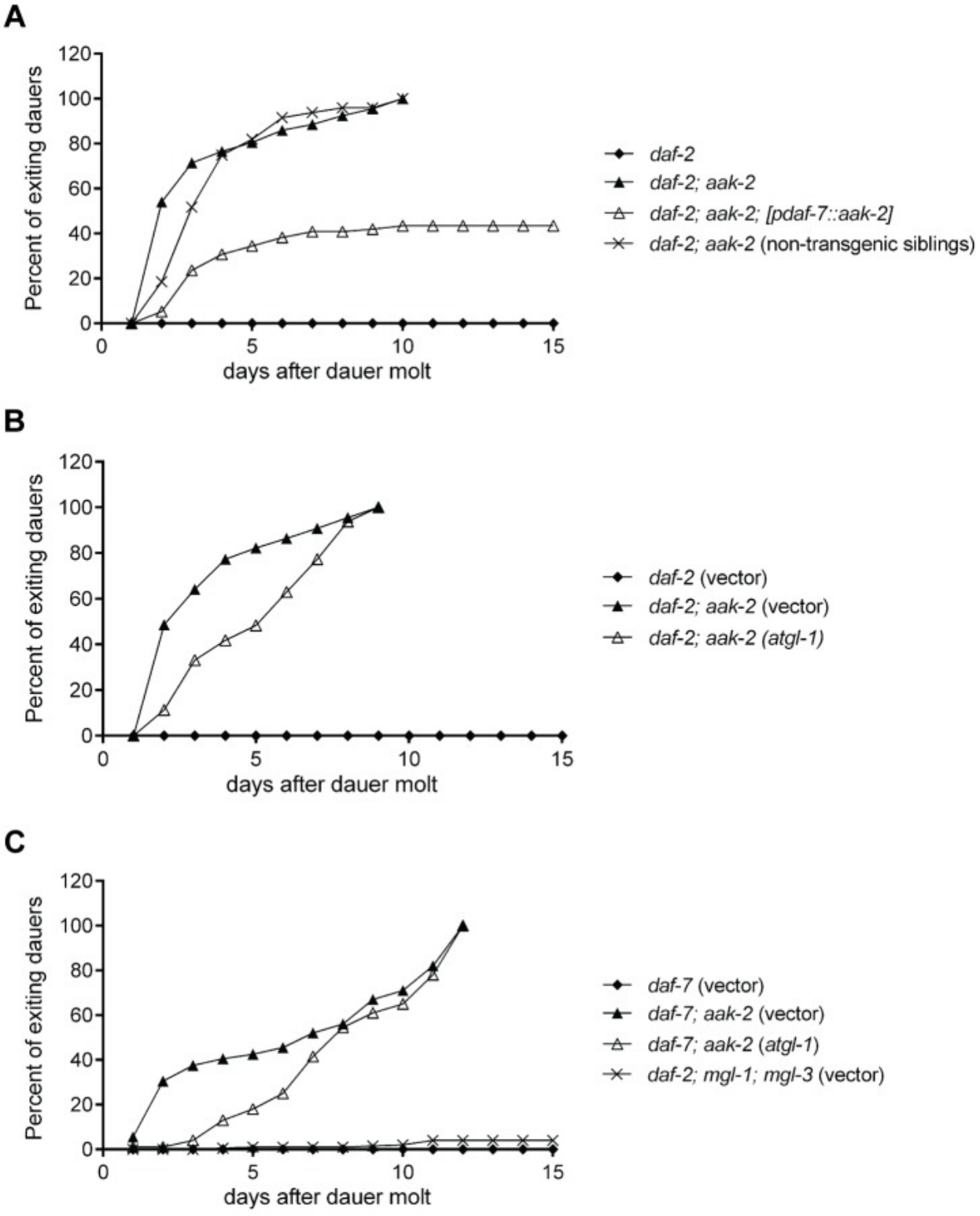
A
Percent of exiting dauers
120
100
80
60
40
20
0
0
5
10
15
days after dauer molt
daf-2
daf-2; aak-2
daf-2; aak-2; [pdaf-7::aak-2]
daf-2; aak-2 (non-transgenic siblings)
B
Percent of exiting dauers
120
100
80
60
40
20
0
0
5
10
15
days after dauer molt
daf-2 (vector)
daf-2; aak-2 (vector)
daf-2; aak-2 (atgl-1)
C
Percent of exiting dauers
120
100
80
60
40
20
0
0
5
10
15
days after dauer molt
daf-7 (vector)
daf-7; aak-2 (vector)
daf-7; aak-2 (atgl-1)
daf-2; mgl-1; mgl-3 (vector)

Figure 1.6. Reconstitution of *aak-2* in ASI partially rescues dauer exit. A. *daf-2; aak-2* animals exit dauer when kept on plates at the restrictive temperature (25 °C), while *daf-2* animals maintain dauer. Reconstitution of *aak-2* in only the ASI neurons restores dauer maintenance to ~60% of *daf-2; aak-2* double mutants. Non-transgenic siblings do not show any improved dauer maintenance. Animals exiting dauers grew to adulthood in each case. We did not examine these dauers beyond day 15 only because it became increasingly difficult to maintain these plates contamination free and prevent the dauers from escaping the plates. **B-C.** RNAi-mediate knockdown of *atgl-1* delays dauer exit for *daf-2; aak-2* (B) and *daf-7; aak-2* (C) animals but does not allow for dauer maintenance beyond the time that a 100% of vector treated animals have exited the stage and resumed growth. While relative to *daf-7* mutants, *daf-7; mgl-1; mgl-3* triple mutants have low fat levels, they maintain dauer as well as *daf-7* mutants (C). Each of the graphed data in A-C reflects the averages of 5 plates of 100 animals per genotype. A representative result is shown. The indicated results were repeated in at least three independent trials.

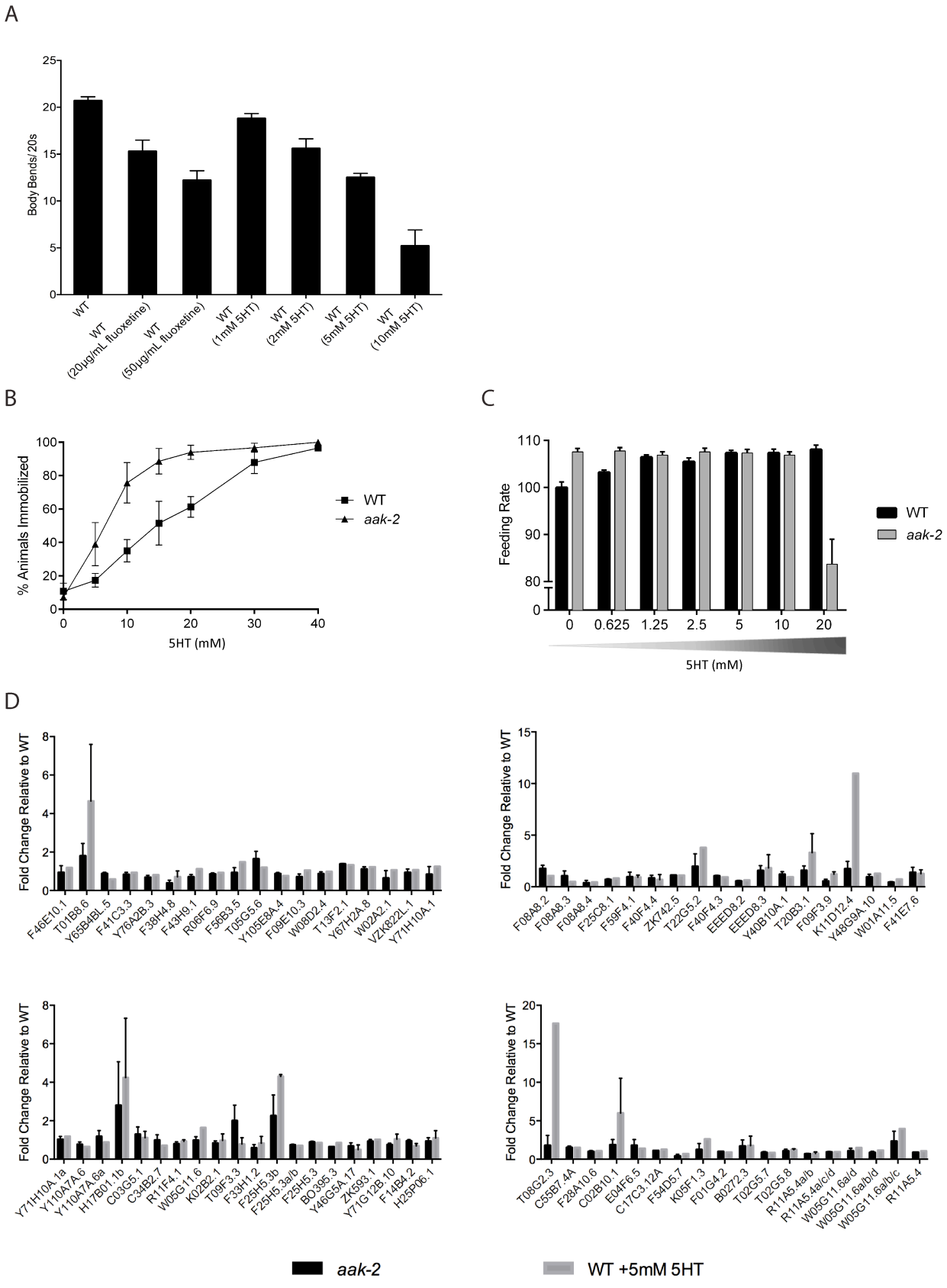
A
Body Bends/ 20s
WT
WT (20µg/mL fluoxetine)
WT (50µg/mL fluoxetine)
WT (1mM 5HT)
WT (2mM 5HT)
WT (5mM 5HT)
WT (10mM 5HT)
B
% Animals Immobilized
5HT (mM)
WT
aak-2
C
Feeding Rate
5HT (mM)
WT
aak-2
D
Fold Change Relative to WT
F46E10.1
T01B8.6
Y65B4BL.5
F41C3.3
Y76A2B.3
F38H4.8
F43H9.1
R06F6.9
F56B3.5
T05G5.6
Y105E8A.4
F09E10.3
W08D2.4
T13F2.1
Y67H2A.8
W02A2.1
VZK822L.1
Y71H10A.1
F08A8.2
F08A8.3
F08A8.4
F25C8.1
F59F4.1
F40F4.4
ZK742.5
T22G5.2
F40F4.3
EEED8.2
EEED8.3
Y40B10A.1
T20B3.1
F09F3.9
K11D12.4
Y48G9A.10
W01A11.5
F41E7.6
Y71H10A.1a
Y110A7A.6
Y110A7A.6a
H17B01.1b
C03G5.1
C34B2.7
R11F4.1
W05G11.6
K02B2.1
T09F3.3
F33H1.2
F25H5.3b
F25H5.3a/b
F25H5.3
BO395.3
Y46G5A.17
ZK593.1
Y71G12B.10
F14B4.2
H25P06.1
T08G2.3
C55B7.4A
F28A10.6
C02B10.1
E04F6.5
C17C3.12A
F54D5.7
K05F1.3
F01G4.2
B0272.3
T02G5.7
T02G5.8
R11A5.4a/b
R11A5.4a/c/d
W05G11.6a/d
W05G11.6a/b/d
W05G11.6a/b/c
R11A5.4
aak-2
WT +5mM 5HT

Figure 1.S1, related to Figure 1.1 Feeding and movement responses of WT and *aak-2* mutants to increasing doses of exogenous 5-HT. **A.** Treatment of wild type animals with increasing doses of exogenous 5-HT causes a progressive reduction in movement and ultimately paralysis. The movement rates of animals treated with 5mM 5-HT were similar to those treated with high concentrations of fluoxetine, suggesting that this dose of exogenous 5-HT mimics the effects of elevating endogenously produced 5-HT. Well-fed animals were washed twice with S-Basal and transferred to assay plates without a bacterial lawn. Locomotion rate was recorded after 5 minutes for a minimum of 10 animals of each genotype per concentration. **B.** Relative to wild type animals, *aak-2* mutants are more sensitive to paralysis caused by escalating doses of 5-HT. At least 30 animals of each genotype per concentration were tested. Movement was scored after a 5-minute exposure to 5-HT. **C.** Effects of various doses of 5-HT on feeding. Treatment of WT animals with increasing doses of 5-HT caused a progressive elevation of pumping rate that reached its maximal levels at 5mM and was not further increased at 10 or 20 mM concentrations of exogenous 5-HT. The already elevated feeding rates of *aak-2* mutants were not further increased by up to 10mM exogenous 5-HT treatment. Consistent with the enhanced susceptibility of *aak-2* mutants to deleterious effects of high exogenous 5-HT, *aak-2* mutants became sickly and displayed lower than wild type feeding at 20mM concentration of 5-HT. **D.** 5mM 5-HT treated wild type animals and untreated *aak-2* animals show significant overlap in transcription expression of indicated metabolic genes relative to untreated wild type animals. Transcript levels of nearly 100 fat and sugar metabolic genes were determined by real-time PCR (RT-PCR). List of the genes and their predicted functions are provided in Table S1. Genes found to be upregulated or downregulated in 5-HT treated wild type animals or in untreated *aak-2* animals were validated using cDNA preparations from two independent nematode growths. Error Bars represent +/-SEM.

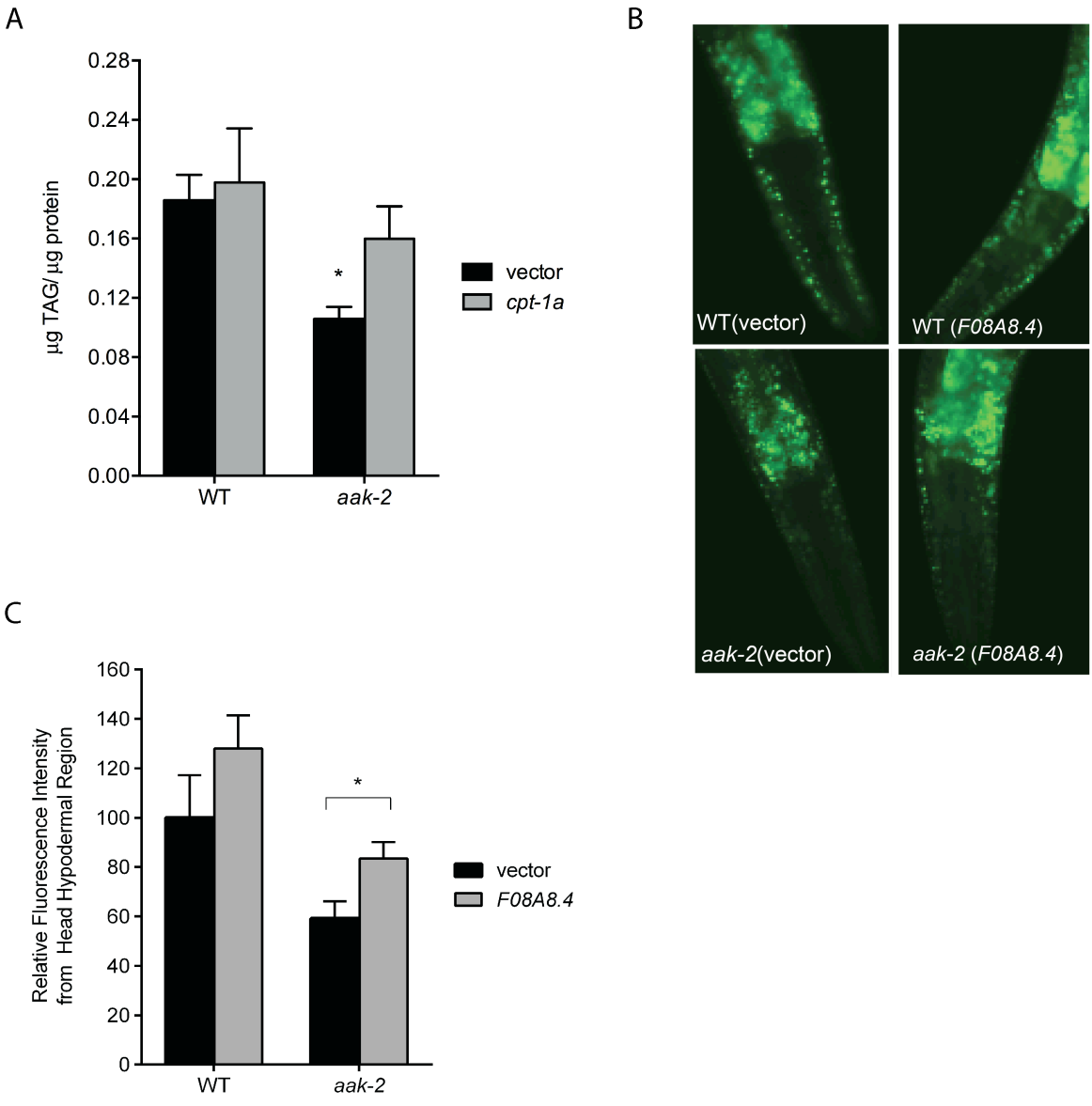

Figure 1.S2, related to Figure 1.1 A. RNAi inactivation of *cpt-1a* (W01A11.5) restored normalized triglycerides (TAG) per protein (TAG/protein) measurement. WT and *aak-2* mutants were grown either on vector RNAi control or on W01A11.5 RNAi. n=3, *p<0.05, Student's t-test. Error bars represent +/-SEM. **B.** Loss of F08A8.4, encoding a putative acyl-CoA oxidase, via RNAi restores BODIPY staining to *aak-2* mutants. Representative images of BODIPY staining. **C.** Quantitation of hypodermal BODIPY fluorescence intensity shown in B. n=5, *p<0.05, one-way ANOVA with Bonferroni correction for multiple comparisons.

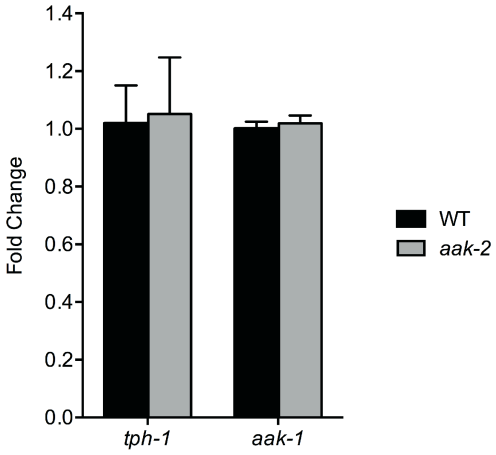

Figure 1.S3, related to Figure 1.1. Transcript levels of *tph-1* and *aak*-1 are unchanged in *aak-2* mutants relative to WT as assessed by RT-PCR assay. In each case, data are normalized to average of the WT levels. n=3, error bars represent +/-SEM

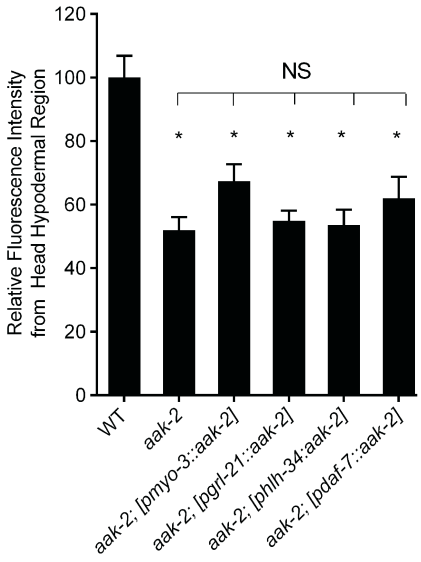

Figure 1.S4, related to Figure 1.1 Quantitation of BODIPY fluorescence intensity shows that reconstitution of *aak-2* in various peripheral tissues or in neurons implicated in feeding or dauer exit does not rescue the low fat of *aak-2* mutants. Data for reconstitution in the body wall muscle (*pmyo-3::aak-2*), hypodermis (*pgrl-21::aak-2*), *hlh-34* neurons, likely AVJ, implicated in feeding elevation upon AAK-2 inactivation (*phlh-34::aak-2*), ASI neurons (*pdaf-7::aak-2*) are shown. n=10, *p<0.05, one-way ANOVA with Bonferroni correction for multiple comparisons. Asterisks indicate significance relative to WT.

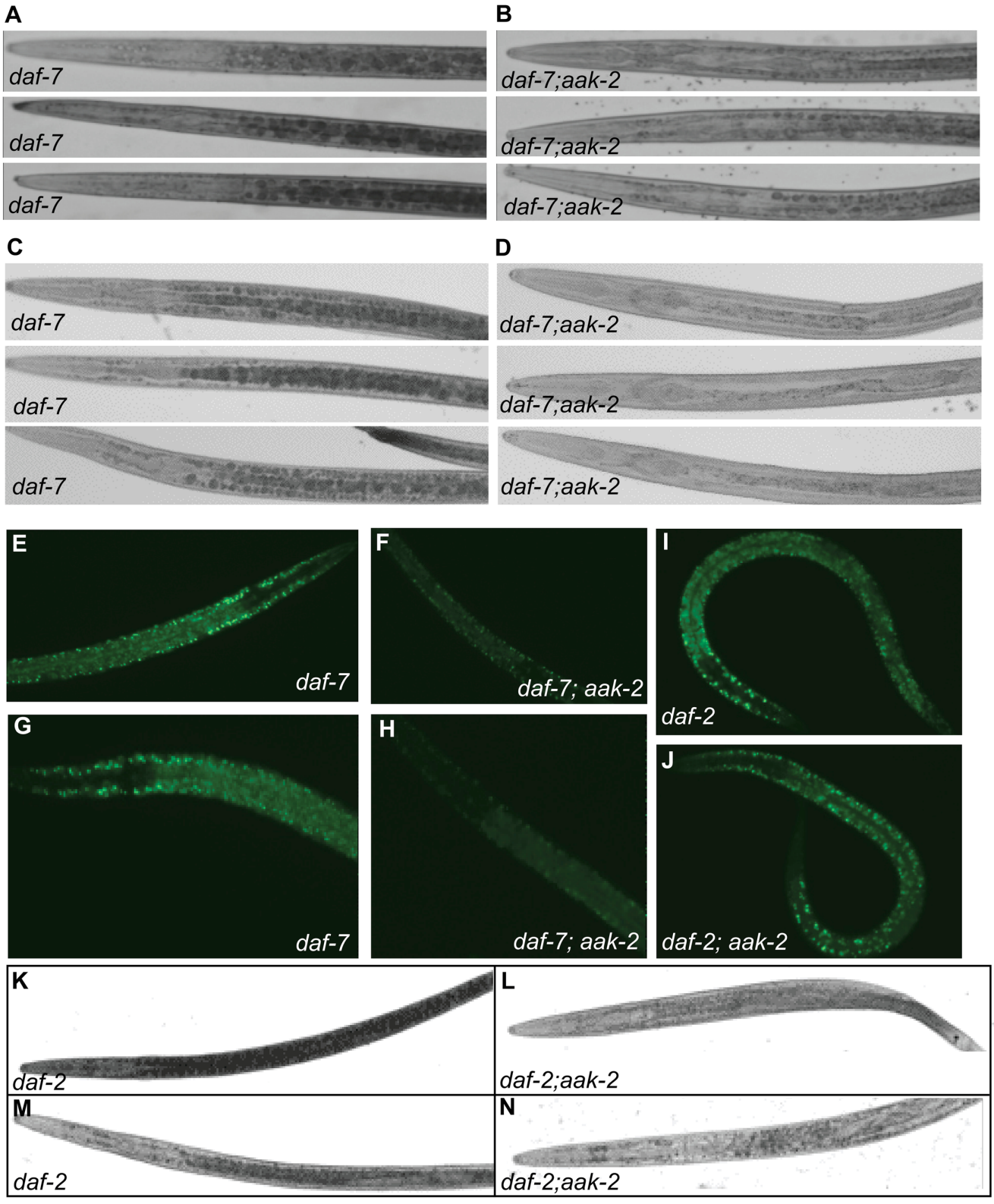
A
daf-7
daf-7
daf-7
B
daf-7;aak-2
daf-7;aak-2
daf-7;aak-2
C
daf-7
daf-7
daf-7
D
daf-7;aak-2
daf-7;aak-2
daf-7;aak-2
E
daf-7
F
daf-7; aak-2
I
daf-2
G
daf-7
H
daf-7; aak-2
J
daf-2; aak-2
K
daf-2
L
daf-2;aak-2
M
daf-2
N
daf-2;aak-2

Figure 1.S5, related to Figure 1.2 *aak-2* deficient dauer animals have reduced fat at all stages. **A-D.** Sudan Black B staining of three representative *daf-7* (A,C) and *daf-7; aak-2* (B,D) animals on day 1 (A,B) and day 4 (C,D) of dauer. **E-H.** Representative BODIPY-labeled fatty acid staining of *daf-7* (E,G) and *daf-7; aak-2* (F,H) as L2 larvae (E,F) and L4 larvae (G,H). **I-J**. Representative images of BODIPY-labeled fatty acid stained *daf-2* (I) and *daf-2; aak-2* (J) L4 larvae. **K-N.** Sudan Black B staining of representative *daf-2* (K, M) and *daf-7; aak-2* (L,N) animals on day 1 (K,L) and day 4 (M,N) of dauer.

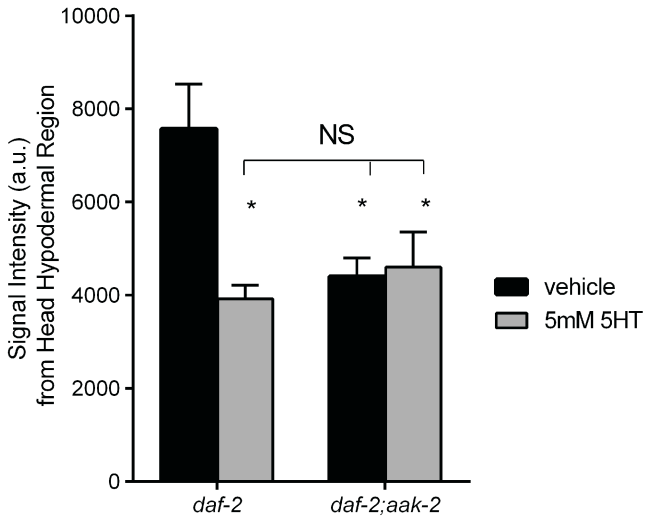

Figure 1.S6, related to Figure 1.2. *daf-2; aak-2* animals have reduced fat relative to *daf-2* animals. Quantitation of signal intensities of coherent anti-Stokes Raman Scattering, CARS, imaging of *daf-2* and *daf-2*; *aak-2* as L4 animals +/- 5mM 5-HT treatment. 5-HT treatment lowered the CARS signal intensities from head hypodermal regions of *daf-2* animals. *daf-2*; *aak-2* mutants had lower signal intensities relative to *daf-2*, which was not further reduced by 5 mM 5-HT treatment. Signal intensities of 5-HT treated *daf-2* were not significantly different than those of *aak-2* +/- 5-HT. n=5, *p<0.05, Student's t-test.

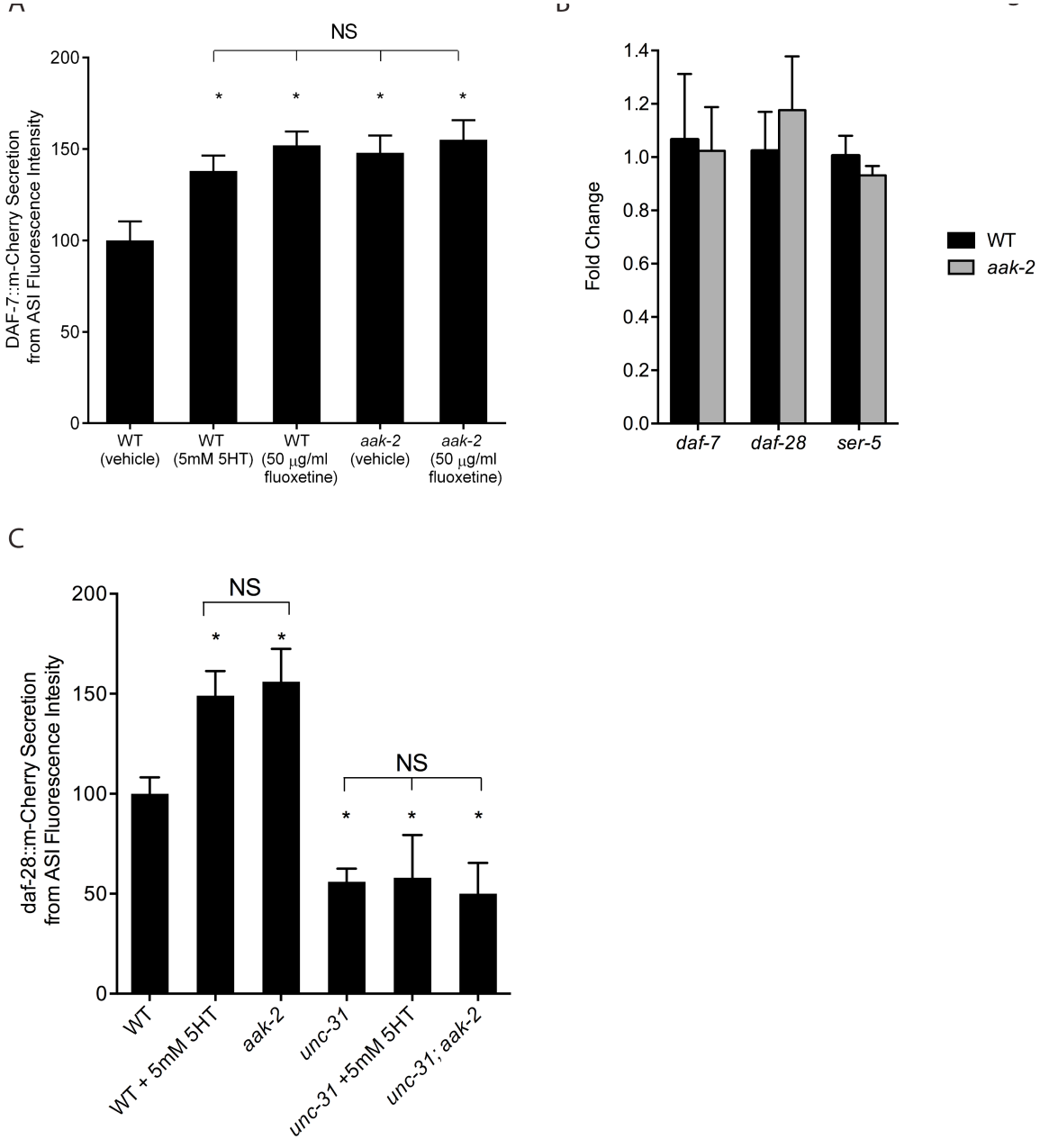
A
NS
DAF-7::m-Cherry Secretion from ASI Fluorescence Intensity
200
150
100
50
0
WT (vehicle)
WT (5mM 5HT)
WT (50 μg/ml fluoxetine)
aak-2 (vehicle)
aak-2 (50 μg/ml fluoxetine)
B
Fold Change
1.4
1.2
1.0
0.8
0.6
0.4
0.2
0.0
daf-7
daf-28
ser-5
WT
aak-2
C
NS
NS
daf-28::m-Cherry Secretion from ASI Fluorescence Intesity
200
150
100
50
0
WT
WT + 5mM 5HT
aak-2
unc-31
unc-31 +5mM 5HT
unc-31; aak-2

Figure 1.S7, related to Figure 1.4 A. As in DAF-28::mCherry (Figure 4), treatment with 5mM 5-HT or loss of *aak-2* promote enhanced secretions of DAF-7::mCherry expressed in the ASI neurons using a *daf-7* promoter, as assessed by the coelomocyte accumulation assay. p*unc-122*::*GFP* was used to mark coelomocytes. The *daf-7::mCherry* transgene was introduced into indicated backgrounds by crossing. WT and *aak-2* mutants were sham treated. Data are shown relative to sham treated WT animals. Each bar represents examination of 20–30 transgenic animals. Error bars represent standard error. *p <0.05, one-way ANOVA with Bonferroni correction for multiple comparisons. **B.** Loss of *aak-2* does not significantly alter gene expressions of *daf-7, daf-28*, or *ser-5* as measured by RT-PCR. In each case, data are normalized to average of the WT levels. n=3, error bars represent +/-SEM **C.** Loss of *unc-31* abrogates the elevated coelomocyte accumulation of DAF-28::mCherry seen upon 5mM 5-HT treatment or loss of *aak-2*. Error bars represent standard error. Asterisks denotes significance relative to sham treated WT animals, *p<0.05, one-way ANOVA with Bonferroni correction for multiple comparisons. An average of 20-30 transgenic animals were examined for each bar. The *daf-28* neuropeptide was tagged with mCherry, while p*unc-122*::*GFP* was used to mark coelomocytes.

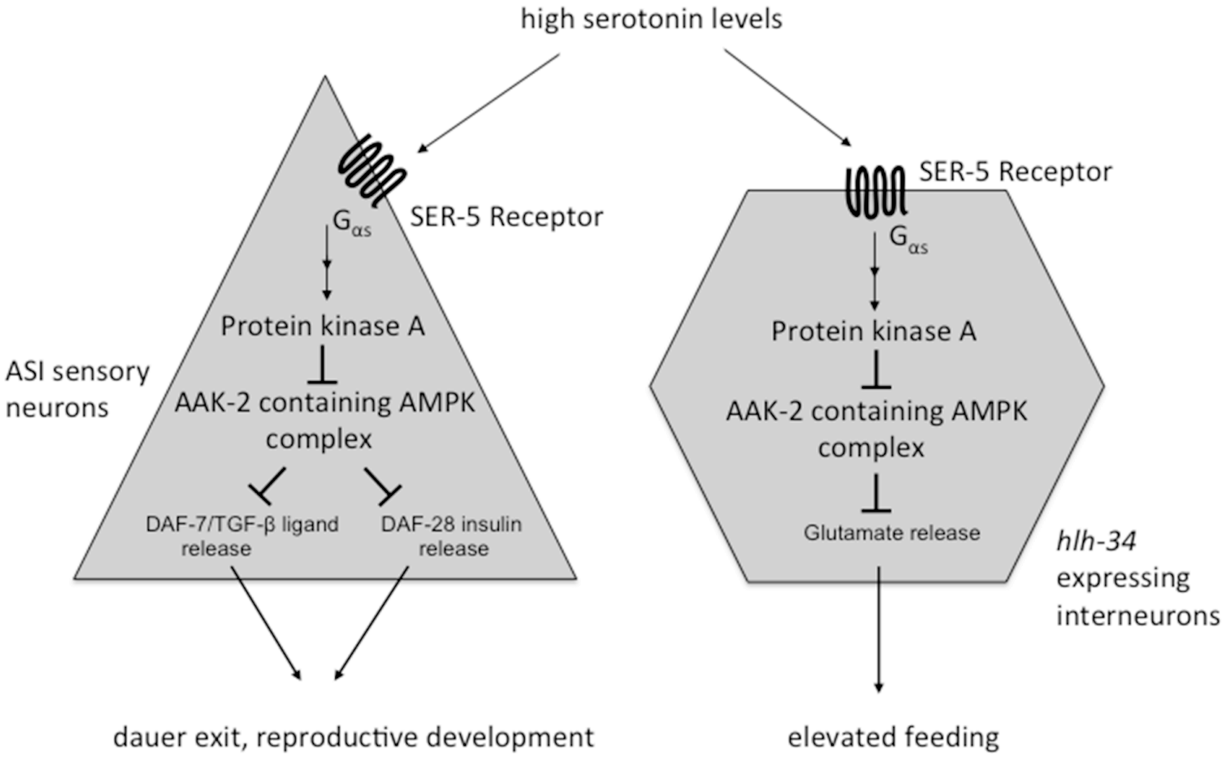

Figure 1.S8 Model Inactivation of AAK-2 in the *hlh-34* expressing AVJ neurons mediate the effects of elevated serotonin signaling on feeding while inactivation of AAK-2 in the ASI neurons mediates the effects of elevated serotonin signaling in enhanced release of the DAF-7 TGF-β ligand and the DAF-28 insulin. In both cases, serotonin signaling through the SER-5 receptor leads to activation of Protein Kinase A, which in turn, causes inhibition of AAK-2.

Table 1.S1 Effects of 5mM 5HT and *aak-2* loss on expression of select metabolic genes. Effects of 5mM 5-HT and *aak-2* loss on expression of select metabolic genes. Predicted annotations for each of the genes are indicated. RT-PCR assays were repeated at least twice for genes whose transcription was altered by addition of 5mM 5-HT or loss of *aak-2*. Data are normalized to untreated WT for each gene.

Gene ID	Putative Function	WT + 5mM 5HT	*aak-2*
	FAT METABOLISM		
F46E10.1	Acyl-CoA Synthetase	1.18	0.93 ± 0.35
T01B8.6	Acyl-CoA Synthetase	4.64 ± 2.94	1.80 ± 0.64
Y65B4BL.5	Acyl-CoA Synthetase	0.59	0.88 ± 0.06
Y76A2B.3	Acyl-CoA Synthetase	0.81	0.68 ± 0.10
F38H4.8	Enoyl-CoA Hydratase	0.70 ± 0.30	0.38 ± 0.15
F43H9.1	Enoyl-CoA Hydratase	1.12	0.71 ± 0.11
R06F6.9	Enoyl-CoA Hydratase	0.92	0.85 ± 0.06
F56B3.5	Enoyl-CoA Hydratase	1.48	0.93 ± 0.25
T05G5.6	Enoyl-CoA Hydratase	1.20	1.64 ± 0.38
Y105E8A.4	Enoyl-CoA Hydratase	0.76	0.87 ± 0.061
F09E10.3	Short-chain Dehydrogenase	1.05	0.71 ± 0.14
K05F1.3	Acyl-CoA Dehydrogenase	2.63	1.26 ± 0.77
F01G4.2	3OH-Acyl CoA Dehydrogenase	0.89	1.01 ± 0.02
B0272.3	3OH-Acyl CoA Dehydrogenase	1.7600 ± 1.24	1.71 ± 0.79
F08A8.2	Acyl-CoA Oxidase-1	1.06	1.77 ± 0.33
F08A8.3	Acyl-CoA Oxidase	0.49	1.05 ± 0.49
F08A8.4	Acyl-CoA Oxidase	0.46	0.38 ± 0.24
F25C8.1	Acyl-CoA Oxidase-1	0.83	0.71 ±0.08
F59F4.1	Acyl-CoA Oxidase-1	0.93 ± 0.20	0.96 ±0.46
T02G5.4	Acetyl-CoA Thiolase	0.92	1.11 ± 0.01
B0303.3	KetoAcyl-CoA Thiolase	1.50	1.22 ± 0.02
W08D2.4	Fat-3 Δ6 Desaturase	0.98	0.87 ± 0.10
T13F2.1	Fat-4 Δ5 Desaturase	1.33	1.37 ± 0.03
Y67H2A.8	Fat-1 Δ3 Desaturase	1.22	1.11 ± 0.12
W02A2.1	Fat-2 Δ12 Desaturase	1.07	0.64 ± 0.39
VZK822L.1	Fat-6	1.07	0.93 ± 0.18
ZK742.5	lbp-6	0.69 ± 0.51	0.83 ± 0.29
T22G5.2	lbp-7	1.12	1.13 ± 0.01
T22G5.6	lbp-8	3.79	1.98 ± 1.23
F40F4.3	lbp-1	0.94	1.06 ± 0.07
EEED8.2	Fatty Acid Binding Protein	0.64	0.57 ± 0.06
EEED8.3	Fatty Acid Binding Protein	1.83 ± 1.28	1.56 ± 0.48
Y40B10A.1	Fatty Acid Binding Protein	0.96	1.20 ± 0.28
C07E3.9	Phospholipase A2	0.86	1.03 ± 0.13

Gene ID	Putative Function	WT + 5mM 5HT	*aak-2*
C42D8.5	Angiotensin Conv Enzyme	1.09	0.68 ± 0.38
C44B7.8	ATP Binding Protein	0.85	0.64 ± 0.01
C25A1.5	Fatty-Acid Hydroxylase	0.50 ± 0.25	0.68 ± 0.18
C44B7.9	Peroxisomal Membrane	2.12	0.82 ± 0.13
Y56A3A.19	Acyl Carrier Protein	0.97	0.86 ± 0.10
T02G5.7	Acetyl-CoA Acetyltransferase	0.84	0.88 ± 0.12
T02G5.8	Acetyl-CoA Acetyltransferase	1.24 ± 0.12	1.07 ± 0.22
C50D2.7	GlucoKinase	0.98	0.97 ± 0.22
T08G2.3	Acyl-CoA Dehydrogenase	17.64	1.79 ± 1.31
C55B7.4A	Acyl-CoA Dehydrogenase	1.51	1.53 ± 0.19
F28A10.6	Acyl-CoA Dehydrogenase	1.08	1.01 ± 0.11
C02B10.1	Acyl-CoA Dehydrogenase	5.99 ± 4.55	1.86 ± 0.69
E04F6.5	Acyl-CoA Dehydrogenase	1.39	1.79 ± 0.76
C17C3.12A	Acyl-CoA Dehydrogenase	1.27	1.10 ± 0.01
F54D5.7	Acyl-CoA Dehydrogenase	0.70	0.40 ± 0.23
F41C3.3	Acyl-CoA Synthase	0.93	0.82 ± 0.11
T20B3.1	Carnitine Palmitoyl Transferase	3.32 ± 1.84	1.58 ± 0.46
F09F3.9	Carnitine Palmitoyl Transferase	1.22 ± 0.25	0.55 ± 0.18
K11D12.4	Carnitine Palmitoyl Transferase	10.98	1.74 ± 0.72
Y48G9A.10	Carnitine Palmitoyl Transferase	1.30	0.95 ± 0.26
W01A11.5	Carnitine Palmitoyl Transferase	0.74	0.46 ± 0.05
F41E7.6	Carnitine Palmitoyl Transferase	1.28 ± 0.38	1.39 ± 0.50
	CARBOHYDRATE METABOLISM		
C05C10.3	Succinyl-CoA;3-ketoacid CoA Transferase	0.95	0.75 ± 0.11
F25B4.6	HMG-CoA Synthase	0.98	0.78 ± 0.01
Y71G12B.10	HMG-CoA Lyase	1.04 ± 0.26	0.75 ± 0.07
F14B4.2	Hexokinase	0.69 ± 0.13	0.94 ± 0.07
H25P06.1	Hexokinase	1.09 ± 0.39	0.93 ± 0.17
Y71H10A.1	6-Phosphofructokinase (both spliceforms)	1.25	0.83 ± 0.41
Y71H10A.1a	6-phosphofructokinase (a spliceform)	1.18	1.03 ± 0.14
R11A5.4	PEPCK (all spliceforms)	1.06	0.89 ± 0.02
W05G11.6	PEPCK (all spliceforms)	1.64	0.98 ± 0.19
F25H5.3	Pyruvate Kinase (all spliceforms)	0.85	0.89 ± 0.03
ZK593.1	Pyruvate Kinase	1.02	0.93 ± 0.09
Y110A7A.6	Phosphofructokinase (both spliceforms)	0.65	0.77 ± 0.12
K02B2.1	Phosphofructokinase	0.97 ± 0.34	0.83 ± 0.11
T09F3.3	Glyceraldehyde-3 Phosphate Dehydroge	0.78 ± 0.32	2.0 ± 0.81
F33H1.2	Glyceraldehyde-3 Phosphate Dehydroge	0.82 ± 0.35	0.59 ± 0.17

Gene ID	Putative Function	WT + 5mM 5HT	*aak-2*
R11A5.4a/b	PEPCK (a and b spliceforms)	0.76 ± 0.19	0.69 ± 0.08
R11A5.4a/c/d	PEPCK (a, c and d isoforms)	0.96	0.94 ± 0.08
W05G11.6a/d	PEPCK (a and d spliceforms)	1.49	1.08 ± 0.33
W05G11.6a/b/d	PEPCK (a,b and d spliceforms)	1.15	0.87 ± 0.17
W05G11.6a/b/c	PEPCK (a,b and c spliceforms)	3.95	2.34 ± 1.29
F25H5.3b	Pyruvate Kinase (b spliceform)	4.31 ± 0.10	2.26 ± 1.07
F25H5.3a/b	Pyruvate Kinase (a and b spliceforms)	0.70	0.75 ± 0.04
Y110A7A.6a	Phosphofructokinase (a isoform)	0.88	1.19 ± 0.30
H17B01.1b	Sugar Transporter (b isoform)	4.24 ± 3.09	2.80 ± 2.25
K07A3.1	fructose, 1,6 bisphosphatase	1.14	0.83 ± 0.20
F54H12.1a/b	aconitase (a and b spliceforms)	0.81	0.80 ± 0.07
F54H12.1a/b/c	aconitase (a, b and c spliceforms)	1.10	0.87 ± 0.01
ZK455.1	aconitase	1.07	0.89 ± 0.17
F20H11.3	malate dehydrogenase	1.06	0.98 ± 0.21
F46E10.10a/c	lactate/malate dehydrogenase (a and c)	0.73	0.99 ± 0.27
F46E10.10a/b	lactate/malate dehydrogenase (a and b)	0.77	0.86 ± 0.07
C05E4.9.a	Isocitrate lyase family/Malate synthase	1.53	1.09 ± 0.39
C05E4.9.b	Isocitrate lyase family/Malate synthase	1.23	1.18 ± 0.51
C03G5.1	succinate dehydrogenase	1.11 ± 0.33	1.29 ± 0.38
C34B2.7	succinate dehydrogenase	0.71	0.98 ± 0.27
R11F4.1	glycerol kinase	0.93 ± 0.08	0.79 ± 0.10

Chapter II: Intestinal peroxisomal fatty acid β-oxidation regulates neural serotonin signaling through a feedback mechanism

Abstract

The ability to coordinate behavioral responses with metabolic status is fundamental to the maintenance of energy homeostasis. In numerous species including *C. elegans* and mammals, neural serotonin signaling regulates a range of food-related behaviors. However, the mechanisms that integrate metabolic information with serotonergic circuits are poorly characterized. Here, we identify metabolic, molecular, and cellular components of a circuit that links peripheral metabolic state to serotonin-regulated behaviors in *C. elegans*. We find that blocking the entry of fatty acyl-CoAs into peroxisomal β-oxidation in the intestine results in blunting of the effects of neural serotonin signaling on feeding and egg-laying behaviors. Comparative genomics and metabolomics revealed that interfering with intestinal peroxisomal β-oxidation results in a modest global transcriptional change but significant changes to the metabolome, including a large number of changes in ascaroside and phospholipid species, some of which affect feeding behavior. We also identify body cavity neurons and an ether-a-go-go related (EAG) potassium channel that functions in these neurons as key cellular components of the circuitry linking peripheral metabolic signals to regulation of neural serotonin signaling. These data raise the possibility that the effects of serotonin on satiety may have their origins in feedback, homeostatic metabolic responses from the periphery.

Introduction

In both invertebrate and vertebrate species, behaviors such as feeding, movement, reproduction and learning are influenced by nutritional and metabolic signals [2–9]. In mammals, the nervous system actively monitors internal nutritional status by directly sensing specific metabolites like carbohydrates, amino acids and fatty acids, in addition

to sensing endocrine signals derived from peripheral tissues [10,11]. These internal nutrient cues are integrated with environmental stimuli and past experiences to orchestrate cohesive and context-appropriate behavioral and physiological responses. Defects in internal metabolic sensing processes contribute to the development of a number of disorders including diabetes, obesity, impaired immune function, neurodegeneration and accelerated aging [9,12–14]. Thus, elucidating the mechanisms by which nutrient status is sensed and communicated between tissues is of critical importance in understanding metabolic homeostasis as well as how metabolism influences myriad physiological and pathophysiological conditions.

Like mammals, *C. elegans* display a range of behavioral and physiological responses to changes in nutrient availability [2,15]. Moreover, as in vertebrate species, the neuromodulator serotonin, 5-hydroxytryptophan, is a key mechanism through which information about food availability is converted to behavioral, physiological, and metabolic responses in *C. elegans* [16–21]. For example, even in the presence of food, worms that lack serotonin display the feeding, egg laying, movement, and metabolic rates that are normally seen when wildtype animals are deprived of food [22]. In contrast, pharmacologic or genetic manipulations that elevate serotonin signaling elicit the range of responses seen when plentiful food supplies are present [20,23,24]. Importantly, serotonin signaling is not simply an *on/off* indicator of food availability but the extent of serotonin signaling allows for animals to fine tune their responses based on their nutritional status and past experiences [4,25,26]. One illustration of this is the effects of varying levels of serotonin signaling on pharyngeal pumping rate, the mechanism by which *C. elegans* ingest nutrients [27,28]. *C. elegans* that have been moved off of their

E. coli food source reduce their serotonin signaling as well as their pumping rates. Both serotonin signaling and pumping rates are elevated as animals are returned to food [29,30]. However, if animals experience a period of fasting before they are returned to food, they exhibit an even further elevation in feeding rate compared to animals that have only been off of food for brief period of time. The hyper-elevated feeding behavior is accounted for by a correspondingly elevated secretion of serotonin from specific neurons [4]. The hyper-secretion of serotonin and the corresponding hyper-elevated feeding are transient and animals eventually resume the intermediate levels of serotonin signaling and feeding rates seen in well-fed animals [4,30]. Thus, the low, high, and intermediate levels of serotonin signaling correspond to the low, high, and intermediate pharyngeal pumping rates, respectively.

In addition to modulating of food intake behavior, serotonin signaling also affects energy metabolism [31]. *C. elegans* that have been returned to food after a period of fasting transition from a metabolic state that favors energy conservation to an active state of energy utilization. This active metabolic state is driven by elevated serotonin signaling [19,32,33]. If elevated levels of serotonin are maintained by pharmacological or genetic interventions, *C. elegans* exhibit fat loss [34,35]. The effects of serotonin on body fat are not simply a byproduct of its effects on food intake as we and other groups have found that molecular and cellular circuits that link serotonin signaling to peripheral energy metabolism are largely independent from those that regulate feeding [19,23,24,32,33,36]. For example, serotonin secreted from the ADF sensory neurons signals through neurally expressed SER-5 serotonergic receptor to modulate feeding. Yet the SER-5 receptor is not required for the serotonergic regulation of peripheral fat metabolism [19,30]. Instead,

serotonin signals through the MOD-1 receptor on URX neurons to promote the release of a neuroendocrine signal that activates triglyceride lipolysis and distinct components of fatty acid oxidation pathways [19,32,33].

In a prior study, we discovered that specific components of lipid oxidation pathways can elicit regulatory effects on feeding behavior [19]. Here, we build upon that finding and describe a feedback mechanism that links peripheral energy metabolism to neuronal serotonin signaling. We find that loss of ACOX-1, a peripheral acyl-CoA oxidase that catalyzes a key step in peroxisomal fat oxidation, affects feeding and egg-laying responses, two serotonin-regulated behaviors. Blunting the utilization of fatty acyl-CoA species, the metabolic substrates of ACOX-1, results in rewiring of peripheral metabolic pathways and ultimately affects the activity of body cavity neurons, which in turn, counteract neural serotonin signaling to influence nutrient-related behaviors.

Results

acox-1 mutants are unresponsive to the feeding stimulatory effects of serotonin

While the serotonergic regulation of fat metabolism is largely distinct from the feeding regulatory pathway, we previously noted two exceptions. RNAi-mediated inactivation of either acox-1, encoding a peroxisomal acyl-CoA oxidase, or cpt-6, encoding a mitochondrial carnitine palmityoltransferase, not only blocked the fat reducing effects of serotonin but also counteracted the effects of elevated serotonin on feeding [19]. Interestingly, acox-1 and cpt-6 function as entry points in the peroxisomal and mitochondrial β-oxidation pathways, respectively [37]. To further investigate how metabolic pathways affect serotonin signaling, we focused on acox-1 given the

availability of a null mutant for this gene at the time that the study was undertaken. Recapitulating our prior RNAi findings, ad-libitum fed acox-1(ok2257) animals exhibit wildtype feeding rates, yet are unresponsive to the feeding stimulatory effects of exogenous serotonin (Figure 1A, Figure S1A). We previously demonstrated that elevated levels of serotonin signaling exert their effects on fat and feeding pathways by inactivating AMP-activated kinase (AMPK) complexes in distinct neurons [24,30]. As in mammals, the catalytic subunit of AMPK can be encoded by one of two distinct genes, aak-1 and aak-2, in C. elegans [38]. Elevated levels of serotonin signaling inactivate the AAK-2 subunit and the hyperactive pumping rate of serotonin-treated wildtype animals is recapitulated by aak-2 mutants [30]. Loss of acox-1 suppressed the elevated feeding rates of aak-2 mutants suggesting that the effects of acox-1 on feeding are not restricted to exogenously supplied serotonin (Figure 1B).

Although the above findings suggested that acox-1 functions downstream or parallel to serotonin signaling, we sought to rule out the possibility that acox-1 affects serotonin biosynthesis. Transcription of tph-1, the gene that encodes the rate-limiting enzyme of de novo serotonin synthesis, is highly dynamic and can be modulated by a range of external and internal cues including food availability, food quality, and stress [25,39–42]. We observed no changes in the transcriptional expression of tph-1 nor in direct quantifications of serotonin levels in acox-1 mutants (Figure S1B and S1C). In mammals, defects in peroxisomal fatty acid oxidation pathways are associated with neurodevelopmental disorders due to toxic accumulation of long and very-long chain fatty acids [43]. We had previously shown that elevation of serotonin signaling from the chemosensory, amphid ADF neurons is sufficient to cause elevated pharyngeal

pumping [30]. We therefore considered the possibility that the lack of response to serotonin in acox-*1* mutants may be the indirect consequence of a defect in the ADF neurons or other sensory neurons. As one broad examination of neural morphology and development, we used DiI dye staining and found that *acox-1* mutants had properly structured amphid sensory neurons (Figure S1D). Collectively, we found no evidence that deficiencies in serotonin biosynthesis or structural or developmental abnormalities in serotonergic sensory neurons account for the inability of serotonin to elevate feeding rate in *acox-1* mutants.

Based on homology to mammalian acyl-CoA oxidase 1, ACOX-1 is predicted to catalyze the first and rate-limiting step in peroxisomal β-oxidation [44,45]. We used fluorescence intensity of BODIPY labeled fatty acids as a measure of fat accumulation since we and others have previously demonstrated that BODIPY fluorescence corresponds to biochemical and label free methods, such as Coherent anti-Stokes Raman Scattering spectroscopy, measurements of fat content [46,47]. We found that animals lacking ACOX-1 accumulate significantly more fat in their hypodermis and intestines, the two major sites of fat storage, consistent with the notion that *acox-1* mutants have a reduced capacity to break down lipids (Figure 1C and 1D). If the inability of *acox-1* mutants to increase their feeding rate represented a homeostatic response to elevated internal energy stores, we predicted that a period of nutrient depletion should reverse *acox-1* mutants' feeding behavior. We fasted *acox-1* mutants for 90 minutes, a period of time shown to elicit a coordinated shift in internal metabolic networks towards fat mobilization and energy production, and reintroduced fasted or *ad-libitum* fed animals to either vehicle or serotonin containing plates [48,49]. Fasting restored the ability of *acox-*

1 mutants to increase their feeding rates in response to exogenous serotonin suggesting that *acox-1* mutants do not simply have a generalized defect in pharyngeal pumping and that a period of starvation can reverse the feeding regulatory effect induced by loss of ACOX-1 activity (Figure 1E). Together, these findings suggest that loss of ACOX-1 activity leads to the generation of a homeostatically regulated signal that can rapidly and reversibly modulate serotoninergic feeding circuits.

Intestinal ACOX-1 regulates feeding behavior

To elucidate the site of ACOX-1 activity in regulating feeding behavior, we performed tissue-specific rescue experiments. As previously reported, ACOX-1 is expressed in the hypodermis and the intestine, the primary sites of lipid metabolism in *C. elegans* [44] (Figure 2A). Expression of a full length wildtype *acox-1* gDNA sequence in the intestine (via the *vha-6* promoter) but not in the hypodermis (via the *dpy-7* promoter) normalized fat levels in *acox-1* mutants (Figure 2B and 2C). The intestine is the primary metabolic organ in *C. elegans* and carries out numerous metabolic functions including food digestion, nutrient absorption, packaging and secretion [50]. We found that the intestinal expression of wildtype *acox-1* was sufficient to restore the capacity of *acox-1* mutants to elevate feeding rates in response to serotonin treatment (Figure 2D). Thus, intestinal ACOX-1 activity can affect neuronal serotonergic feeding circuits.

Modulation of feeding by ACOX-1 requires fatty acyl-CoA synthesis

Acyl-CoA oxidases regulate the rate of metabolic flux through peroxisomes as they govern the first and rate-limiting reaction in peroxisomal metabolic pathways, specifically catalyzing the desaturation of long and very-long chain fatty acyl-CoA esters to 2-trans-

enoyl-CoAs [45,51–53]. The *C. elegans* genome encodes seven acyl-CoA oxidases that form homo and heterodimer complexes with distinct substrate specificities [51,54,55]. Structural and biochemical analyses suggest that ACOX-1 homodimers are capable of accommodating a wide-range of fatty acyl-CoA substrates and contribute to peroxisomal β-oxidation of ascaroside lipids [56,57]. Given the enzymatic function of ACOX-1, we hypothesized that its loss leads to an accumulation of fatty acyl-CoA species, which in turn, elicit the anorectic effect. Fatty acyl-CoAs are generated by acyl-CoA synthases (ACS), a family of enzymes that esterify free fatty acids with Co-enzyme A (CoA) [58,59]. To prevent the formation of acyl-CoA thioesters, we acutely exposed animals to Triacsin C, an inhibitor of acyl-CoA synthase activity [60]. This treatment restored the ability of serotonin to cause elevated feeding rate in *acox-1* mutants suggesting that fatty acid esterification is required in order for ACOX-1 to regulate serotonergic feeding cascades (Figure 3A). There at least 20 known or predicted acyl-CoA synthases encoded in the *C. elegans* genome. As a strategy to validate the Triacsin C results and identify the specific synthases involved, we screened through 18 of 20 *acs* genes for which RNAi clones were available. RNAi treatment against multiple *acs* genes, most notably those of *acs-18*, *acs-20* or *acs-22*, suppressed the feeding defects of *acox-1* mutants, suggesting that a degree of redundancy among *C. elegans* acyl-CoA synthases (Figure S3A). As we did not validate the efficacy of each of the 18 RNAis we cannot rule out the possibility that other ACS enzymes also contribute to acyl-CoA pools used by ACOX-1. To further test the notion that fatty acyl-CoAs modulate feeding, we treated animals with oleic acid, a dietary fatty acid, and noted a reduction in pharyngeal pumping rate (Figure 3B). The oleic acid-induced feeding suppression was abrogated in animals that were pretreated with Triacsin

C, suggesting that the anorectic effect is induced by oleoyl-CoA or a downstream metabolic derivative.

To directly evaluate whether loss of *acox-1* causes accumulation of acyl-CoAs, we employed an HPLC-based extraction and detection method from whole animal extracts [61,62]. We found that acyl-CoAs levels were not grossly altered in *acox-1* mutants (Figure 3C). One possible explanation for the absence of elevated acyl-CoA species in *acox-1* mutants is that only a small fraction of total acyl-CoAs in the animals are directed to peroxisomal β-oxidation such that a change in their abundance may not be detectable by our assay. Moreover, acyl-CoA metabolism is known to be highly spatially regulated and acyl-CoA products are selectively synthesized or partitioned in specific tissues [63,64]. Yet another possibility is that acyl-CoAs are substrates for numerous metabolic processes and can be converted into a variety of signaling molecules like ceramides, ascarosides and eicosanoids [55,59,65]. Thus, blocking acyl-CoA utilization by inactivating ACOX-1 may shunt these intermediates into a variety of other metabolic derivatives that ultimately elicit anorectic effect.

Loss of *acox-1* results in modest transcriptional upregulation of compensatory fat oxidation pathways

To better understand molecular responses to the loss of *acox-1*, we compared the transcriptome *acox-1* mutants to that of wildtype animals using RNA-sequencing. Loss of *acox-1* had a surprisingly limited effect on global gene expression. Our analyses revealed that only 36 out of ~17,000 genes were differentially expressed in *acox-1* mutants, with only three genes significantly upregulated. Among the differentially expressed genes, the majority were expressed in the intestine, consistent with our finding

that this tissue is a major site of action for ACOX-1. Gene Ontology analysis revealed an enrichment for genes involved in “lipid metabolic” and “innate immune” related processes (Table 1). Among the differentially regulated genes, several are predicted to encode for components of peroxisomal β-oxidation including a homolog of acyl-CoA oxidase (ACOX-2), an enoyl-CoA hydratase (ECH-*1.1*) and an ortholog of human bile acid-CoA:amino acid N-acyltransferase (K05B2.4). Two lipases, LIPL-2 and K03H6.2, whose activities are predicted to promote lipid mobilization, were downregulated. Collectively, we interpret these results to mean that the transcriptional responses elicited upon loss of *acox-1* likely compensate for peroxisomal dysfunction by limiting lipid mobilization and by upregulating alternative lipid utilization pathways. Using RNAi, we asked whether inactivation of any of the upregulated genes could counteract the resistance of *acox-1* mutants to serotonin induced feeding elevation but the experiment yielded no such candidates.

Loss of *acox-1* perturbs fatty acid ethanolamine signaling

Next, we sought to obtain a comprehensive overview of the impact of loss of *acox-1* on the *C. elegans* metabolome. For this purpose, we compared the *acox-1* mutant and wildtype metabolomes via untargeted metabolomics using high-pressure liquid-chromatography-high-resolution mass spectrometry (HPLC-HRMS) and the XCMS software platform [66,67]. These analyses revealed that knockout of *acox-1* has a dramatic impact on the *C. elegans* metabolome. Of more than 10,000 significant features detected in the wildtype metabolome, over 500 were at least 3-fold downregulated in *acox-1* mutants. Conversely, we detected more than 500 features that were at least 3-fold upregulated in *acox-1* mutants. To facilitate structural classification of the vast number of detected differential features, we employed molecular networking based on

analysis of MS/MS fragmentation patterns [68,69]. These analyses enabled characterization of several metabolite families up- or downregulated in *acox-1* mutants. As expected from previous reports, we found that biosynthesis of most ascaroside pheromones with fatty acid side chains shorter than 9 carbons is abolished or strongly reduced in *acox-1* mutants, whereas abundances of ascarosides with saturated side chains of 9 to 15 carbons are 10- to 50-fold increased [56,57]. In addition, a large number of diacylglycerophosphoethanolamines (DAGPEs), primarily derived from saturated and mono-unsaturated fatty acids with 14 to 18 carbons, were reduced 5- to 20-fold in *acox-1* mutants. Among the metabolites most strongly upregulated in *acox-1* mutants, thiamine and several thiamine derivatives were most prominent, alongside ascr#18 and ascr#22, ascarosides with 11 and 13 carbon sidechains, respectively (Figure 4, Supplemental Table 1).

The very large number of metabolites affected by loss of *acox-1* prevented a comprehensive examination of each of the metabolites. Nevertheless, we used a combination of chemical, genetic, and metabolite add-back experiments to broadly investigate the noted metabolomics changes. We began by considering the possibility that perturbations in ascaroside biosynthesis underlie the feeding defect observed in *acox-1* mutants. Originally identified as constituents of the dauer pheromone, ascarosides are large class of excreted small molecules that regulate development and behavior and whose synthesis can be influenced by metabolic status [70–72]. The acyl-CoA thiolase, DAF-22, catalyzes the terminal step in peroxisomal β-oxidation and plays an essential role in shortening the fatty acid-like-side chains of ascarosides [73]. Though *daf-22* mutants lack ascarosides they still exhibit wildtype feeding rates and are still

responsive the feeding increasing effects of serotonin, suggesting that ascaroside biosynthesis and serotonergic feeding regulation are independent of one another (Figure S4A). Though a number of ascaroside species were strongly reduced in *acox-1* mutants, we detected a nearly 30-fold accumulation of ascaroside #18 (ascr#18). To determine if an accumulation of ascr #18 underlies the suppressed feeding response of *acox-1* mutants, we treated wildtype animals with ascr#18 and serotonin. Surprisingly, rather than suppressing feeding, ascr#18 dramatically increased pharyngeal pumping rates of wildtype animals in a manner that was additive with serotonin (Figure S4B). Together, these results suggest that while certain ascarosides species can have feeding regulatory effects, they are unlikely to underlie the specific feeding responses elicited in *acox-1* mutants.

Thiamine and thiamine derivatives were also significantly accumulated in *acox-1* mutants. We next asked if thiamine supplementation was sufficient to block the feeding enhancing effects of serotonin, though did not find this to be the case (Figure S4C). As in mammals, *C. elegans* does not produce thiamine and obtains this essential cofactor from its diet [74]. Given the pervasive changes to *C. elegans* metabolism upon loss of *acox-1*, we speculate that thiamine accumulation in these mutants reflects a general downregulation of enzyme activities that use thiamine derivatives as cofactors.

We next turned our attention to the finding that loss of *acox-1* perturbs the biosynthesis of ethanolamine containing lipid species. Most prominently, we find that diacylglycerophosphoethanolamine (DAGPEs) synthesis is strongly reduced in *acox-1* mutants. DAGPEs likely represent intermediates in the biosynthesis of *N*-acylethanolamines (NAEs), a diverse family of signaling molecules with range of

biological roles including in nutrient sensing and mammalian appetite regulation [75–79]. This family of lipids includes the mammalian orexigenic endocannabinoid arachidonoyl ethanolamine (AEA) and anorectic factor oleoyl ethanolamine (OEA) [80]. To test if a reduction in NAEs contributes to ACOX-1 mediated feeding regulation, we inactivated fatty acid amide hydrolase (*faah-1*), an enzyme involved in the hydrolytic degradation of NAEs. We found that inhibition of FAAH-1, which was shown to increase endogenous NAE abundance [81], stimulates pharyngeal pumping rates of both wildtype and *acox-1* mutants (Figure S4D). Thus, in *C. elegans* as in mammals, NAE signaling regulates feeding behavior. As the feeding increasing effects of increasing NAEs were not restricted to *acox-1* mutants, we cannot definitively know that reduced NAE synthesis accounts for the inability of *acox-1* mutants to respond to serotonin. Though this data is intriguing, it is also possible that an as of yet unidentified metabolite or a complex combination of metabolites blunt serotonergic modulation of feeding in *acox-1* mutants.

ACOX-1 mediated regulation of serotonergic feeding circuits requires EGL-2 activity

We next sought to identify the neural mechanisms that link changes elicited by loss of *acox-1* to serotonergic mechanisms of feeding. The clue that guided us towards an answer emerged unexpectedly by following another phenotype that we had noted in *acox-1* mutants. Relative to wildtype animals, *acox*-1 mutants hold more eggs *in utero* and lay embryos at a later developmental stage (Figure 5A, Figure S4A). This was intriguing since serotonin is also a key modulator of egg-laying behavior [82]. Serotonin controls the excitability of the egg-laying neuromuscular circuit and governs the activity and timing of egg-laying in response to various sensory cues [16–18,83–88]. We found that *acox-1*

mutants were markedly less responsive to exogenous serotonin and resistant to the effects of fluoxetine, a serotonin reuptake inhibitor consistent with a reduced response to the excitatory effects of serotonin at the level of the neuromuscular junction (Figure 5C, Figure S4B). As in the context of feeding, reconstitution of *acox-1* in the intestine but not the hypodermis also rescued egg-laying defects of these mutants (Figure 5D and 5E).

The egg-laying neuromuscular circuit has been extensively studied in *C. elegans* and it is well established that egg-laying behavior is strongly influenced by potassium channel activity [89]. Potassium channels are a highly diverse and evolutionarily conserved family of proteins that modulate cellular excitability by regulating the flow of potassium ions (K+) across cellular membranes [90,91]. Gain-of-function mutations in distinct potassium channels have been shown to reduce the excitability of neurons or vulval muscles, and in turn causing egg-laying defects [92–95]. We therefore considered the possibility that aberrant potassium channel activity contributes to the egg-laying dysfunction in *acox-1* mutants. We conducted an RNAi screen of potassium channels with documented roles in egg-laying and assessed their capacity to rescue the egg-laying defect in *acox-1* mutants. RNAi knockdown of the EGL-2 potassium channel normalized egg-laying responses in *acox-1* mutants without influencing baseline egg-laying rates (Figure S4C and S4D). To validate our RNAi results, we crossed *acox-1* mutants with *egl-2*(lf) mutants and found that double mutants resembled wildtype animals in their egg-laying responses (FIGURE 5F and 5G). *egl-2* encodes an ether-a-go-go (EAG) voltage-gated potassium channel that has been shown to modulate the excitability of neuromuscular circuits in response to starvation states, suggesting they may more generally serve as a link between internal nutrient status and neuronal activity [96–98].

To determine if EGL-2 plays a role in ACOX-1 mediated feeding regulation, we took advantage of gain-of-function mutations in *egl-2.* These mutations cause a negative shift the voltage-dependence of these channels and cause pleotropic sensory and behavioral defects by reducing the excitatory capacity of cells in which they are expressed [99,100]. It has been previously reported that *egl-2*(gf) mutants are resistant to the egg-laying inducing effects of serotonin [95,101]. We find that *egl-2*(gf) mutants are also resistant to the feeding enhancing effects of serotonin and thus mimic *acox-1* mutants in their blunted responses to the excitatory effects of serotonin signaling in the context of both egg-laying and feeding (Figure 6A). Both the egg-laying and pharyngeal pumping phenotypes of *egl-2*(gf) mutants can be fully suppressed by *egl-2* RNAi knockdown suggesting that the behavioral effects of aberrant EGL-2 activity can be normalized by inactivating the channel (Figure 6A, Figure S5A). Similarly, RNAi inactivation of *egl-2* restores the ability of *acox-1* mutants to elevate their pumping rates upon exposure to serotonin signaling but without affecting the basal pumping rate in *acox-1* mutants (Figure 6B). Validating the RNAi results, we find that double *acox-1;egl-2(*lf) mutants exhibit wildtype feeding responses to exogenous serotonin (Figure 6C). Finally, we find that the feeding reducing effects of oleic acid also require EGL-2 (Figure 6D). Together, these results suggest that an EGL-2 containing circuit can serve as a regulatory link between metabolic status and feeding behavior.

Loss of acox-1 suppresses URX body cavity neuron activity to limit feeding responses

Our results with *egl-2* provided us the opportunity to pinpoint neurons that may serve as a link between peripheral metabolic signals and processes regulated by

serotonin signaling. In hermaphrodites, *egl-2* is expressed in a limited subset of sensory neurons including AFD, ALN, AQR, ASE, AWC, BAG, IL2, PLN, PQR and URX [99]. We were intrigued by the expression of *egl-2* channels in body cavity neurons (AQR ,PQR and URX), as these are the only neurons with dendritic projections within the pseudocoelom, the rudimentary circulatory fluid utilized by *C. elegans* (Figure 7A) [102]. Given their unique anatomic position, these neurons are hypothesized to mediate bidirectional communication between nervous system and peripheral tissues as they have the capacity to both release and detect circulating signals. Interestingly, neural serotonin signaling is thought to promote intestinal fat metabolism through the release of an neuroendocrine signal from URX neurons [32,33] and fluctuations in peripheral fat metabolism modulate the tonic activity of URX [103]. We find that targeted expression of *egl-2(*gf*)* in only the body cavity neurons is sufficient to block the feeding increasing effects of serotonin and mimic the effects of loss of *acox-1* (Figure 7B).

To our knowledge, body cavity neurons have not previously been implicated in the regulation of feeding behavior. To further study this role, we examined the effect of prolonged activation of body cavity neurons on pharyngeal pumping. Activation of PKC-1 has been shown to promote synaptic transmission and neuropeptide release from expressing neurons [104]. We examined the feeding responses of wildtype and *acox-1* mutants expressing constitutively active protein kinase C [PKC-1(gf)] in body cavity neurons and found that this manipulation strongly stimulates pharyngeal pumping in both wildtype and *acox-1* mutants. Importantly, this feeding enhancement could not be further elevated by addition of serotonin, suggesting a common regulatory circuit (Figure 7C).

As genetic inhibition of body cavity neurons by *egl-2(*gf*)* did not modulate baseline feeding rates, our data suggests that these neurons likely fine-tune feeding responses in distinct conditions rather than governing basal feeding behavior.

To directly assess the effects of ACOX-1 activity on body cavity neuron function, we measured intracellular Ca^{2+} transients from the URX body cavity neurons using the genetically-encoded calcium reporter GCaMP5K [103,105]. We selected URX neurons as calcium dynamics from these cells have been well documented and intriguingly their activity has recently been shown to be modulated by internal metabolic cues and starvation [103,106–108]. URX neurons play a well-documented role in oxygen sensing and are robustly and rapidly activated under atmospheric conditions (21% oxygen) (Figure 8A and 8C) [106,109–111]. To determine if loss of ACOX-1 modulates URX activity, we imaged O_2-evoked calcium transients in URX neurons in wildtype and *acox-1* mutants. We observed no significant difference in URX responses in wildtype and *acox-1* mutants at 10% oxygen, a concentration at which the tonic URX neurons are held in the "off" state [106]. This result suggests that ACOX-1 does not modulate basal activity of URX (Figure 8B and 8F). However, whereas URX neurons in wildtype animals robustly activate at 21% oxygen as previously documented, O_2-evoked calcium transients were dramatically inhibited in *acox-1* mutants (Figure 8D and 8D). This reduction in maximal activation ($F\Delta/F_o$) could not be attributed to altered promoter activity or drift in expression across the tested lines as the level of a co-expressed *flp-8*::mCherry reporter was not measurably different *acox-1* mutants (Figure 8E and 8G). Together, this data suggest that loss of ACOX-1 decreases the sensitivity of URX neurons to excitatory stimuli, supporting the model that body cavity neuron activity is suppressed in *acox-1* mutants

We previously showed that regulation of feeding responses by ACOX-1 requires the generation of fatty acyl-CoA species. We thus asked whether we could rescue the suppression of URX neuron activity by inhibiting the synthesis of fatty acyl-CoA species. To assess the effects of fatty acyl-CoA species on URX activity, we treated wildtype and *acox-1* animals with the acyl-CoA synthase inhibitor, Triacsin C for 60 minutes prior to assessing URX responses. Paradoxically, reducing the synthesis of fatty acyl-CoAs suppresses the activity of URX neurons in wild-type animals but slightly enhances the activity of this neuron in *acox-1* mutants though these trends are not statistically significant (Figure S6).

These results are complicated to interpret. Though this experiment suggests that Triacsin C does not significantly rescue the defects in URX activity, we must consider the limitations of this experimental approach. GCaMPs are powerful tools, they offer indirect and oft-crude representations of neuronal activity that lack in spatial and temporal resolution. It possible that our particular methodology and experimental set up is not sensitive enough to resolve the small but perhaps biologically relevant increase in URX activity in *acox-1* mutants treated with Triacsin C. Of particular relevance to this study, the electrophysical properties of neurons cannot easily be interpreted from GCaMP recordings. Our model suggest that ACOX-1 may influence body cavity neuron activity in a mechanism involving EGL-2 potassium channels. Potassium channels play significant roles in shaping the frequency, duration and firing pattern of action potentials and it is not entirely clear how these properties are reflected at the level of Ca^{2+} dynamics. To clarify the influence of fatty acyl-CoAs on URX neurons, it will be necessary to use alternative reporters of URX neuronal activity. Body cavity neurons are peptidergic neurons as it has

been reported that activity of these neurons can be assessed by monitoring the secretion of fluorescently-tagged neuropeptides[107]. This read-out may offer a more physiologically representative and sensitive measure of URX activity.

Our data supports a model in which loss of ACOX-1 leads to the generation of a metabolic signal derived from a fatty acyl-CoA that regulates the activity of the URX body cavity neuron in an EGL-2 dependent manner. In turn, this circuit modulates the excitability of serotonergic circuits to link internal metabolic information with behavioral responses.

Discussion

Animals adopt distinct behavioral and physiological states in response to changes in internal metabolic status. In this study, we show that peripherally generated signals act to modulate neurally regulated processes in *C. elegans*. Specifically, we found that loss of an intestinal peroxisomal acyl-CoA oxidase leads to the production of interoceptive signals of metabolic status that modulate serotonergic regulation of feeding and egg laying. These signals are generated when acyl-CoAs that would normally be destined for peroxisomal β-oxidation via ACOX-1 are redirected into other pathways resulting in a vast change to the animal's metabolome despite a very modest transcriptional effect. Moreover, we found that the metabolic changes in the periphery affect the activity of a specific neuron, URX, a ring neuron that is anatomically well positioned to sense peripheral signals. A change in the activity of URX dampens the effects of elevated serotonin signaling on feeding and egg laying. The precise mechanisms by which URX neurons intersect with serotonergic circuits of feeding and egg-laying remain to be determined.

Our genetic and pharmacological analyses suggest that the feeding regulatory response begins with an accumulation of a fatty acyl-CoA species. Physiological condition in which generation of acyl-CoAs exceeds their utilization predicted to occur during periods of nutrient excess, thus the feeding reducing effects of these signals are consistent with satiety-like signals. In mammals, pharmacologic or dietary manipulations that lead to elevated circulating fatty acyl-CoA levels inhibit food intake [112,113]. Fatty acyl-CoAs are short-lived species that are substrates for numerous enzymatic pathways and it is unclear in mammals whether the anorectic effect is mediated directly by specific fatty acyl-CoAs or downstream metabolic derivatives [114]. While we could not measure an obvious increase in acyl-CoA pools extracted from *acox-1* mutants, our metabolomic analyses revealed many hundreds of differentially expressed features in *acox-1* mutants, the majority of which remain structurally unidentified. The enormous metabolomic change made it unrealistic for us to pinpoint the precise metabolic species that underlies the effects of loss of *acox-1* on serotonergic signaling. Nevertheless, our metabolomics analyses revealed several classes of compounds including a variety of phospholipid species that may underlie the noted behavioral changes. Several *N*-acylethanolamines have well-known effects on mammalian feeding behavior and mood [79,115–118]. Their identification here highlighting the deep evolutionary origins of the links between metabolic state and neural mechanism that influence behavior.

We found that body cavity neurons, most prominently URX, serve as key components of the sensory circuit linking peripheral metabolic information with feeding behavior. Body cavity neurons are known to regulate oxygen sensing and social aggregation behaviors though to our knowledge they have not been implicated in

regulation of pharyngeal pumping [109,111,119,120]. Given their unique anatomical placement, these neurons have long been hypothesized to facilitate bi-directional communication between the nervous system and peripheral tissues, particularly in the context of energy homeostasis. Several lines of evidence, in addition to our findings, offer experimental credence to this hypothesis. First, these neurons are in direct synaptic contact with environment sensing neurons like ADF and release modulatory signals to influence peripheral processes such as body growth, lifespan control and lipid metabolism [103,107,121,122]. Second, these neurons have the capacity to sense internal metabolic cues and integrate this information with external cues of nutrient availability to orchestrate cohesive and context-appropriate physiological responses [103]. Lastly, our data and a recent study suggest that internal nutrient sensing pathways modulate the activity of these neurons to regulate nutrient-dependent behavioral states [123]. Skora *et al.* suggest that prolonged nutrient deprivation increases the activity of URX neurons to control starvation-induced quiescence behaviors in a mechanism that involves DAF-2/IGF signaling. This data complements our findings and suggests that states of nutrient excess and nutrient deprivation have inverse effects on URX activity.

An important future challenge is to determine how the vast metabolic changes in the periphery are sensed by the body cavity neurons including URX. In principle, it is possible that some of the peripheral metabolites leave their intestinal sites of generation to directly act on the URX neurons. Alternatively, it is possible that an endocrine response originating in the intestinal cells communicates the metabolic status of the intestine to the URX neurons. Regardless of which model may ultimately be valid, our findings point to *egl-2* as a modulator of URX activity. EGL-2 is a *C. elegans* potassium channel with close

homology to human ether-a-go-go related channels [99,124]. While mammalian EAG channels have not yet been implicated in the control of nutrient-dependent behavioral plasticity, numerous potassium channels have well-documented roles in metabolic sensing and energy homeostasis. For example, hypothalamic Kir6.2 K_{ATP} channels are responsive to circulating glucose levels and regulate appetite and glucose homeostasis [125–127]. Ketogenic diets, which increase circulating ketone body levels, have been shown to suppress the excitability of GABAergic neurons and reduce seizure susceptibility in a K_{ATP} channel dependent manner [128–130]. Numerous metabolites including phospholipids, polyunsaturated fatty acids, eicosanoids, fatty acyl-CoAs and oxygen can directly bind certain potassium channels to modulate channel activity [131–133]. Alternatively, metabolic information can be coupled to potassium channels by indirect signaling events involving second messengers like Ca^{2+} and cAMP, neurotransmitters or post-transcriptional modifications [134,135].

In both mammals and *C. elegans*, elevating serotonin signaling is associated with fat loss [19,34,35,136]. In mammals, this has been primarily attributed to the anorectic effects of serotonin. By contrast, detailed analysis of serotonergic effects in *C. elegans*, revealed that distinct molecular mechanisms underlie the fat and feeding effects of serotonin and that serotonin induced fat reduction in *C. elegans* is primarily driven by upregulation of peripheral mechanisms of triglyceride lipolysis and β-oxidation [19,32,33]. Although it is general overshadowed by the feeding behavioral data, the existing data indicate that serotonin also causes an increase in metabolic rate and increase fat oxidation in mammals [31,137–139]. In this study, we found that if β-oxidation pathways cannot utilize the influx of acyl-CoAs that are generated upon mobilizing stored

triglycerides, a homeostatic signal is generated to blunt serotonergic effects, including effects on feeding. The complexity of the mammalian fat and feeding pathways has made it difficult to pinpoint the precise mechanisms through which serotonin levels act as satiety signals. Our findings raise the possibility that in both worms and mammals, increasing serotonin signaling may result in peripheral metabolic changes that, in turn, feedback to the nervous system to modulate food intake.

Materials and Methods

Worm Strains and General Maintenance

C. elegans strains were cultured under standard growth conditions [140]. The Bristol N2 strain was used as wildtype in all experiments and the following mutant alleles and transgenic strains were analyzed: *acox-1(ok2257), aak-2(ok524), egl-2(rg4), egl-2(n2656), daf-22(m130),* CX10386 *kyEx2491*[*gcy-36::pkc-1*(gf)::SL2::GFP; *ofm-1::dsRed*], SSR1070 *flp-8::mCherry; flp-8::GCaMP5k*. When generating double mutants, genotypes were confirmed by PCR or sequencing. Unless stated otherwise, animals were cultured on NGM agar plates with OP50 *E. coli* at 20^{o}C. For all experiments, worms were plated as synchronized L1 populations after hypochlorite treatment of gravid adults.

Plasmid construction and transgenesis

Plasmids were constructed using Gateway Cloning Technology (Life Technologies). Promoter regions were amplified from wildtype genomic DNA using Phusion DNA polymerase (New England Biolabs) and sub-cloned into the pDONR-P4-P1R Gateway entry vector by BP recombination. Unless otherwise specified, primers pairs were designed based on Promoterome recommendations. For *acox-1* tissue specific rescue

lines, full *F08A8.1* genomic coding sequence was amplified from wildtype genomic DNA was subsequently sub-cloned into the P221 Gateway entry vector by BP recombination. Transgenic animals were generated by injecting purified plasmids into the gonads of wildtype or mutant animals. Transgenes and an *unc-122*::*gfp* co-injection marker were injected at a concentration of 50 ng/µl. At least two independent and stably expressing lines were maintained and analyzed.

Serotonin, Fluoxetine, Oleic Acid and Triacsin C Treatments

Stock solutions of serotonin hydrochloride (TCI America, S0370) and fluoxetine hydrochloride (Matrix Scientific, 047891) were prepared in water. For feeding experiments, synchronized L1 animals were grown on OP50 plates containing 5mM serotonin and assayed at the day 1 adult stage. To determine egg-laying responses, animals were exposed to 0.5mg/mL fluoxetine in M9 buffer or 5mg/mL serotonin in M9 buffer for 20 minutes prior to counting released eggs. Oleic acid and Triacsin C treatments were conducted as previously described [19]. Briefly, Oleic Acid (Sigma-Aldrich, O1383) was solubilized in 45% (w/v in dH_2O) 2-hydroxypropyl-ß-cyclodextrin (Sigma-Aldrich, H5784) to 1M, and then added to OP50 plates to a final concentration of 1µM. Triacsin C (Enzo Life Sciences, BML-EI218) was solubilized in DMSO and used at 1µM on OP50 plates.

Pharyngeal Pumping

Contractions of the posterior pharyngeal bulb were counted during a 10 second interval as previously described [19]. For measurements on fasted then refed animals, ad-libitum fed day 1 adults were washed 3 times in S-basal buffer to remove residual E. coli and subsequently placed on sterile NGM plates. Animals were fasted on plate for the indicated

time then transferred to either vehicle (OP50 *E. coli*) or treatment (5mM serotonin + OP50) containing plates for 90 minutes to assay post-fast feeding responses.

RNAi Treatment

Overnight cultures of HT115 *E. coli* containing RNAi plasmids were induced with 6mM IPTG for 4 hours at 37°C. Cultures were concentrated 2X and added to RNAi plates containing IPTG, carbenicillin, and tetracyclin. Synchronized L1 animals were added to plates and grown for 3 days at 20°C and assayed as day 1 adults.

Microscopy

Animals were mounted on 2% agarose pads, paralyzed with NaN_3 and imaged using a Zeiss Axioplan 2 microscope with a 16X (0.55 NA) oil immersion objective. DIC images of eggs retained *in utero* were acquired from animals at the Day 1 adult stage.

Acyl-CoA Quantification

We adapted an HPLC-based acyl-CoA extraction, derivatization and quantification protocol from Larson et al., 2008 [62]. Briefly, 15,000 synchronized L1s were grown in liquid S-medium culture at 20°C on a rotary shaker. Animals were grown to the L4 stage and washed 3X in S-Basal then snap frozen in liquid nitrogen and stored at -80°C until further processing. To prepare lysates, pellets were thawed on ice and resuspended in 300µL of freshly prepared extraction buffer (2mL 2-propanol, 2mL pH 7.2 50mM KH_2PO_4, 50µL glacial acetic acid, 80µL 50mg/ml BSA). ~500 mg of zirconium oxide beads (NextAdvance, 0.5 mm diameter, 5.5 g/ml) were added to each sample and animals were lysed using a bead beater (5 cycles - 30s ON, 1 min OFF) at 4 °C. Lysates were separated from beads by pipet and an aliquot was preserved for protein quantification (Bio-Rad, DC

Protein Assay). Lysates were then washed of lipids and pigments in 200µL petroleum ether (40-60°C) saturated 1:1 with 2 propanol:water. 5µL of saturated $(NH_4)_2SO_4$ was added to samples before extracting acyl-CoAs with 600µL 2:1 methanol:chloroform. Samples were vortexed and incubated at room temperature for 30 minutes before centrifugation. Supernatants were transferred to glass tubes and dried at 40°C in a GeneVac (~2hrs). Once dry, samples were reconstituted in 55µL of chloroacetaldehyde derivatizing reagent (0.15 M sodium citrate, 0.5% SDS (w/v), 0.5 M chloroacetaldehyde, pH 4) and incubated in an 80°C water bath for 20 minutes. Samples were again clarified by centrifugation, before being transferred to HPLC sample tubes. 20µL of each sample was injected into an equilibrated C18 reversed-phase HPLC column (Phenomenex Luna, 4.6 mm x 150 mm, 5 µm silica particle, 100 Å pore size). A linear gradient of 0.25% (v/v) triethylamine in water and 90% (v/v) acetonitrile in water at a 0.5mL/min flow rate was used to elute acyl-CoAs. Full elution protocol described in [62]. Derivatized acyl-CoAs were detected using a fluorimeter with flash rate 100Hz and with excitation wavelength at 230nM, emission wavelength at 420nM and slid width at 20nM. Peak areas were integrated and quantified using Agilent ChemStation software.

RNA-Seq Sample Preparation

Total RNA was extracted from ~10,000 synchronized L4 animals using the standard Trizol, chloroform, isopropanol protocol with on-column DNAse digest. Sample quality and quantity were assessed on the Agilent Bioanalyzer using RNA 600 Nano chips and only samples with RIN score ≥9 were used for library construction. mRNA was enriched from 1µg of total RNA using NEXTflex™ Poly(A) Beads (Bioo Scientific, NOVA-512979) and strand-specific directional libraries were generated using the NEXTflex™ Rapid

Directional RNA-Seq Kit (Bioo Scientific). For each genotype, samples were prepared from 3 biological replicates and indexed with distinct barcodes. Quality and fragment size distribution of synthesized cDNA libraries were assessed on the Agilent Bioanalyzer using DNA 1000 chips. Library concentrations were quantified using the NEBNext Library Quant Kit (E7630S) and each library was normalized to 10nM in TE buffer prior to pooling. Multiplexed libraries were sequenced using 100bp pair-end reads on the Illumina HiSeq 4000 platform at the UCSF Center for Advanced Technologies.

RNA-Seq Analysis

Transcriptomic analyses were performed on the Galaxy Platform [141]. Sequencing reads were filtered and trimmed to remove barcode sequence using fastx_trimmer (http://hannonlab.cshl.edu/fastx_toolkit/). Clipped paired-end sequences were aligned to the *C. elegans* ce11 reference genome using TopHat version 2.1.1 [142]. Read counts for each gene were quantified using *htseq-count* based on gene annotations from reference annotation WS235 [143]. Differential expression analysis was conducted using the DESeq2 package (3.8) in R(3.4.1) using size factor normalization [144]. P-values were adjusted for multiple comparisons using the Benjamini-Hochberg method and a permissive false discovery threshold of $q \leq 0.1$ was applied to identify differentially expressed transcripts.

Metabolomic sample preparation

Mixed stage worms were grown in liquid and fed OP50 on days 1, 3 and 5 during the 7-day culture period, while shaking at 22 °C and 220 rpm. The cultures were centrifuged at 4 °C, and worm pellets and supernatant were frozen separately, lyophilized, and each extracted with 35 mL of 95% ethanol at room temperature for 12 h. The extracts were

dried *in vacuo*, resuspended in 200µL methanol, and analyzed by LC-HRMS. All cultures were grown in at least three biological replicates.

Mass spectrometric analysis

LC-MS analysis was performed on a Dionex 3000 UHPLC coupled with a ThermoFisher Q Exactive high-resolution mass spectrometer. Metabolites were separated using a water–acetonitrile gradient on Agilent Zorbax Eclipse XDB-C18 column (150 mm x 2.1 mm, particle size 1.8 µm) maintained at 40 °C. Solvent A: 0.1% formic acid in water; Solvent B: 0.1% formic acid in acetonitrile. The solvent gradient started at 5% B for 5 min after injection and increased linearly to 100% B at 12.5 min, and continued at 100% B for 5 min. The gradient was rapidly brought down to 5% B (over 30s) and held for 2 min for re-equilibration.

The UHPLC-MS data were collected in the profile MS mode, based on instrument specifications. Metabolites were detected as $[M-H]^-$ ions or $[M+Cl]^-$ adducts in the negative ionization mode (ESI+), or as $[M+H]^+$ ions or $[M+Na]^+$ adducts in the positive ionization mode (ESI+), using a spray voltage of 3 kV. Compound identities were confirmed based on their high-resolution masses (accuracy < 1 ppm), MS/MS fragmentation spectra, and/or comparison with authentic standards. Data analysis was carried out using the Bioconductor package XCMS [66,145]. The matched filter algorithm in XCMS for peak picking in the profile data was used.

GCaMP Calcium Imaging

Animals were exposed to different oxygen concentration (10% or 21%) using a microfluidic chamber constructed with the oxygen-permeable poly(dimethylsiloxane) (PDMS) as described [106]. A Valvebank II (AutoMate Scientific, Inc.) was used to control

input from two pressurized pre-mixtures of oxygen and nitrogen containing either 10% oxygen or 21% oxygen (Praxair, Inc.). The gas flow rate was measured by a VWRTM traceable pressure meter and set to 0.26 psi. At the time of experiment, an individual day 1 adult animal was picked without using any food and consecutively transferred to two unseeded plates immediately before imaging. The transferred animal was immobilized in S basal containing 5 mM levamisole and transported into the microfluidic chamber via Tygon tubing (Norton). To avoid drying, the animal was constantly submerged in S-Basal buffer while inside the chamber and GCaMP5K fluorescence was visualized at 40x magnification using a spinning disk confocal microscope (Olympus) with MetaMorphTM software (version 6.3r7, Molecular Devices). As described earlier, worms were pre-exposed to 10% oxygen for 5 min in the microfluidic chamber [106]. GCaMP5K fluorescence was recorded by stream acquisition for 2 min at a rate of 8.34 frames/second, with an exposure time of 20ms using a 12-bit Hamamatsu ORCA-ER digital camera. Each animal was recorded once, and GCaMP5K-expressing neurons were marked by a region of interest (ROI). The change in fluorescent intensity as per neuronal excitation and position of the ROI was tracked using the “Track Objects” function in MetaMorphTM. To subtract background from the total integrated fluorescence intensity of the ROI, an adjacent ROI was selected in the same image. MATLAB (MathWorks,Inc.) was used to analyze the data. Fluorescence intensity is presented as the percent change in fluorescence relative to the baseline ($\Delta F/F0$). F0 was measured in worms exposed to 10% oxygen during the first 9-13 seconds for each recording and calculated as an average over that period. The number of animals used for each condition is denoted in the figures.

Statistics

Graphpad Prism 8.0 software package was used to calculate all p-values unless otherwise specified. Where only 2 conditions were compared, a two-tailed students t-test was performed. ANOVAs with appropriate post-test corrections were used when comparing multiple conditions.

Acknowledgements

We thank the *Caenorhabditis* Genetics Center (CGC), which is funded by the NIH Office of Research Infrastructure Programs (P40 OD010440), for providing some of the strains used in this study. We also thank the De Bono lab for sharing the *gcy-32*::*egl-2*(gf) construct and the Bargmann Lab for the generous gift of the CX10386 strain. Lastly, we thank George Lemieux for helpful advice and discussion and members of the Ashrafi lab for comments on the manuscript.

Figure 1

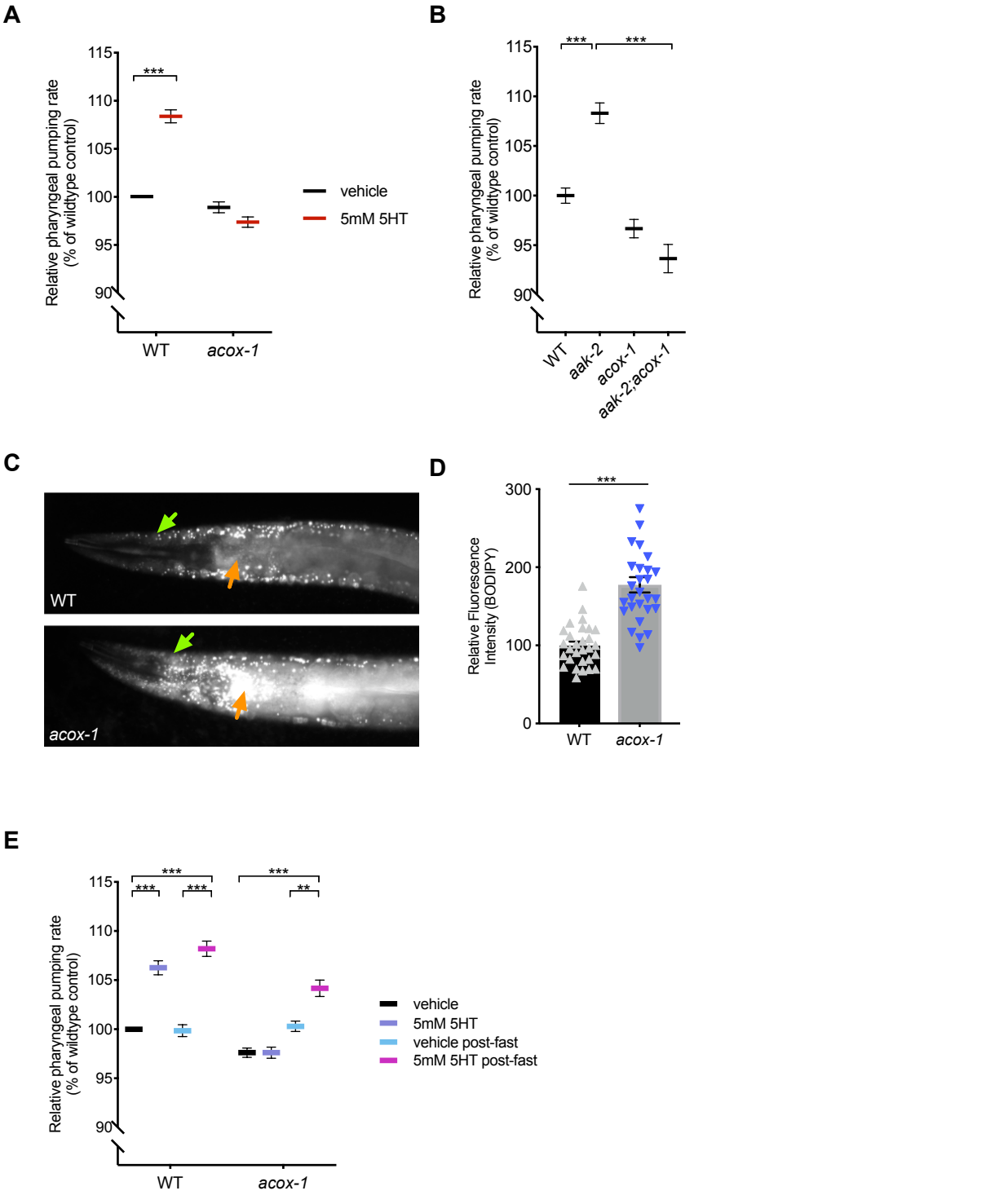
A
Relative pharyngeal pumping rate (% of wildtype control)
115
110
105
100
95
90
***
WT
acox-1
vehicle
5mM 5HT
B
Relative pharyngeal pumping rate (% of wildtype control)
***
***
WT
aak-2
acox-1
aak-2;acox-1
C
WT
acox-1
D
Relative Fluorescence Intensity (BODIPY)
300
200
100
0
***
WT
acox-1
E
Relative pharyngeal pumping rate (% of wildtype control)
***
***
***
***
**
WT
acox-1
vehicle
5mM 5HT
vehicle post-fast
5mM 5HT post-fast

Figure 2.1. *acox-1* mutants are insensitive to the feeding stimulatory effects of serotonin

(A) *acox-1(ok2257)* mutants are resistant to pharyngeal pumping increasing effects of 5mM serotonin. All feeding data is expressed as a percentage of vehicle treated wildtype animals. (B) Loss of *acox-1* suppresses the elevated feeding rates of *aak-2* animals. In both (A) and (B) error bars indicate +/- SEM from mean, n = 50 animals per strain. *** $p < 0.0001$ ANOVA (Tukey) (C - D) *acox-1* mutants accumulate significantly more fat than wildtype animals as assessed by hypodermal (green arrows) and intestinal (orange arrows) BODIPY fluorescence levels. Representative images of BODIPY staining (C) and corresponding quantifications of hypodermal BODIPY fluorescence levels (D) *** $p<0.001$, students t-test. (E) Fasting *acox-1* mutants for 90 minutes restores their ability to elevate feeding in response to 5mM serotonin. Day 1 adult animals were either fed *ad-libitum* or fasted for 90 minutes than plated on vehicle or 5mM 5HT plates for 60 minutes before assessing pharyngeal pumping rates. Error bars indicate +/- SEM from mean, n = 15 animals per condition. ** $p < 0.01$, *** $p < 0.001$ ANOVA (Tukey).

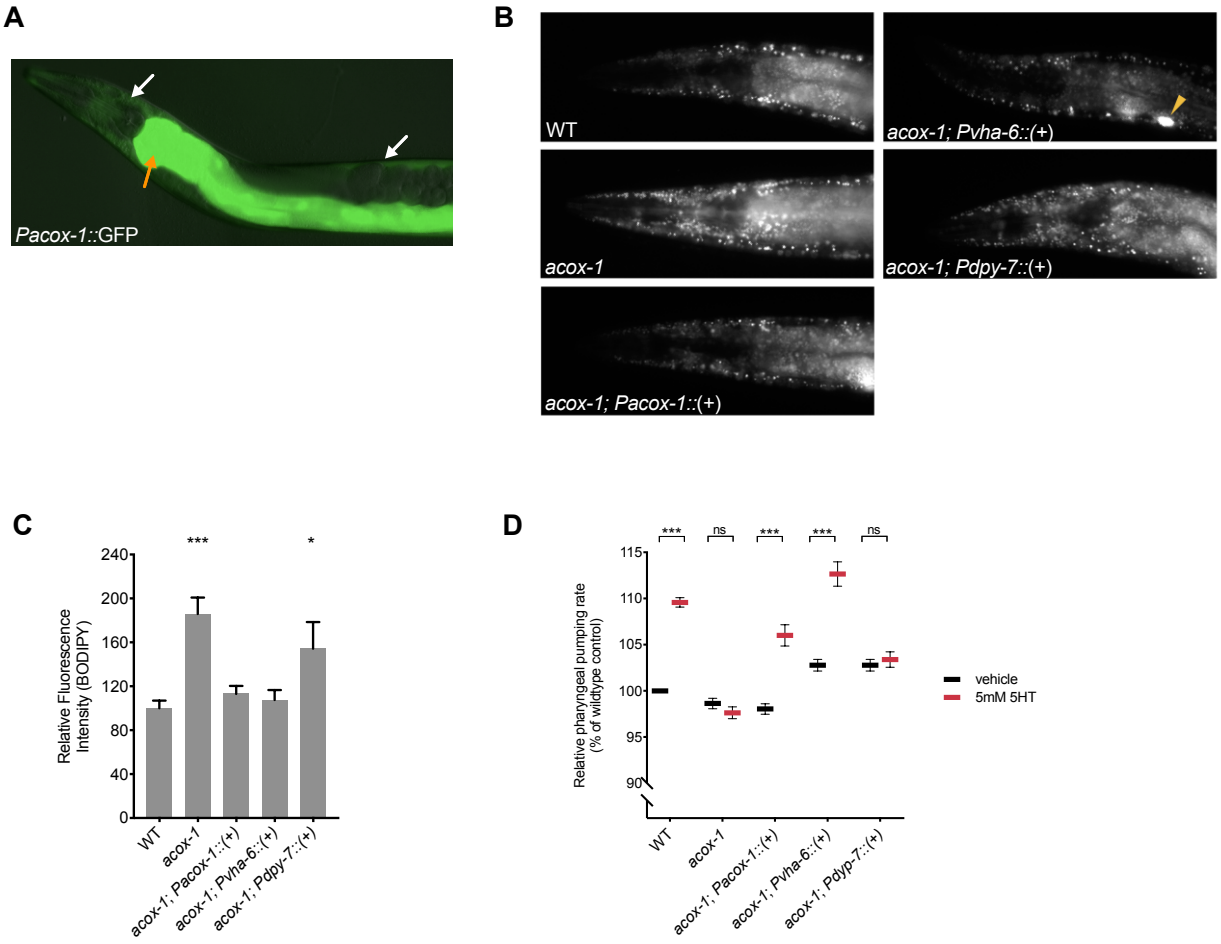

Figure 2.2 Reconstitution of *acox-1* in the intestine rescues fat and feeding phenotypes

(A) *acox-1* is expressed in hypodermal (white arrows) and intestinal (orange arrow) tissues. Merged DIC and green epifluorescent image of a transgenic animal expressing a *acox-1p::gfp* transcriptional reporter. (B-C) Reconstitution of *acox-1* gDNA under its own promoter (*Pacox-1*) and under an intestine specific promoter (*Pvha-6*) but not under a hypodermal-specific promoter (*Pdpy-7*) normalizes BODIPY fat levels. Representative images of BODIPY staining (B) and corresponding quantifications (C) expressed as fluorescence intensity relative to wildtype animals. The yellow arrow in (B) indicates a coelomocyte co-injection marker used during transgenic strain generation. Error bars indicate +/- SEM from mean, n>20 per strain. *p<0.05, ***p<0.001, ANOVA (Tukey) (D) Reconstitution of *acox-1* gDNA under an intestine specific promoter (*Pvha-6*) restores serotonin responsiveness. Relative pharyngeal pumping rates of indicated strains. Error bars indicate +/- SEM from mean, n > 15 per strain. ***p<0.001, ANOVA (Tukey).

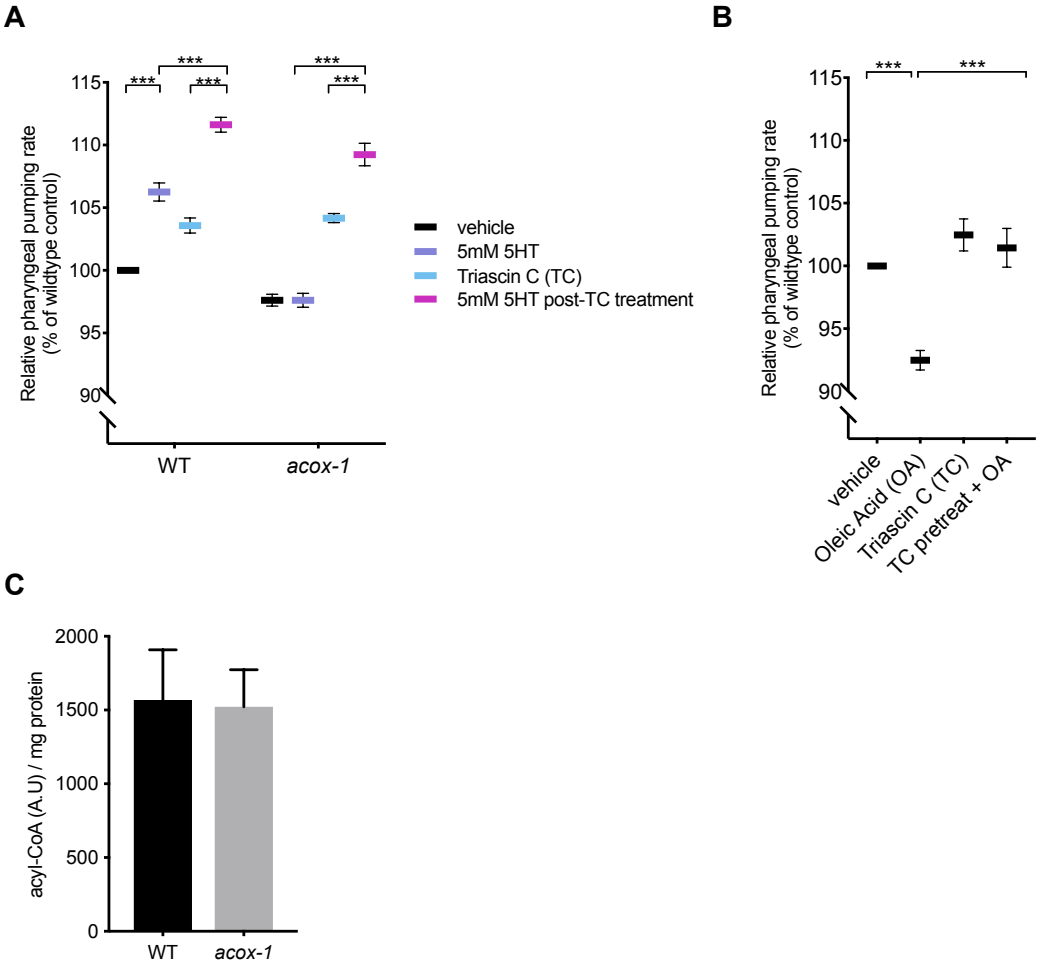

Figure 2.3 Modulation of feeding by ACOX-1 requires fatty acyl-CoA synthesis
(A) Inhibiting acyl-CoA synthesis (ACS) in *acox-1(ok2257)* animals restores the ability to elevate feeding in response to 5mM serotonin. Day 1 adult animals were pre-treated with vehicle or 1µM ACS inhibitor Triacsin C for 90 minutes before being plated on vehicle or 5mM 5HT plates. Feeding was assayed after 60 minutes on assay plates. Error bars indicate +/- SEM from mean, n = 15 animals per condition. ** $p < 0.01$, *** $p < 0.001$ ANOVA (Tukey). (B) Animals were treated with 1mM oleic acid (OA) or 1µM Triacsin C (TC) for one hour, or pre-treated with 1µM TC or one hour prior to OA treatment before feeding was assayed. Error bars indicate +/- SEM from mean, n > 15 per strain. ***p<0.001, ANOVA (Tukey) (C) Acyl-CoA levels in *acox-1* mutants are unchanged relative to WT. Acyl-CoA species were separated and quantified by HPLC and normalized to protein concentrations, n = 3 independent extractions.

Table 2.1: Loss of *acox-1* results in modest transcriptional changes in intestinal and fatty acid metabolic pathways

WormBase ID	Gene Name	log2(FC)	Cellular Process	Putative Function	P-value	Adjusted p-value
UPREGULATED						
WBGene00008681	*scrm-4***	2.50	membrane phospholipids	phospholid scramblase	7.83E-11	1.48E-06
WBGene00019404	*K05B2.4***	1.98	peroxisomal fatty acid metabolism	ortholog of human bile acid-CoA: amino acid N-acyltransferase (BAAT)	1.18E-04	8.71E-02
WBGene00013540	*Y75B8A.3*	1.89	fatty acid metabolism	carboxylic ester hydrolase type B	1.83E-04	1.15E-01
DOWNREGULATED						
WBGene00011487	*T05E12.6***	-1.64	unknown	unknown	5.88E-05	5.83E-02
WBGene00019619	*asp-14***	-1.97	innate immune response	aspartic endopeptidase	3.93E-05	5.54E-02
WBGene00007875	*dod-24***	-2.09	innate immune response	unknown	2.33E-05	3.98E-02
WBGene00009429	*irg-5*	-2.10	innate immune response	unknown	4.51E-05	5.54E-02
WBGene00009773	*lipl-2***	-2.15	fatty acid metabolism	ortholog of human triglyceride Lipase F	2.67E-04	1.36E-01
WBGene00012671	*Y39B6A.9*	-2.17	unknown	unknown	2.24E-04	1.17E-01
WBGene00019368	*K03H6.2***	-2.18	fatty acid metabolism	putative lipase	2.18E-04	1.17E-01
WBGene00001150	*ech-1.1***	-2.18	fatty acid metabolism	enoyl-CoA hydratase, 3-hydroxyacyl-CoA dehydrogenase activity	9.90E-05	8.24E-02
WBGene00014562	*Y17D7B.7*	-2.24	unknown	unknown	4.67E-05	5.54E-02
WBGene00019495	*sdz-24*	-2.28	larval development	SKN-1 dependent zygotic transcript	1.96E-04	1.15E-01
WBGene00007331	*pho-11*	-2.29	metabolic process	ortholog of human acid phosphatase 2	7.81E-06	1.47E-02
WBGene00020560	*T19C3.2*	-2.29	unknown	unknown	1.25E-04	8.75E-02
WBGene00007916	*C34C6.3*	-2.30	unknown	unknown, contains an EGF-like domain	1.90E-04	1.15E-01
WBGene00006636	*tsp-10***	-2.30	unknown	putative tetraspanin	5.29E-05	5.54E-02
WBGene00194708	*Y36E3A.2*	-2.31	membrane biology	unknown	1.20E-04	8.71E-02
WBGene00008584	*irg-4*	-2.32	innate immune response	unknown	2.23E-06	7.00E-03
WBGene00000747	*col-174*	-2.43	structural protein/collagen	collagen	1.04E-04	8.24E-02
WBGene00021337	*Y34F4.2***	-2.47	membrane biology	putative tight-junction/claudin	7.44E-05	7.01E-02
WBGene00008565	*acox-2***	-2.48	peroxisomal fatty acid metabolism	acyl-CoA oxidase	2.64E-06	7.11E-03
WBGene00009904	*F49E12.12*	-2.51	GPI anchor maturation	PGAP2 ortholog	5.07E-05	5.54E-02
WBGene00022375	*Y94H6A.2*	-2.56	unknown	unknown	2.22E-04	1.17E-01
WBGene00008905	*F17B5.1*	-2.61	redox biology	putative thioredoxin	1.47E-04	9.53E-02
WBGene00022730	*ZK402.3*	-2.64	unknown	unknown, contains a SPK domain	4.80E-05	5.54E-02
WBGene00020083	*R57.2***	-2.65	unknown	unknown	1.44E-04	9.53E-02
WBGene00011665	*T09F5.1*	-2.66	protein glycosylation	putative galactosyltransferase	9.29E-05	8.24E-02
WBGene00008564	*acox-1***	-2.74	peroxisomal fatty acid metabolism	acyl-CoA oxidase	2.01E-09	1.26E-05
WBGene00008698	*F11D11.3***	-2.76	innate immune response	putative transmembrane glycoprotein	2.03E-04	1.16E-01
WBGene00022731	*ZK402.5*	-2.86	unknown	unknown, contains a SPK domain	1.05E-04	8.24E-02
WBGene00022156	*Y71G12B.18***	-2.92	unknown	unknown	6.98E-06	1.46E-02
WBGene00015268	*BE0003N10.3*	-2.93	zinc ion binding	unknown	2.78E-07	1.31E-03
WBGene00010102	*F55C9.5***	-3.05	unknown	unknown	3.07E-05	4.82E-02
WBGene00017020	*D1014.7*	-3.26	unknown	unknown	1.27E-06	4.79E-03
WBGene00017019	*D1014.6*	-4.17	protein glycosylation	unknown, putative galactosyltransferase activity	2.57E-10	2.42E-06

** indicates intestinally expressed gene products

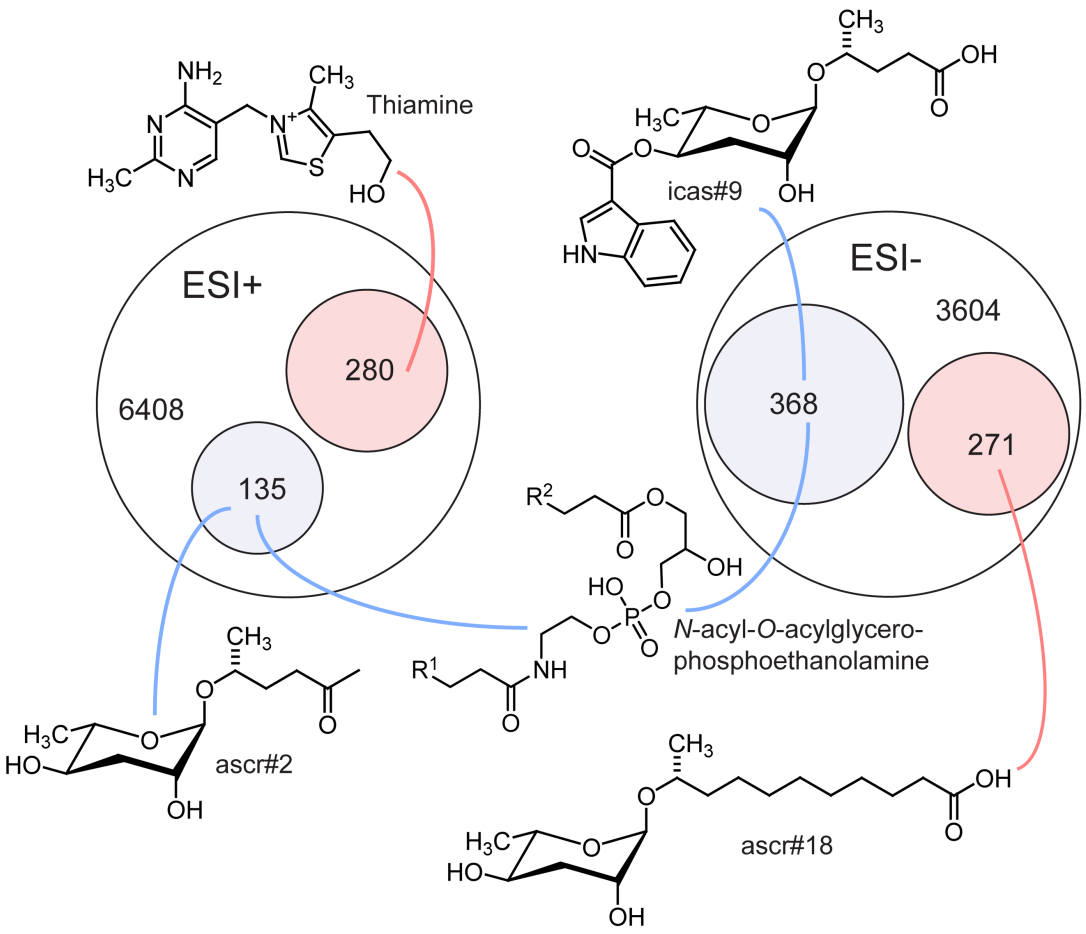

Figure 2.4 Loss of *acox-1* results large-scale changes to the global metabolome Venn diagrams showing total numbers of detected features (6408 and 3604) and numbers of metabolites more than three-fold upregulated (pink) or downregulated (blue) in LC-HRMS using positive-ion (ESI+) and negative-ion (ESI-) electrospray ionization in *acox-1* mutants. Though most differentially detected features were unidentifiable, the chemical structures shown here represent examples of the most significantly up or down regulated compounds in identifiable metabolic classes. See Supplemental Table 1.

Figure 5

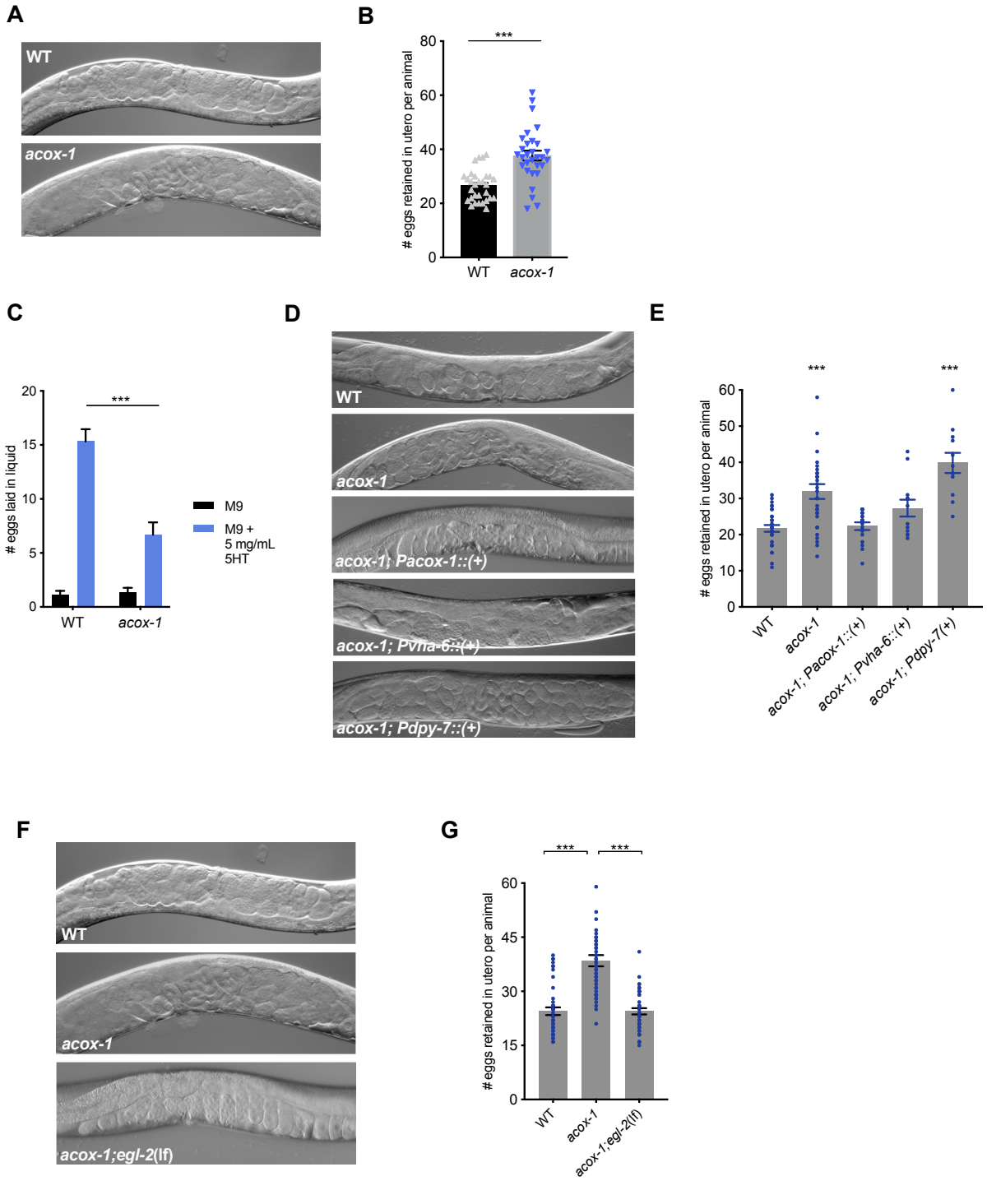
A
WT
acox-1
B
***
eggs retained in utero per animal
0
20
40
60
80
WT
acox-1
C
***
eggs laid in liquid
0
5
10
15
20
WT
acox-1
M9
M9 +
5 mg/mL
5HT
D
WT
acox-1
acox-1; Pacox-1::(+)
acox-1; Pvha-6::(+)
acox-1; Pdpy-7::(+)
E
***
***
eggs retained in utero per animal
0
10
20
30
40
50
60
WT
acox-1
acox-1; Pacox-1::(+)
acox-1; Pvha-6::(+)
acox-1; Pdpy-7(+)
F
WT
acox-1
acox-1;egl-2(lf)
G
***
***
eggs retained in utero per animal
0
15
30
45
60
WT
acox-1
acox-1;egl-2(lf)

Figure 2.5 *acox-1* mutants exhibit egg-laying defects
(A-B*) acox-1*(ok2257) mutants accumulate significantly more eggs *in utero* than wildtype animals. Representative DIC images (A) and quantification (B) of eggs retained *in utero*. Error bars indicate +/- SEM from mean, n = 30 animals per genotype. *** $p < 0.001$ unpaired student's t-test. (C) *acox-1* animals are less responsive to the egg-laying inducing effects of serotonin. Egg-laying response of wildtype and *acox-1* in control buffer (M9) or 5mg/mL serotonin in M9 buffer. Data represents the number of eggs released per animal after a 20-minute exposure to vehicle or drug. Error bars represent +/- SEM from mean. n = 20 animals per condition, *** $p < 0.001$ ANOVA (Sidak) (D-E) Reconstitution of *acox-1* gDNA under an intestine specific promoter (*Pvha-6*) but not a hypodermal specific promoter (*Pdpy-7*) restores egg-laying capacity to *acox-1* mutants. Representative DIC images (D) and quantification (E) of eggs retained *in utero*. Error bars indicate +/- SEM from mean, n = 30 animals per genotype, *** $p < 0.001$ unpaired student's t-test, against a wildtype control. (F-G) Loss of *egl-2* rescues *acox-1* egg-laying defects. Representative DIC images of each genotype (F) and quantification (G) of eggs retained *in utero*. Error bars indicate +/- SEM from mean, n = 30 animals per genotype. *** $p < 0.001$ unpaired student's t-test.

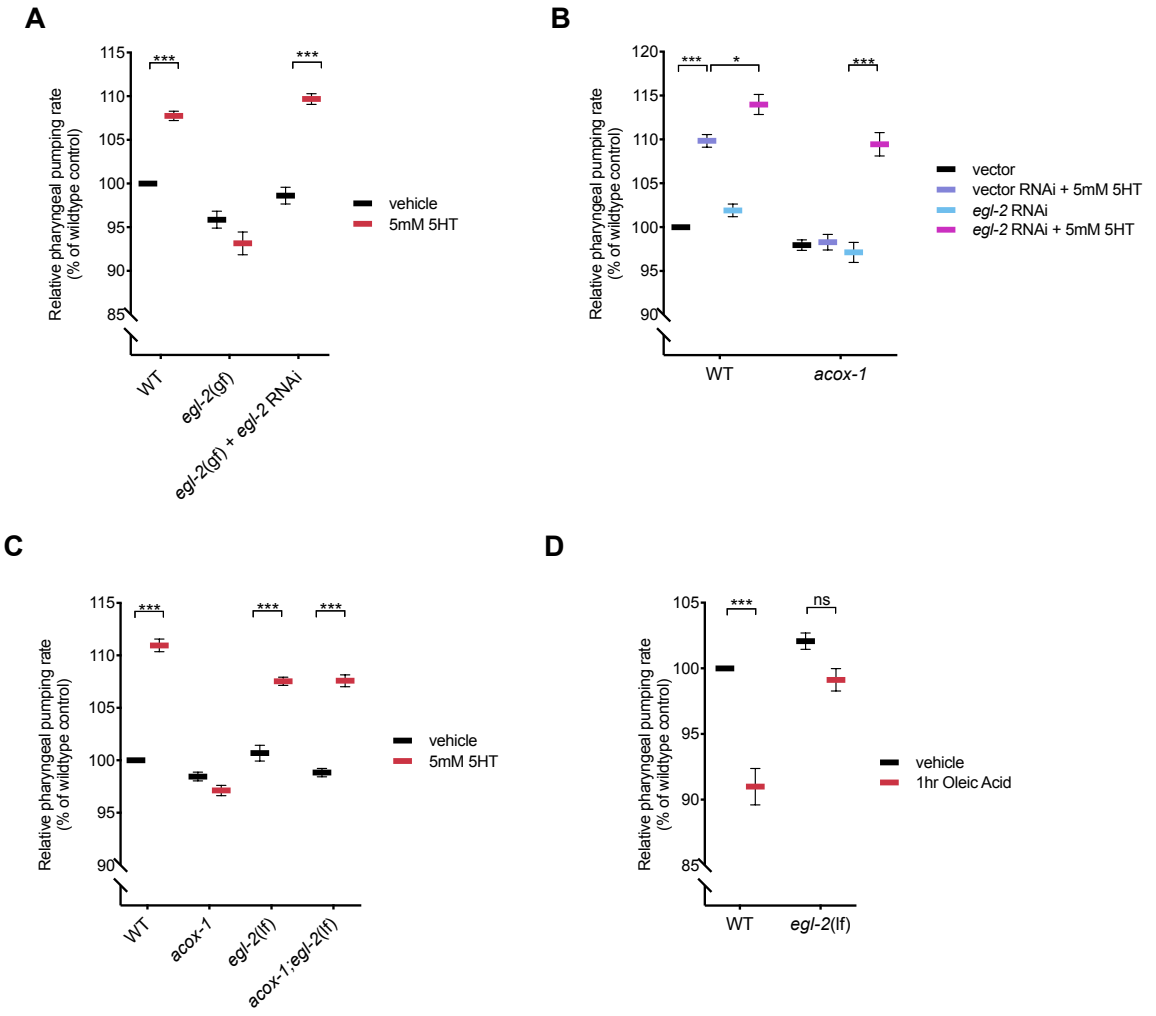

Figure 2.6. ACOX-1-mediated regulation of serotonergic feeding responses requires the EGL-2 K+ channels

(A) Pharyngeal pumping rates of wildtype, *egl-2*(n698), and *egl-2* RNAi treated *egl-2*(n698) mutants on vehicle or 5mM 5HT containing plates. (B) Pharyngeal pumping rates of wildtype and *acox-1(*ok2257) animals treated with vector RNAi or *egl-2* RNAi and vehicle or 5mM 5HT (C) Pharyngeal pumping rates of indicated strains treated with vehicle or 5mM 5HT. Error bars indicate +/- SEM from mean, n=20 animals per condition. *p<0.05, *** p < 0.001, ANOVA (Tukey) (D) EGL-2 is required for animals to reduce feeding in response to oleic acid. Animals were exposed to 1mM Oleic Acid for one hour before feeding was assayed. n> 15 per strain, Error bars indicate +/- SEM from mean, ***p<0.001, ANOVA (Tukey). All feeding data are expressed as a percentage of vehicle treated wildtype animals.

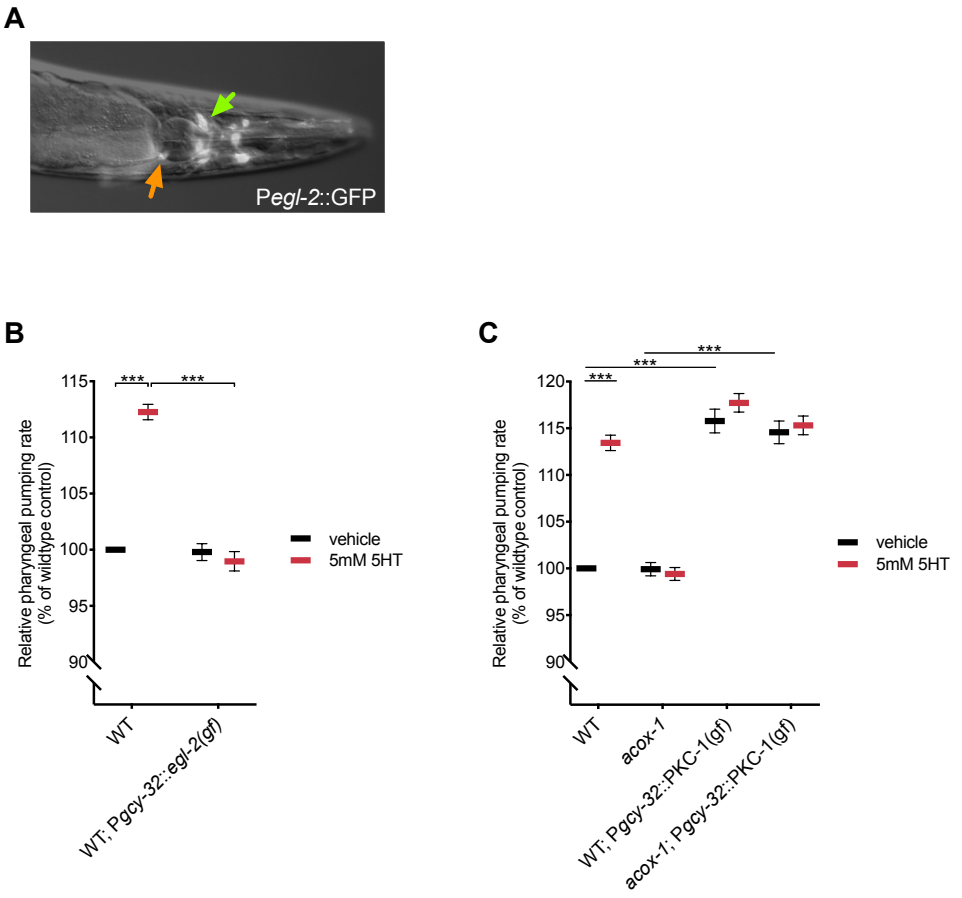

Figure 2.7. Body cavity neurons modulate feeding behavior
(A) EGL-2 is expressed in a limited subset of sensory neurons. Epifluorescent image of a transgenic animal expressing *egl-2p::gfp* transcriptional reporter. Yellow and green arrows indicate the AQR and URX body cavity neurons, respectively. (B) Animals expressing *egl-2*(gf) in body cavity neurons do not elevate feeding in response to 5mM 5HT. Pharyngeal pumping rates of wildtype and *pgcy-32::egl-2*(gf) expressing animals treated vehicle or 5mM 5HT. (C) Constitutive activation of synaptic release from body cavity neurons stimulates feeding. Pharyngeal pumping rates of wildtype, *acox-1*(ok2257), CX10386 *pgcy-32::pkc-1*(gf) and *acox-1;* CX10386 *pgcy-32::pkc-1*(gf) animals on vehicle or 5mM 5-HT. In (B) and (C) data are expressed as a percentage of vehicle treated wildtype animals. Error bars indicate +/- SEM from mean, n=15 animals per condition. *** $p < 0.001$ two way ANOVA (Tukey).

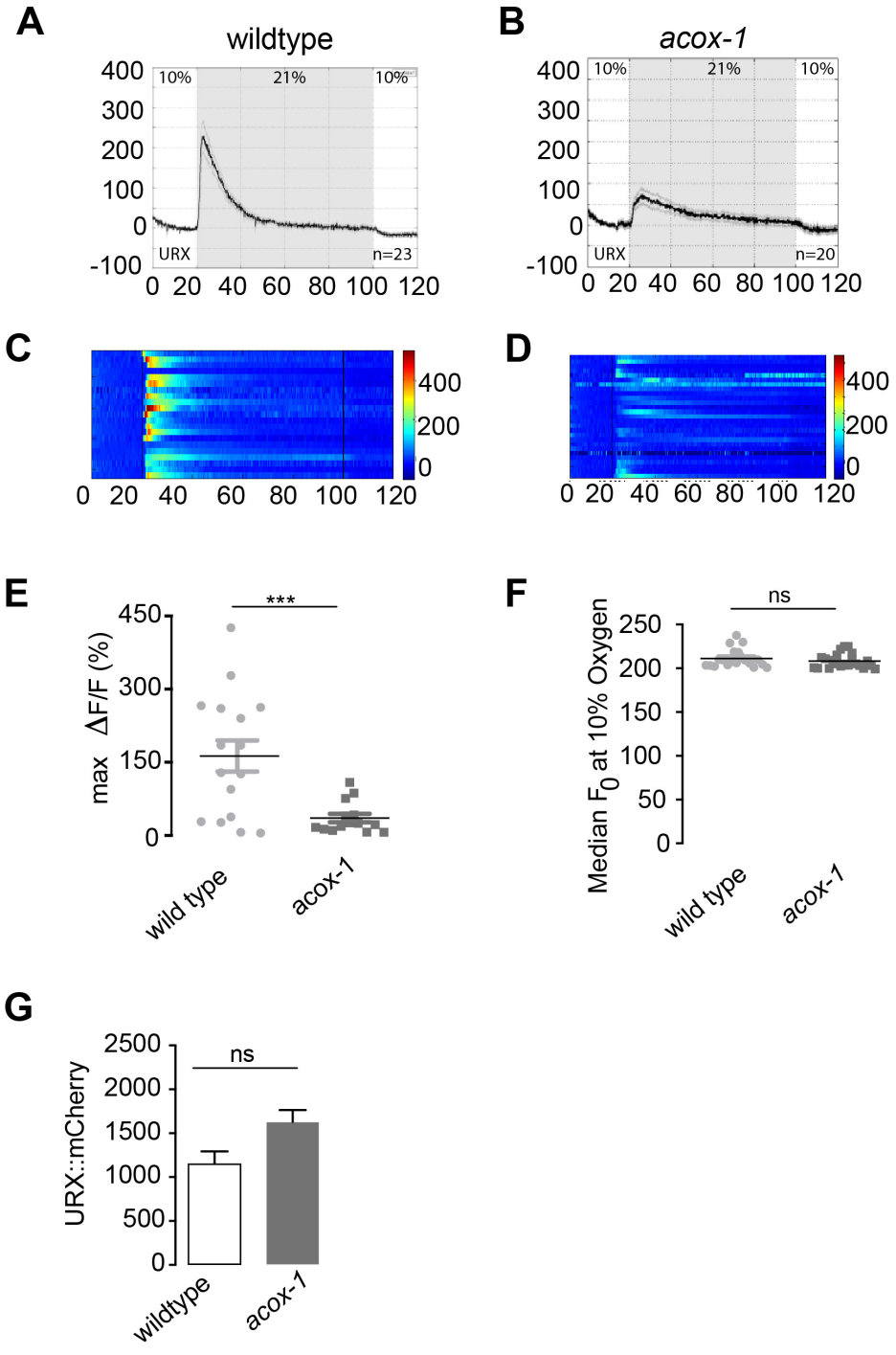
A
wildtype
400
300
200
100
0
-100
10%
21%
10%
URX
n=23
0 20 40 60 80 100 120
B
acox-1
400
300
200
100
0
-100
10%
21%
10%
URX
n=20
0 20 40 60 80 100 120
C
400
200
0
0 20 40 60 80 100 120
D
400
200
0
0 20 40 60 80 100 120
E
***
max ΔF/F (%)
450
300
150
0
wild type
acox-1
F
ns
Median F0 at 10% Oxygen
250
200
150
100
50
0
wild type
acox-1
G
ns
URX::mCherry
2500
2000
1500
1000
500
0
wildtype
acox-1

Figure 2.8 Loss of *acox-1* suppresses URX body cavity neuron activity
(A-D) Activity of URX neurons in each indicated genotype using Ca^{2+} imaging by GCaMP5K under the control of the URX specific *flp-8* promoter. Oxygen concentrations in the microfluidic chamber were 10% and 21% as indicated. (A-B) For each genotype, black traces show the average percent change of GCaMP5k fluorescence ($F\Delta/F_0$) and gray shading indicates SEM. The number of animals used for each condition is shown in the figure. (C-D) Individual URX responses are shown for each genotype; each row represents one animal. (E) Maximal ($F\Delta/F_0$) values are shown for individual animals in wildtype and *acox-1* animals. Bars indicate the average value within each genotype. ***p<0.001 by students t-test. (F) Individual baseline fluorescence (F_0) values at 10% oxygen are shown for individual animals in wildtype and *acox-1* mutants. Bars indicate the median value within each genotype; n.s., not significant by students t-test (G) We imaged mCherry fluorescence in wildtype and *acox*-1 mutant animals expressing both GCaMP5K and mCherry under the control of the *flp-8* promoter. Images were taken in animals exposed to 10% oxygen. For each genotype, the fluorescence intensity was imaged at the same exposure, determined to be within the linear range. Fluorescence intensity was quantified and is expressed as the mean +/- SEM (n = 23). n.s., not significant by students t-test.

Figure S1

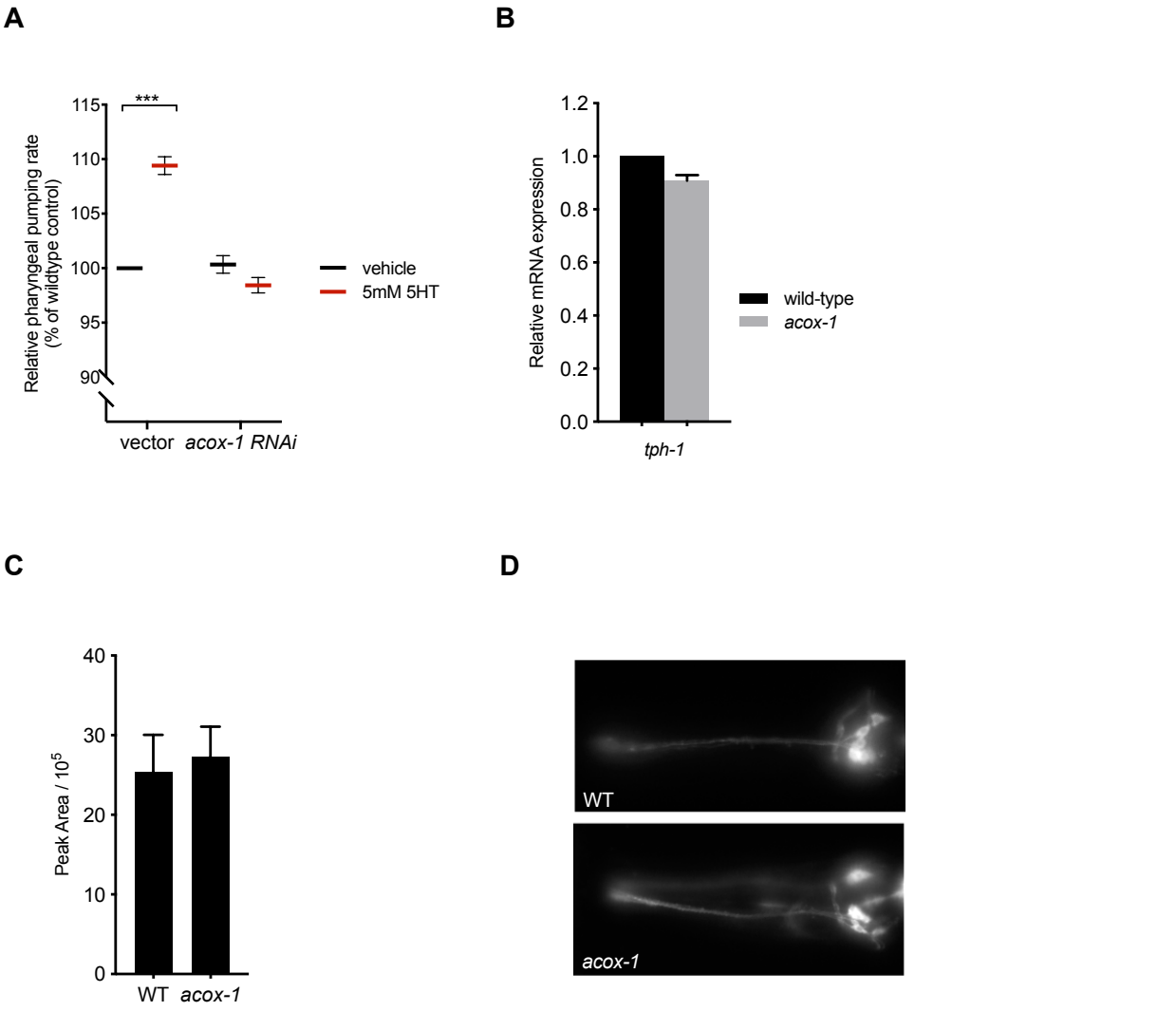

Figure 2.S1, related to Figure 2.1
(A) Knocking down *acox-1(F08A8.1)* by RNAi suppresses the feeding elevating effects of exogenous serotonin (5mM 5HT). Animals were treated with RNAi from L1 stage and feeding was assayed at day 1 adult stage. Feeding data is expressed as a percentage of vehicle treated wildtype animals. Error bars indicate +/- SEM from mean, n = 20 animals per strain. *** $p < 0.001$ ANOVA (Tukey) (B) Loss of *acox-1* does not influence the transcriptional expression of tryptophan hydroxylase (*tph*-1) as measured by qPCR. Error bars indicate +/- SEM from mean n = 3 independent assays (C) Relative abundance of 5-HT in wildtype and *acox-1* mutants, as determined by LC-HRMS. Error bars indicate +/- SEM from mean, n = 4 independent experiments. (D) Loss of *acox-1* does not grossly alter amphid neuron morphology. DiI staining of amphid chemosensory neurons in wildtype and *acox-1* mutants. Images acquired at day 1 adult stage.

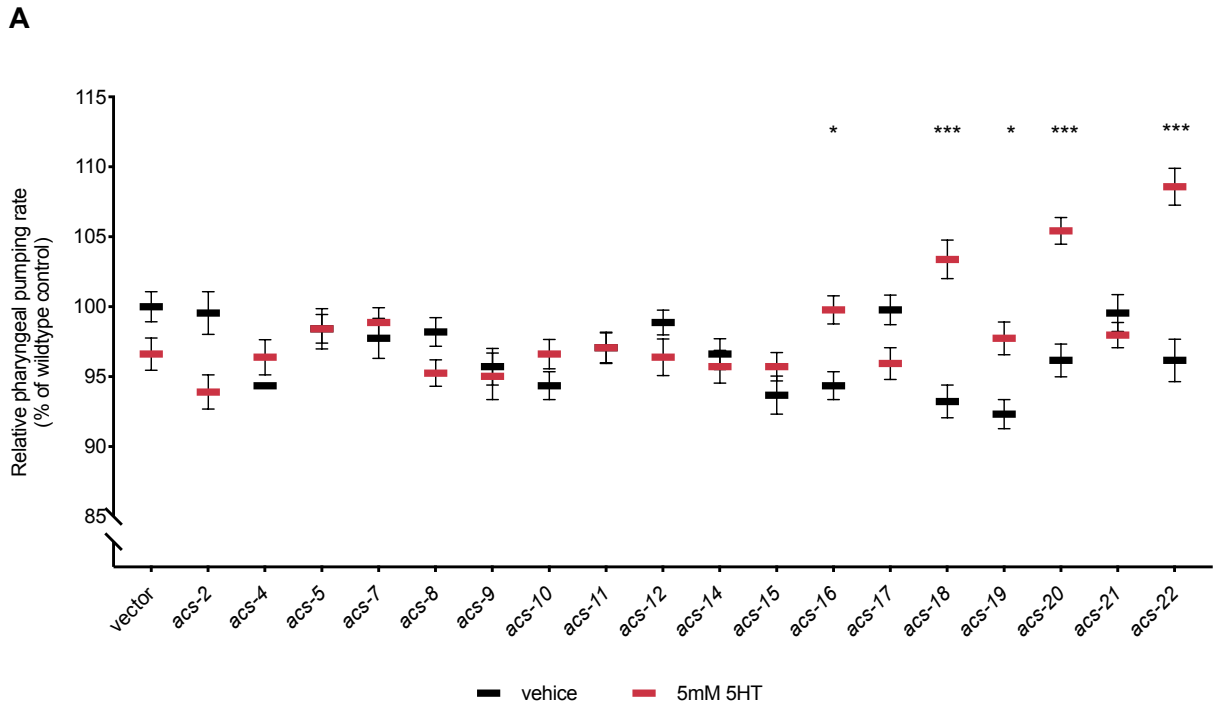

Figure 2.S2, related to Figure 2.3
(A) RNAi-mediated inactivation of distinct acyl-CoA synthases suppress feeding defects in *acox-1(ok2257)* animals. Animals were treated with respective RNAi clones from L1 stage and feeding was assayed at day 1 adult stage. Feeding data is expressed as a percentage of vehicle treated wildtype animals. Error bars indicate +/- SEM from mean, n = 15 animals per strain. *<0.05, *** p < 0.001 two way ANOVA (Tukey).

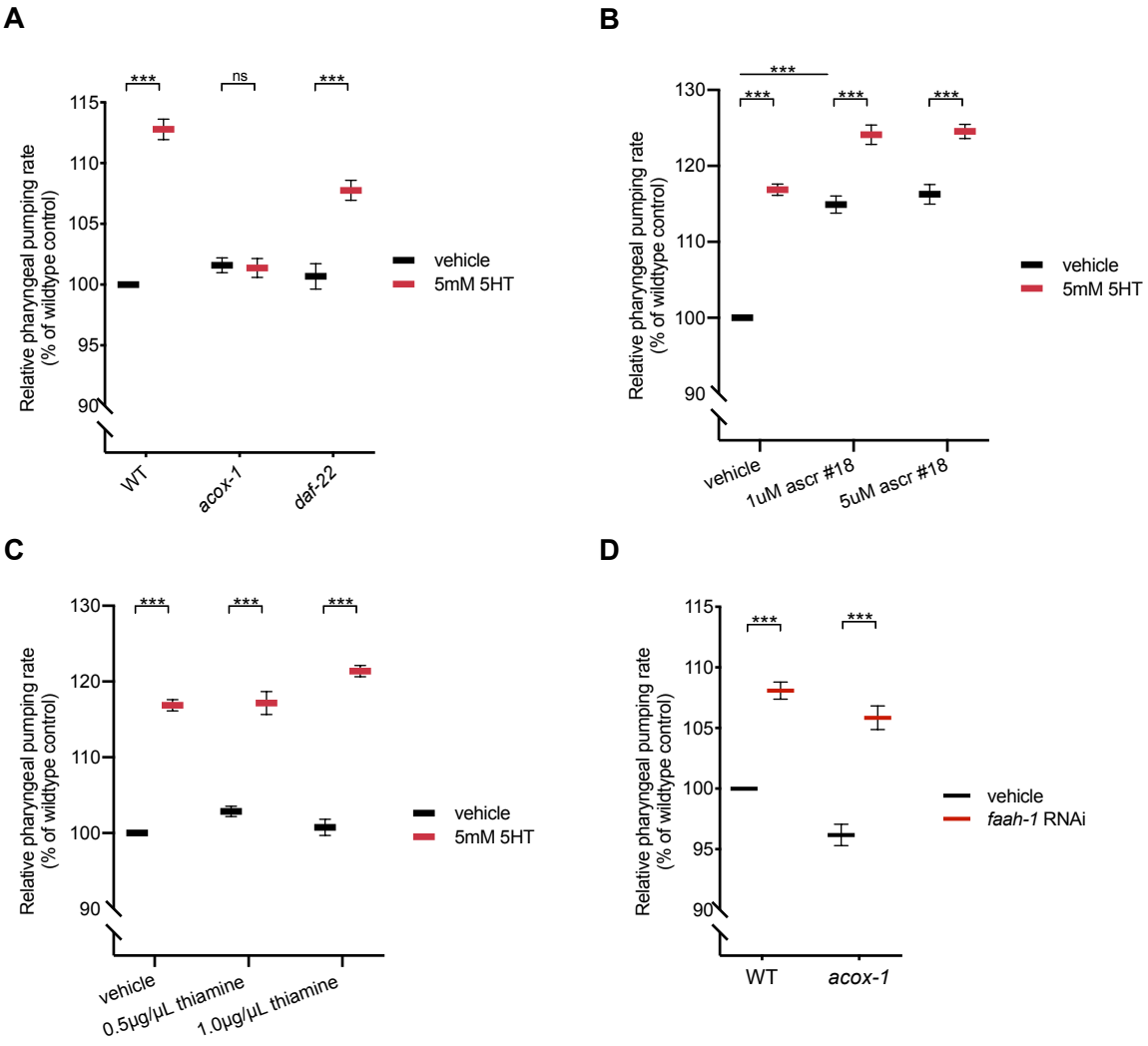

Figure 2.S3, related to Figure 2.4
(A) *daf-22(ok693)* animals are still responsive to the feeding elevating effects of 5mM serotonin. n=10 animals per condition **(B)** Feeding responses of wildtype animals to ascaroside #18 (ascr #18). Animals were exposed to 1µM and 5µM ascr#18 from L1 stage and pharyngeal pumping rates were determined at day 1 adult stage. n = 15 animals per condition **(C)** Feeding responses of wildtype animals to thiamine. Animals were exposed to 0.5 µg/µL thiamine and 1.0 µg/µL thiamine from L1 stage and pharyngeal pumping rates were determined at day 1 adult stage. n = 15 animals per condition **(D)** RNAi-mediated inactivation of fatty acid amide hydrolase (*faah-1*) elevates feeding responses of wildtype and *acox-1* mutants. Animals were grown on *faah-1* RNAi from L1 stage and feeding was assayed at day 1 adult stage. n = 10 animals per condition. All feeding data is expressed as a percentage of vehicle or vector treated wildtype animals. Error bars indicate +/- SEM from mean, *** $p < 0.001$ two way ANOVA (Tukey).

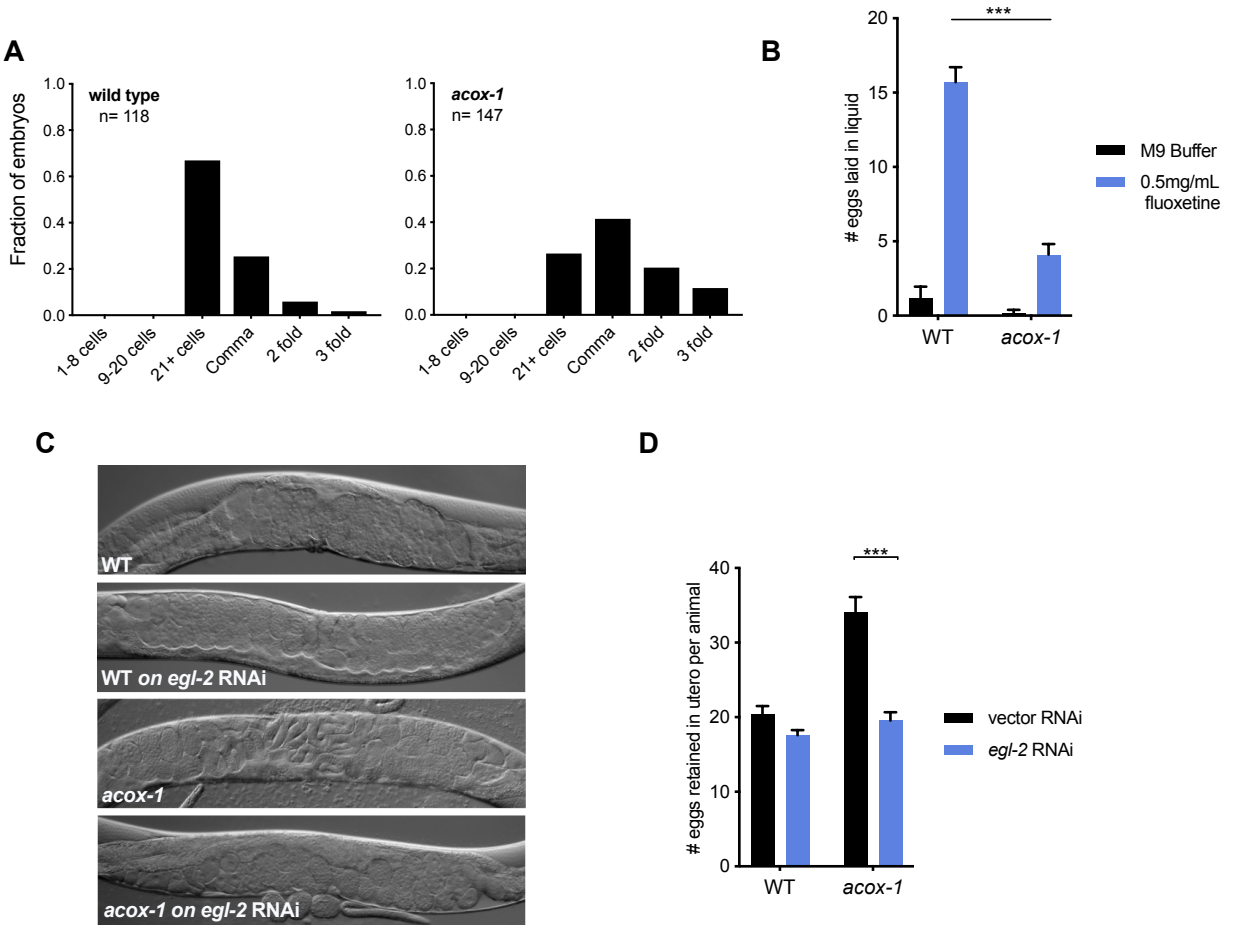

Figure 2.S4, related to Figure 2.5
(A) *acox-1(ok2257)* mutants lay eggs at a later developmental stage that wildtype animals, suggesting that *in utero* retention time is increased. Histograms indicate the distribution of embryos at each developmental stage. (B) *acox-1* mutants are less responsive to the egg-laying inducing effects of serotonin. Egg-laying response of wildtype and *acox-1* mutants in control buffer (M9) or 0.5mg/mL fluoxetine. Data represents the number of eggs released per animal after a 20-minute exposure to vehicle or drug. Error bars represent +/- SEM from mean. n = 15 animals per condition, *** $p < 0.001$ ANOVA (Sidak) (C-D) Inactivation of *egl-2* via RNAi rescues *acox-1* egg-laying defects. Representative DIC images of day 1 adults of each genotype (C) and quantification (D) of eggs retained *in utero*. Error bars indicate +/- SEM from mean, n = 15 animals per genotype. *** $p < 0.001$ unpaired student's t-test.

A

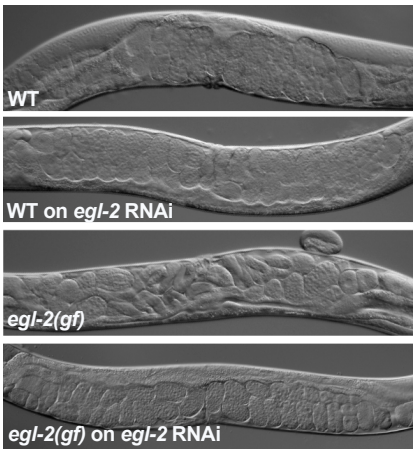

Figure 2.S5, related to Figure 2.6(A) RNAi-mediated knockdown of *egl-2* rescues egg-laying defects associated with aberrant channel activity *egl-2(n698)* mutants. Representative DIC images acquired from day 1 adults.

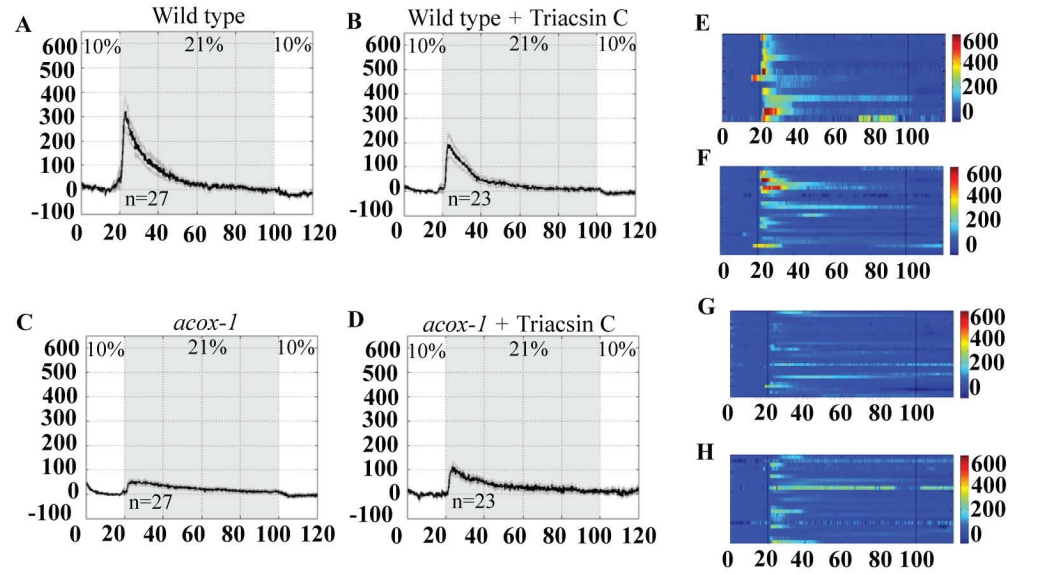
A
Wild type
B
Wild type + Triacsin C
C
acox-1
D
acox-1 + Triacsin C
10%
21%
10%
n=27
n=23
E
F
G
H
600
400
200
0
0 20 40 60 80 100

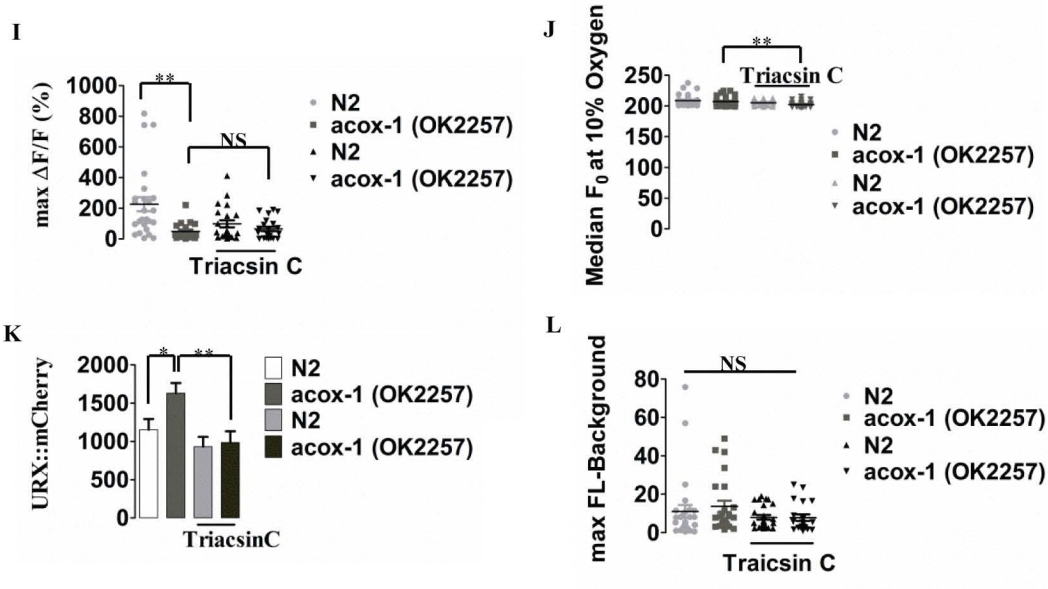
I
max ΔF/F (%)
**
NS
N2
acox-1 (OK2257)
Triacsin C
J
Median F0 at 10% Oxygen
Triacsin C
K
URX::mCherry
*
**
TriacsinC
L
max FL-Background
NS
Traicsin C

Figure 2.S6. Effects of Triacsin C on URX body cavity neuron activity
(A-H) Activity of URX neurons in each indicated genotype and treatment using Ca^{2+} imaging by GCaMP5K under the control of the URX specific *flp-8* promoter. Oxygen concentrations in the microfluidic chamber were 10% and 21% as indicated. (A-D) For each genotype and treatment group, black traces show the average percent change of GCaMP5k fluorescence ($F\Delta/F_0$) and gray shading indicates SEM. The number of animals used for each condition is shown in the figure. (C-D) Individual URX responses are shown for each genotype and treatment; each row represents one animal. (I) Maximal ($F\Delta/F_0$) values are shown for individual animals in wildtype and *acox-1* animals +/- Triacsin C. Bars indicate the average value within each genotype. ***$p<0.001$ by students t-test. (J) Individual baseline fluorescence (F_0) values at 10% oxygen are shown for individual animals in wildtype and *acox-1* mutants. Bars indicate the median value within each genotype; n.s., not significant by students t-test (K) We imaged mCherry fluorescence in wildtype and *acox*-1 mutant animals expressing both GCaMP5K and mCherry under the control of the *flp-8* promoter. Images were taken in animals exposed to 10% oxygen. For each genotype, the fluorescence intensity was imaged at the same exposure, determined to be within the linear range. Fluorescence intensity was quantified and is expressed as the mean. (L) The background-subtracted maximum fluorescence (max FL) at 21% (high) oxygen is shown for each genotype and treatment group. Bars indicate the median value within each genotype or treatment group. +/- SEM (n = 23). n.s., not significant by students t-test.

Chapter III: CPT-6 is expressed in the nervous system and regulates social feeding behavior

Introduction

We previously reported that RNAi inhibition of either F08A8.1/acox-1 and W01A11.5/cpt-6 suppress the feeding increasing effects of serotonin. *cpt-6* encodes an orthlogue of mammalian carnitine palmitoyl transferase I (CPT1), an enzyme that catalyzes the conversion of long chain fatty acyl-CoAs to fatty acyl-carnitines for translocation across the outer mitochondrial membrane. Like ACOX-1 in peroxisomal fatty acid oxidation, CPT-6 is hypothesized to control the rate of flux of cytosolic fatty acyl-CoAs into the mitochondrial matrix and thus function as a gate-keeper of mitochondrial fatty acid oxidation [37]. As loss of either CPT-6 and ACOX-1 abrogates the increased feeding rate of serotonin treated animals, we hypothesized that an accumulation of fatty acyl-CoAs, the metabolic substrates of these enzymes initiates an anorexigenic response. In mammals, pharmacologic manipulations that increase levels of hypothalamic fatty acyl-CoAs also inhibit feeding suggesting these moieties may play a conserved role in feeding regulatory circuits[112].

Though ACOX-1 has not previously been implicated in mammalian feeding regulation, a growing body of literature implicates mammalian carnitine palmitoyl transferase in the hypothalamic control of feeding. In particular, CPT1c, a brain specific isoform of the enzyme has emerged as key regulator of organismal energy homeostasis[146]. Mice lacking CPT1c have reduced food intake and body fat than their wildtype counterparts yet paradoxically, these animals are more susceptible to obesity when fed a high-fat diet[146]. This is hypothesized to be due in part due to disruption of hypothalamic leptin and ghrelin signaling pathways. Specifically, CPT1c KO animals are resistant to the anorectic effects of leptin and ghrelin [147,148]. In addition, a recent study

suggests that CPT1c activity in the mediobasal hypothalamus is required for the induction of brown adipose tissue thermogenesis by leptin [149].

CPT1c has a shares a high degree of homology with CPT1a and CPT1b, the liver and muscle specific isoforms of the enzyme. Though all three isoforms share the capacity to bind fatty acyl-CoAs, CPT1c curiously lacks capacity to transfer fatty acyls to carnitine and is expressed uniquely in the endoplasmic reticulum (ER) suggesting it may play a non-canonical role in lipid metabolism [146] [150]. Metabolomic profiling of CPT1c KO mice confirms the notion that this isoform plays a limited role in mitochondrial fatty acid oxidation as no changes in metabolites associated with fatty acid oxidation were detected. Loss of CPT1c does significantly reduce the levels of certain fatty acyl ethanolamines and increase ceramide production [151]. These two lipid families have well established roles in the regulation of feeding and have been proposed as potential downstream effectors of CPT1c [147].

Despite a clear role for CPT1 in the regulation of feeding, the precise role of this enzyme in the nervous system remains unclear. Moreover, though this enzyme has been shown to mediate the effects of peripherally derived endocrine signals (i.e ghrelin, leptin), no studies have examined the influence of CPT1 on neuroendocrine circuits that regulate feeding behavior. Our data suggests that CPT1 enzymes may exert their effects on feeding by modulating serotonergic signaling circuits.

Here, we describe the generation and preliminary phenotypic analysis of a novel allele of *cpt-6,* an ortholog of mammalian CPT-1. We find that CPT-6 is expressed broadly within the *C. elegans* nervous system and may play a role regulating pharyngeal pumping and social feeding behaviors.

Results

We previously reported that RNAi inhibition of W01A11.5/cpt-6 suppress both the fat reducing and feeding increasing effects of serotonin. To investigate how loss of *cpt-6* influences serotonin signaling, we utilized CRISPR/Cas9-directed genome editing to generate *cpt-6* mutants as no genetic mutants for this gene currently exist. Using a dual sgRNA-directed strategy with non-homologous end joining dependent repair, we generated a novel deletion allele of *cpt-6* [152]. Guide RNAs were designed to target PAM sites that flank the first exon and a portion of the second exon resulting in a ~397bp deletion (Figure 1A-D).

The developmental timing, size and health of the resulting *cpt-6* mutants appear grossly wildtype. *cpt-6* mutants however have reduced rates of pharyngeal pumping and are partially unresponsive to the feeding increasing effects of serotonin (Figure 2A). In addition to the noted feeding defects, *cpt-6* mutants exhibit a preference for low oxygen regions at the border of bacterial lawns and demonstrate a social feeding behavior. To examine the expression pattern of CPT-6, we generated a translation reporter consisting of a full length *cpt-6* cDNA fused to a C-terminal GFP under the control of the endogenous *cpt-6* promoter. CPT-6 is expressed broadly within the nervous system with notable expression in the ventral cord motor neurons and over 50 distinct head neurons. Slight expression was also noted in the intestine and vulva. Closer examination, particularly with co-injection markers illuminating known neurons, will be required to more specifically identify the neurons in which CPT-6 is expressed.

Discussion

We have generated a novel deletion allele of W01A11.5/*cpt-6* using CRISPR/Cas9 editing. This deletion removes ~400bp region of the gene that represents the first exononic region and the beginning portion the second. This mutation is presumed a null given the large deletion, however we cannot entirely rule out the possibility that a downstream ORF gives rise to a partially functional gene product. The feeding phenotype of this novel mutant recapitulated the result attained with RNAi knockdown against CPT-6 supporting the notion that this mutation results in a loss of CPT-6 function.

CPT-6 is predominantly expressed in the *C. elegans* nervous system though the specific neurons or neuronal subtypes remain unknown. This result was unexpected given the previously held notion that this protein was uniquely expressed in peripheral tissues. In mammals, it is the neuronal function of CPT-1c that is largely thought to contribute to the regulation of whole energy homeostasis. It is possible that CPT-6 plays a similar enzymatic and mechanistic function in *C. elegans* neurons. To further explore this possibility it will be interesting to examine the localization patterns of the remaining 5 CPT-1 orthologs to determine if any CPTs are expressed within the nervous system. Importantly, it will be important to determine the subcellular localization of CPT-6 as the feeding regulatory effects of CPT-1c stem from its function in the endoplasmic reticulum rather than the canonical mitochondrial role. Preliminary metabolomic analyses suggest that numerous metabolic and lipidomic species including phospholipids, ascarosides and short polypeptides are altered in *cpt-6* mutants (Schroeder Data). Further biochemical analyses will be required to more specifically determine the nature of the metabolic changes arising in *cpt-6* mutants.

It is intriguing that loss of CPT-1c in mammals results in altered fatty acid ethanolamine synthesis as these species were also among the most differentially expressed in *acox-1* null animals. Fatty acid ethanolamines may represent a common regulatory node in through which ACOX-1 and CPT-6 influence feeding behavior. Closer examination of the role of fatty acid ethanolamines in regulating serotonergic circuits and feeding behavior should be prioritized.

The most notable phenotype exhibited by *cpt-6* mutants is the bordering phenotypes. These mutants exhibit a preference for low oxygen environments, a well-studied behavior known to be under the control of the URX-RMG hub-and-spoke circuit [33,103,120,123]. This is particularly intriguing considering the purported role for URX body cavity in energy homeostasis and metabolic sensing as shown by our recent study and other groups [103,107,121,122]. It will be important to determine whether CPT-6 is expressed in URX, RMG or other body cavity neurons. Follow-up experiments could probe the role of URX or RMG neurons in regulating oxygen preferences in *cpt-6* mutants by determining whether activation or ablation of these neurons rescues the bordering phenotype.

cpt-6 and *acox-1* were originally identified as suppressors of the feeding increasing effects of serotonin from the same experiment[19]. Interestingly, these two proteins are expressed in distinct tissues, *acox-1* is only expressed with peripheral tissues whereas *cpt-6* is predominantly expressed in the nervous system. In mammals, changes in lipid metabolism either in peripheral tissues or directly within feeding regulatory regions within the hypothalamus can influence feeding behavior and changes in hypothalamic lipid metabolism can influence distant peripheral metabolic circuits [10,12,112,146,153].

We have demonstrated that URX and oxygen sensing neurons play a key role in mediating the effects *acox-1* on feeding behavior. It is therefore highly intriguing that loss of *cpt-6* modulates social feeding behavior and normoxia avoidance as it suggests that URX neurons and oxygen sensing circuits may represent a common mechanism through which peripherally and neuronally derived lipid metabolic species influence the behaviors and physiologies that underlie energy homoeostasis.

A

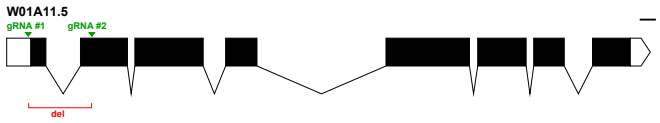

B

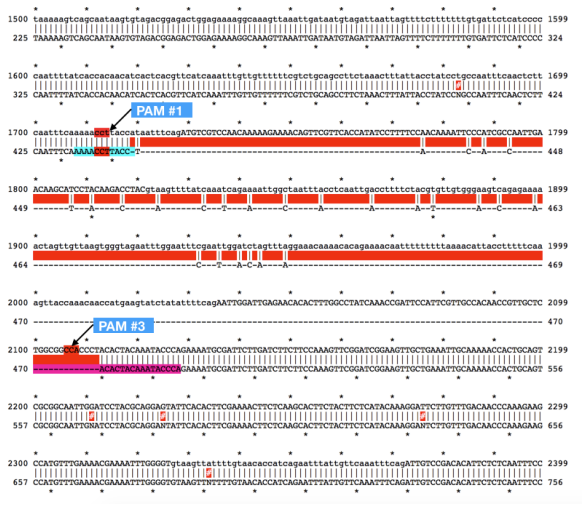

C

Primer ID	Sequence	Target Sequence	Source
cpt-6 guide RNA PAM #1	cctcctattgcgagatgtcttgCGACATCTGAAATTATGGTAgtttaagagctatgctgg	Targets: CGACATCTGAAATTATGGTA(AGG) in antisense	From ChopChop
cpt-6 guide RNA PAM#3	cctcctattgcgagatgtcttgTGGGTATTTGTAGTGTAGGGgtttaagagctatgctgg	Targets TGGGTATTTGTAGTGTAGGG (TGG) in antisense	From crispr.mit.edu
genotyping forward	cgctcattcaacaacacgga		
genotyping reverse	gaatgtttccagcttggcga		

D

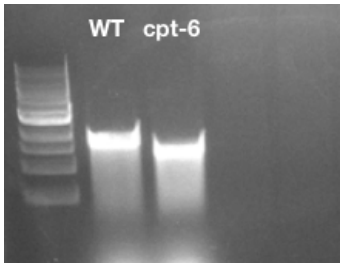

Figure 3.1 Generation of a novel allele of W01A11.5/*cpt-6*

We have generated a novel allele of cpt-6 using CRiSPR/Cas9 (A) Map of the exonic and intronic regions of W01A11.5/*cpt-6* with the location of the ~ 397bp deletion indicated in red brackets. (B) Alignment of DNA sequence of wild-type and the novel *cpt-6* allele. (C) Guide RNAs and sequencing primer sequences. Guide RNAs designed was aided with ChopChop or crispr.mit.edu software as indicated. (D) PCR confirmation of resulting deletion event. Expected wildtype product = 1695bp and mutant product = ~1300bp.

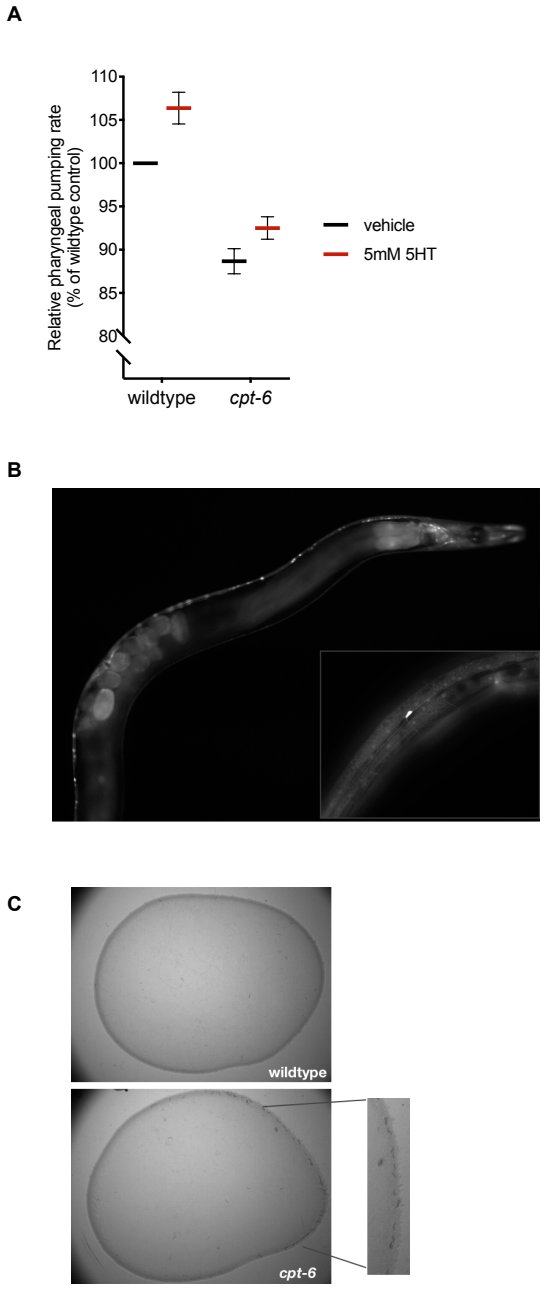

Figure 3.2 CPT-6 is expressed in the nervous system and plays a role in regulating feeding behavior and oxygen preference

(A) *cpt-6* mutants have reduced feeding rates and are partially insensitive to the feeding increasing effects of serotonin. Feeding data is preliminary in nature and represents an n=10 animals. (B) Expression of a *cpt-6p*::*cpt-6*cDNA::GFP suggest that CPT-6 primarily functions in the nervous system (C) *cpt-6* mutants exhibit social feeding behavior and a preference for low oxygen regions on the border *E. coli* source.

Chapter IV: Reflections and Future Directions

In this study, we uncover the architecture of a novel gut-to-brain regulatory axis that links peripheral metabolic information with neuroendocrine signaling circuits that regulate nutrient-related behaviors. This work offers mechanistic insight into how nutrient cues can modulate neuromodulatory circuits implicated in the control of mood, cognition and behaviors. Two areas of investigation should be prioritized in follow-up studies.

1. Investigating the influence of body cavity neurons on serotonergic circuits

We identified the body cavity neurons as a key link between peripheral metabolic cues and serotonergic signaling. We hypothesize that these neurons are capable of sensing numerous metabolic cues from the coelomic fluid and serve as an entry point into a circuit that links peripheral metabolic information with neuroendocrine circuits. However, it is still currently unclear what signals are released by URX neurons to regulate feeding (and potentially egg-laying) nor which cells are downstream recipient of these signals. Constitutive activation of synaptic vesicle and dense-core vesicle release from these neurons strongly stimulates feeding though intriguingly and somewhat perplexingly, genetic ablation of these neurons restore serotonin sensitivity to *acox-1* mutants (Figure 1). Taken together, these results paint a complicated role for body cavity neurons in this circuit as it seems that their activity is required to both suppress and activate feeding responses. Further investigation is required to more specifically determine the specific role and influence of body cavity neurons in the regulation of feeding behavior as it is possible that multiple signals are released from these neurons to control feeding. One area of investigation should focus on more specifically defining

contributions of AQR, PQR and URX neurons to feeding behavior. Given our GCaMP results, examining the contribution of URX neurons should be prioritized. Such an experiment would consist generating transgenic animals in which *egl-2(*gf) and *pkc-1*(gf) are expressed the URX specific *flp-8* promoter and determining the effects of inhibition and activation of URX neurons on feeding behavior. We hypothesize that inhibition of URX neurons will suppress serotonergic responses while activation of these neurons will stimulate feeding.

Next, it will be important to determine the nature of the signal(s) released from URX/body cavity neurons in the control of pharyngeal pumping. URX neurons are both cholinergic and peptidegic and specifically secrete a number FMRFamide-like peptides (*flp*), a family of neuropeptides involved in the control of most complex behaviors including feeding and egg-laying [83,154–156]. We showed that activation synaptic vesicle and dense core vesicle release stimulates feeding behavior suggesting that either a cholinergic or peptidergic signal from these neurons functions to enhance feeding responses. To resolve the role of neuropeptides specifically, an important experiment will be to selectively suppress dense-core vesicle release from URX neurons. RAB-5 is a Rab GTPase that is required for dense-core vesicle release but plays no role in synaptic vesicle release. It's been previously shown that expression of a constitutively active version of this protein, *rab-5*(Q78L) blocks neuropeptide release in a cell-autonomous manner [157]. If neuropeptide release from URX neurons is required to stimulate feeding responses, we would expect an animal expressing the *rab-5*(Q78L) transgene under a *flp-8* promoter to have blunted responses to exogenous serotonin in a manner that phenotypically recapitulates the responses of *acox-1* mutants. If this is

the case, a screen for specific neuropeptides should be carried out perhaps utilizing a strain with RNAi sensitivity specifically in URX neurons. If animals lacking peptidergic signaling from URX neurons still retain full responsiveness to serotonin, it could suggest that a cholinergic tone rather than a peptidergic signal from these neurons regulates feeding.

There is some preliminary evidence that acetylcholine signaling is altered in *acox-1* mutants. Acetylcholine plays a key role in mediating excitatory neuromuscular responses and stimulates pharyngeal pumping [158–161]. Animals defective in acetylcholine synthesis or release have reduced feeding rates of pharyngeal pumping [162,163]. It has also been proposed that the experience of starvation modulates pharyngeal muscle excitability in turn influencing feeding behavior in a mechanism that involves the GAR-3 muscarinic cholinergic receptor [29]. A few pieces of data that suggest that altered acetylcholine signaling may contribute to the feeding and egg-laying defects noted in *acox-1* mutants. Both *acox-1* and *acox-1;aak-2* mutants are partially resistant to the paralyzing effects of the acetycholinerase inhibitor, aldicarb suggesting that acetylcholine release or transmission is reduced in these animals (Figure 2). Preliminary data from direct biochemical measurements of acetetylcholine and choline, the rate-limiting substrate in the synthesis of acetylcholine suggests that levels of this neurotransmitter in whole animal lysates are indeed reduced in *acox-1* and *cpt-6* mutants (Figure 3, Yan Yue, Schroeder Lab – communicated findings). As choline levels are unchanged in these animals, it remains possible that either the synthesis of acetylcholine is slowed by reduced levels or activity of choline acetyltransferase (ChAT) or the breakdown of acetylcholine is increased by higher levels or activity of

acetylcholine esterase, the enzyme involved in breakdown of acetylcholine. Reexamination of our RNAseq data suggest that a putative acetylcholine esterase (Y75B8A.3) is indeed 2.5 fold higher in *acox-1* and *aak-2;acox-1* mutants. This gene was not included in our screen of RNAseq hits, and it will be interesting to determine if contributes to the behavioral responses of *acox-1* mutants. If reduced cholinergic signaling leads to reduced excitability of serotonergic responses, inactivation or knock-down of acetylcholine esterase levels would be hypothesized to rescue the noted behavioral phenotypes of *acox-1* mutants.

Acetylcholine signals through two broad families of receptors, the metabotropic/G-protein coupled muscarinic receptors (mAChRs) and the ionotropic nicotinic receptors (nAChRs) [164]. To begin exploring the influence of cholinergic signaling on feeding, we first explored the influence of muscarinic acetylcholine signaling on feeding responses. Transient treatment with atropine, a muscarinic receptor antagonist suppresses the pharyngeal pumping rates of both wildtype and *aak-2* mutants (Figure 3A). Conversely, treatment with arecoline, a muscarinic receptor agonist did not restore high feeding rates to *aak-2;acox-1* (Figure 3B). These preliminary experiments suggest that muscarinic signaling is required for serotonin-mediated feeding increases, but not sufficient to stimulate feeding or to rescue the suppression induced by loss of ACOX-1. As both muscarinic and nicotinic acetylcholine signaling have been shown to regulate serotonin responses in both the pharyngeal and vulval neuromuscular, a follow-up set of experiments could explore the role of nicotinic cholinergic signaling [165–167]. It is well established that animals lacking EAT-2, a nicotinic cholinergic receptor, have reduced feeding responses [159,167]. The roles of

nicotine or other nicotinic cholinergic receptor agonists on *C. elegans* behaviors are less well defined. Transient exposure to nicotine has been shown to stimulate egg-laying behavior and excite dissected pharyngeal muscles [167,168]. If reduced nicotinic signaling contributes to the suppression of serotonergic feeding responses in *acox-1* mutants, nicotine supplementation may rescue feeding and egg-laying defects. If this is the case, the role and site of action of specific nicotinic acetylcholine receptors (nACrRs) should be probed. Such experiments could help elucidate mechanistic and cellular components that lie downstream of URX and body cavity neurons in the regulation of feeding and egg-laying behavior.

2. **Characterizing the role of *N*-acylethanolamines in regulating feeding behavior**

Our metabolomic analyses suggest that the synthesis of fatty acyl ethanolamine synthesis may be altered in *acox-1* mutants. Metabolic intermediates in the biosynthesis of N-acylethanolamines were among the most significantly altered. *N*-acylethanolamines, endogenous ligands of cannabinoid receptors, are potent neuromodulators and regulate numerous behaviors and physiologies including appetite, lifespan, mood and cognition [79,115–118]. We find that inactivation of fatty acid amide hydrolase (*faah-1*), an enzyme involved in the hydrolytic degradation of NAEs, stimulates both feeding and egg-laying responses in wildtype, *acox-1, aak-2;acox-1* mutants (Figure S4D-1, Figure 4A). To place FAAH-1 within an existing feeding regulatory framework, we performed an epistasis analysis with known components of serotonergic feeding circuits**.** Animals deficient in serotonin due to a mutation in *tph-1* fail to increase pharyngeal pumping rates on *faah-1* RNAi (Figure 4B). This suggest that the effects of NAEs on feeding behavior require serotonin signaling.

NAEs are synthesized by N-acyl phosphatidylethanolamine phospholipase D (*nape-1*), an enzyme that hydrolyses N-acylphosphatidyethanolamines to produce N-acylethanolamines and phosphatidic acid. RNAi inactivation of *nape-1* generates an "anxiety-like" phenotype where animals exhibit extremely rapid bouts of feeding after mechano-stimulation (ex. movement of plates) before eventually stabilizing back to wildtype levels (data not shown). This curious phenotype merits closer investigation and may suggest that NAPE-1 and NAE products play roles in gating the excitability of sensory circuits.

How might NAEs regulate feeding and egg-laying behavior and sensory responsiveness? Endocannabinoids are potent neuromodulators and play a key role in regulating neuronal excitability in part due to their actions on serotonergic systems [169]. Indeed, there is high degree of overlap in the behaviors and physiologies regulated by endocannabinoid and serotonergic signaling and cannabinoid-driven effects often require the involvement of serotonergic signals [79,118,169]. Endocannabinoids have been shown to modulate the release of serotonin, alter the expression and activity of serotonin and influence the excitability of serotonergic neurons [170,171]. In mammals, most of these effects require the activity of the canonical $G\alpha_o$- coupled cannabinoid receptors, CB1 and CB2 [172].

Though *C. elegans* synthesize endocannabinoids, they were long thought to lack clear orthologs for mammalian CB1 and CB2 receptors [173–175]. However, a recent report suggests that the neuropeptide receptor *npr-19* binds at least two major endocannabinoids 2-arachidonoylglycerol (2-AG) and N-arachidonoylethanolamide (AEA) and functions as a cannabinoid receptor [176]. Intriguingly, *npr-19* is expressed in

a limited subset of neurons including the URX body cavity neuron and the M3 pharyngeal motoneuron where it mediates the effect of 2-AG and AEA on numerous behaviors, including feeding, nociception and locomotion. It is highly intriguing that *npr-19* is expressed in the URX body cavity neurons as it suggests that it may play a role in mediating the effects of loss of ACOX-1 on feeding. Cannabinoids are known to have state-dependent and counterbalancing effects. If cannabinoid signaling through NPR-19 is required to block feeding increasing effects of serotonin, we would expect an *acox-1;npr-19* animals to have wildtype feeding responses. Alternatively, certain cannabinoid species may stimulate feeding through NPR-19 in which case, it is possible that *npr-19* mutants resemble *acox-1* mutants and fail to respond to serotonin. It will also be important to determine if *npr-19* is required for the feeding increasing effects of *faah-1* RNAi or the regulation of URX neuron activity.

NPR-19 long evaded BLAST searches for cannabinoid receptors as it only shares 23% homology with human CB1. There are still numerous orphaned neuropeptide receptors that may play a role in mediating the effects of cannabinoids in *C. elegans*. It is also possible that *npr-19* or other NPR/CB-like receptors play no role in mediating the effects of ACOX-1 or FAAH-1 on feeding. Indeed it has been established in mammalian systems that not all not fatty acylethanolamines bind or activate cannabinoid receptors though the mechanisms of action for the receptor-inactive acylethanolamines remain poorly understood [177]. Given the lack of clear CB homologs, *C. elegans* are likely an excellent model to identify novel and perhaps more evolutionarily ancient mechanisms that underlie the influence of cannabinoids and fatty acylethanolamines on behavior and physiology.

Lastly, the contribution of individual N-acylethanolamines and their precursors in the regulation of feeding should be examined. We conducted a preliminary supplementation analysis and found that addition of docosahexaenoic acid (DHA), docosahexaenoylehanolamine (DHEA) and arachidonic acid (AA) stimulate feeding in wildtype animals while DHA, DHEA and the eicosapentaenoic acid (EPA) derivative eicosapentaenoic ethanolamine (EPEA) elevate feeding rates in *acox-1* mutants (Figure 6). DHA, AA and EPA are major components of neuronal phospholipids and play significant and conserved roles in the development and function of the nervous system. Though our screen was limited, it is notable that the only fatty acid "hits" (AA, EPEA, DHA and DHEA) belong or are derived to the omega-3 and omega-6 family of fatty acids. There is an overwhelming amount of literature highlighting the protective role of these lipids on the incidence and severity of wide range of psychiatric, neurological and neurodegenerative conditions through their precise contribution to neuronal and cognitive health remain unclear. Some of these protective influences of omega-3/6 fatty acids are hypothesized to require the conversion of these lipids to their cognate N-acyl ethanolamines [178–180].

Despite the physiologically essential role of omega 3 fatty acids, virtually all vertebrate species are incapable of catalyzing the sequential desaturation reactions required to synthesize these lipids *de novo.* Instead, these lipids must be acquired from dietary sources or synthesized from the essential fatty acid precursor, α-linoleic acid (ALA, 18:3n-3). In vertebrates, ALA is progressively desaturated and elongated to tetracosapentaenoic acid (24:6n-3) in the endoplasmic reticulum. Tetracosahexaenoic acid is subsequently translocated to the peroxisomal matrix where it is shortened to DHA

in part through the action of ACOX-1 [181]. Unlike mammals, *C. elegans* and other nematodes seem to have the capacity to generate DHA *de novo* though it is unclear how much is generated via a *de novo* pathway versus the ACOX-1 and ALA dependent circuit [182,183]. It will be important to re-mine the metabolomics data to determine if *acox-1* mutants have altered levels of DHA, EPA and other related polyunsaturated fatty acid derivatives (i.e fatty acyl ethanolamines). It is hypothesized that the ratio of omega-3 to omega-6 fatty acids contributes to pathogenic or dysfunctional states so it will be important to access both absolute and relative levels of these lipids in *acox-1* mutants [184]. As polyunsaturated fatty acids are major structural components of cellular membranes and functional modulators of cellular function these preliminary data are highly intriguing. Long chain poly/unsaturated fatty acids like DHA and EPA have been shown to be essential for efficient serotonergic and cholinergic neurotransmission. For example, animals deficient in *fat-3*, the Δ6-desaturase that mediates the first step in the conversion of α-linolenic acid (ALA) to EPA and DHA show behavioral defects consistent with inefficient serotonin and acetylcholine transmission. Like *acox-1* mutants, *fat-3* mutants exhibit egg-laying defects and aldicarb resistance, phenotypes that can be rescued with exogenous supplementation of arachidonic acid and docosahexaenoic acid [185]. Though the precise mechanisms remain unclear, modulation of neuronal PUFA composition seems to influence synaptic vesicle formation and fusion at synaptic terminals in turn altering neurotransmission. It is possible that loss of ACOX-1 alters the composition of neuronal PUFAs in turn, causing behavioral phenotypes due to altered serotonergic and cholinergic release. The role of PUFAs in mediating the behavioral deficits of *acox-1* mutants should be more carefully assessed. Dose response

experiments with each PUFA should be conducted to understand the ability of each PUFA to rescue the phenotypes of *acox-1* mutants. As PUFAs serve as essential precursors to numerous signaling molecules including NAEs, sphingolipids and eicosanoids, experiments with unmetabolizable variants of each PUFA could be a starting place to disentangle the contributions of the PUFAs themselves from their derivatives.

A

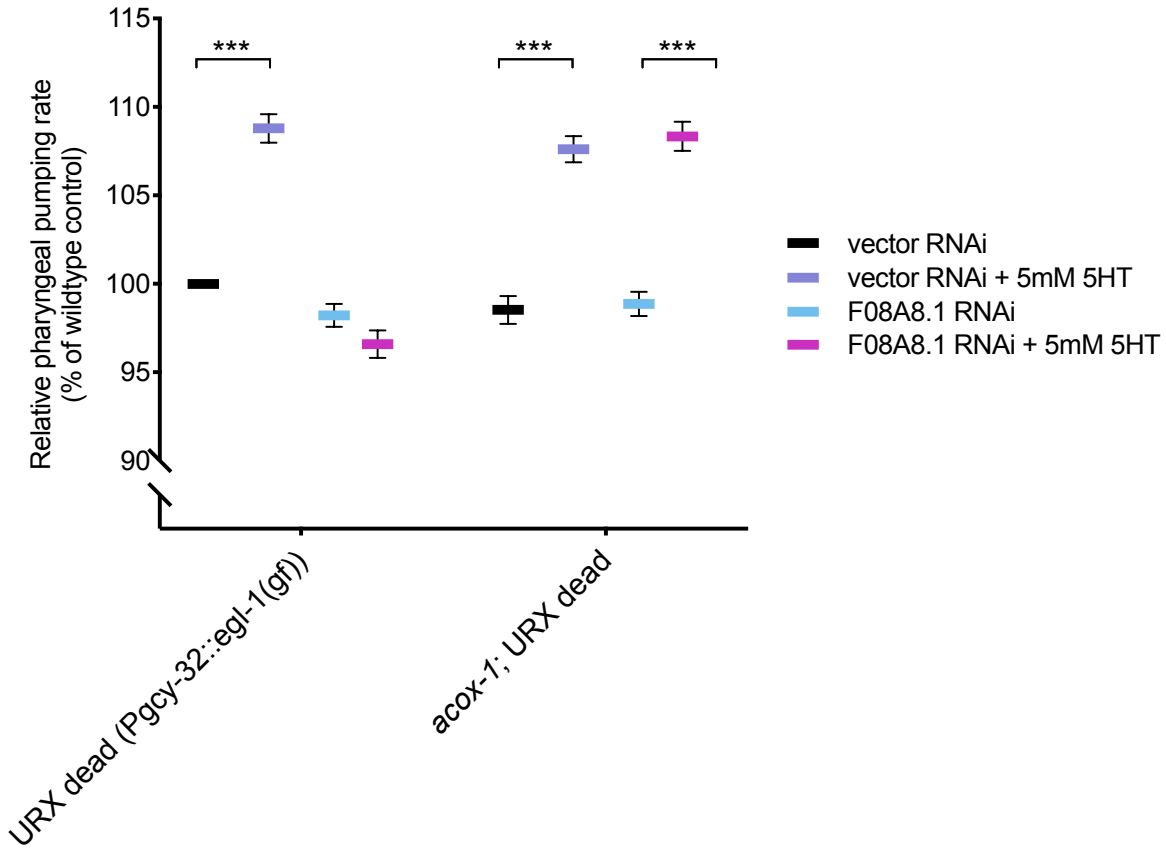

Figure 4.1 ACOX-1-mediated regulation of serotonergic feeding responses requires the EGL-2 K+ channels

(A) Body Cavity Neurons are required for ACOX-1 to modulate serotonergic feeding responses. AQR, PQR and URX neurons were genetically ablated using a gain-of-function allele of the EGL-1 caspase. Pharyngeal pumping rates of CX7102 (URX dead) and *acox-1(*ok2257); CX7102 animals treated with vehicle or 5mM 5HT. Error bars indicate +/- SEM from mean, n=10 animals per condition. *p<0.05, *** p < 0.001, ANOVA (Tukey)

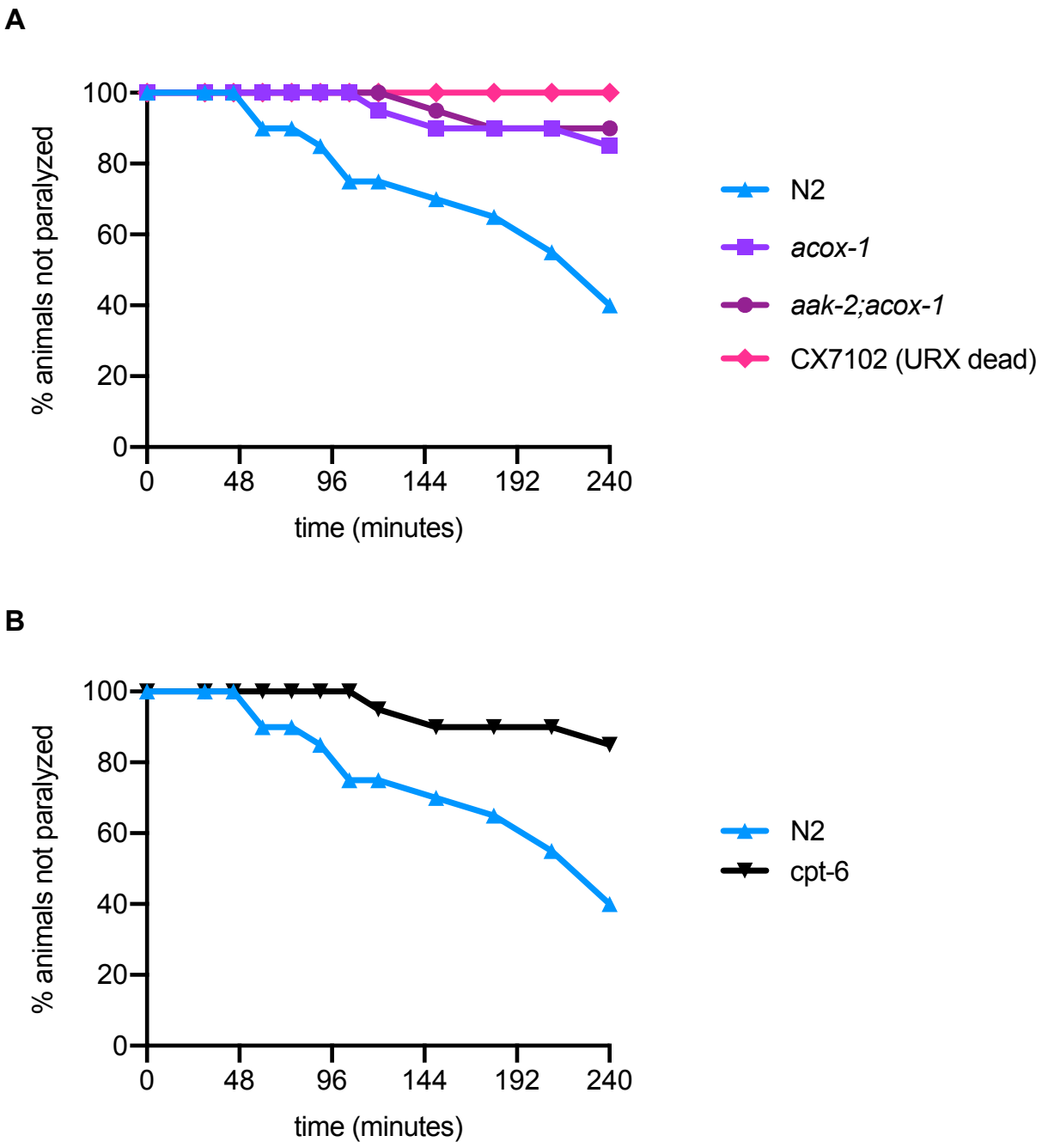

Figure 4.2 ACOX-1, CPT-6 and Body Cavity Neurons regulate acetylcholine signaling
(A, B) Aldicarb induced paralysis assay suggests that acetylcholine signaling may be reduced in *acox-1*, *aak-2;acox-1, cpt-6* and URX dead animals (CX7102) Animals were placed on plates containing 1mM of the acetylcholinesterase inhibitor Aldicarb. Animals were observed and scored as moving or paralyzed every 30 minutes.

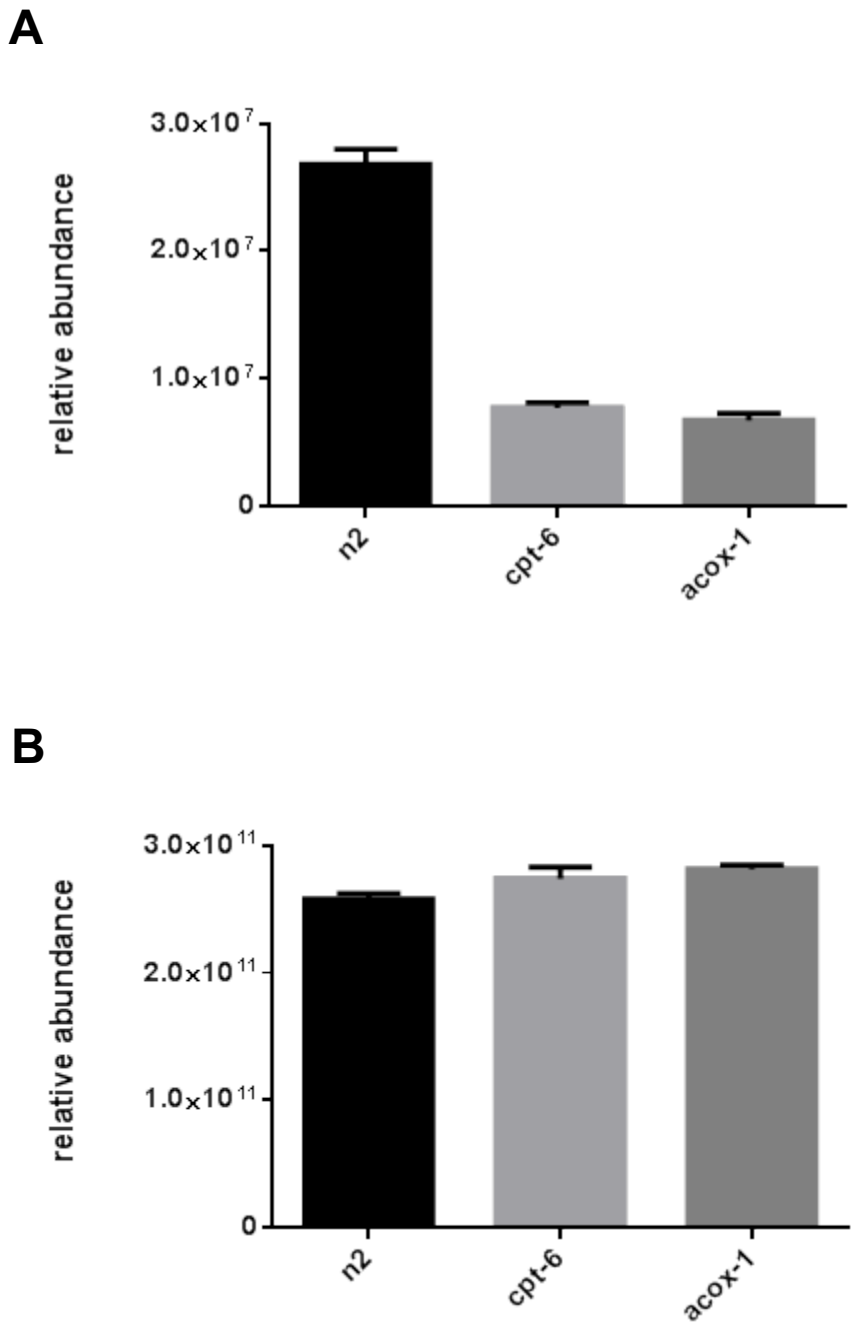

Figure 4.3 Loss of *acox-1* and *cpt-6* reduces acetylcholine but not choline levels
(A) Pharyngeal pumping rates of wildtype and *aak-2* animals treated with vehicle or 1mM atropine for one hour. . Error bars indicate +/- SEM from mean, n=10 animals per condition. (B) Pharyngeal pumping rates of wildtype and *acox-1*;*aak-2* animals treated with vehicle or 1mM arecoline for one hour. Error bars indicate +/- SEM from mean, n=10 animals per condition

A

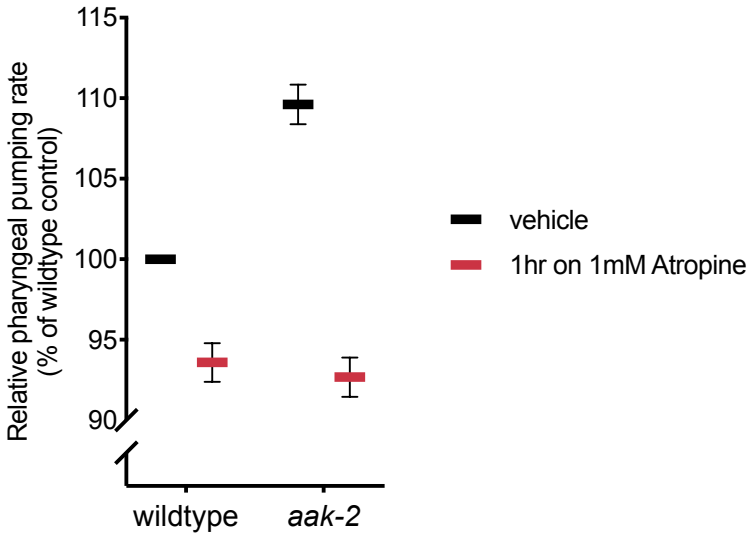
Relative pharyngeal pumping rate
(% of wildtype control)
115
110
105
100
95
90
wildtype
aak-2
vehicle
1hr on 1mM Atropine

B

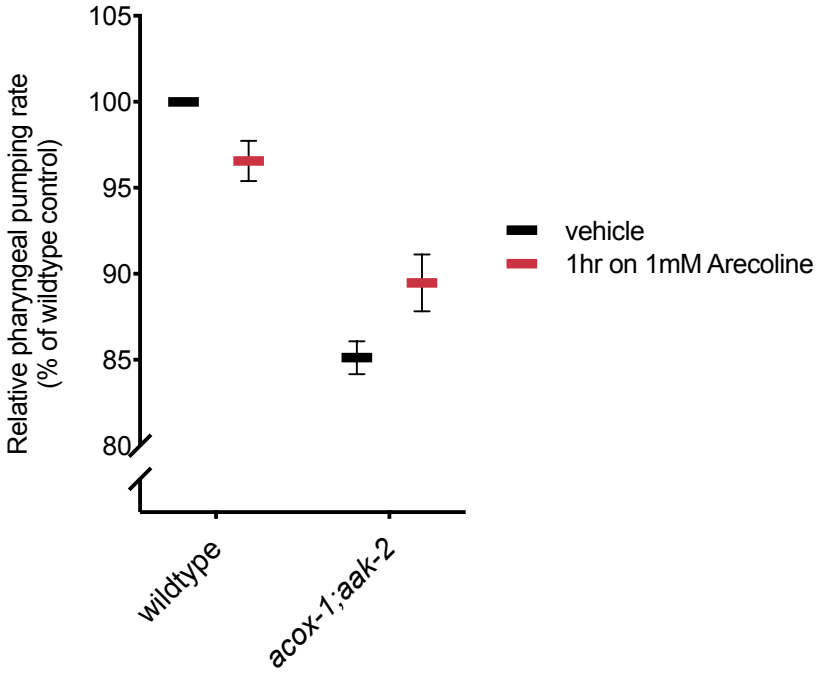
Relative pharyngeal pumping rate
(% of wildtype control)
105
100
95
90
85
80
wildtype
acox-1;aak-2
vehicle
1hr on 1mM Arecoline

Figure 4.4 Inhibition of muscarinic acetylcholine signaling suppresses elevated feeding responses of *aak-2* mutants

(A) Pharyngeal pumping rates of wildtype and *aak-2* animals treated with vehicle or 1mM atropine for one hour. . Error bars indicate +/- SEM from mean, n=10 animals per condition. (B) Pharyngeal pumping rates of wildtype and *acox-1*;*aak-2* animals treated with vehicle or 1mM arecoline for one hour. Error bars indicate +/- SEM from mean, n=10 animals per condition

A

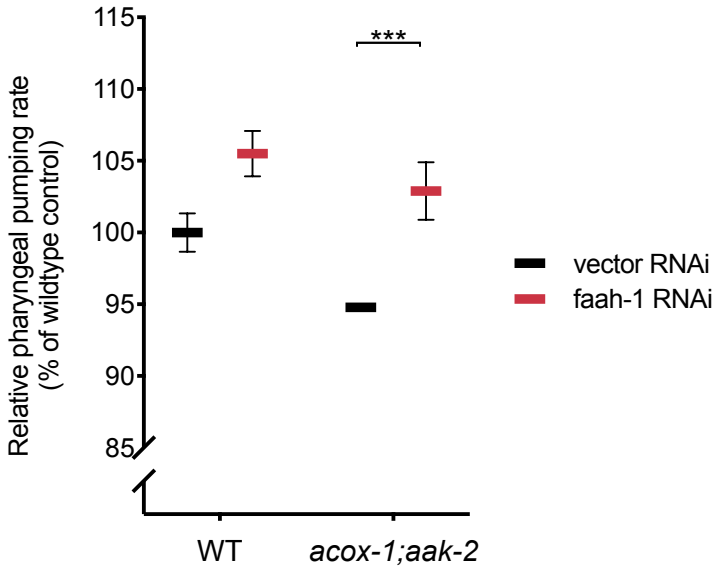
Relative pharyngeal pumping rate
(% of wildtype control)
115
110
105
100
95
90
85
***
vector RNAi
faah-1 RNAi
WT
acox-1;aak-2

B

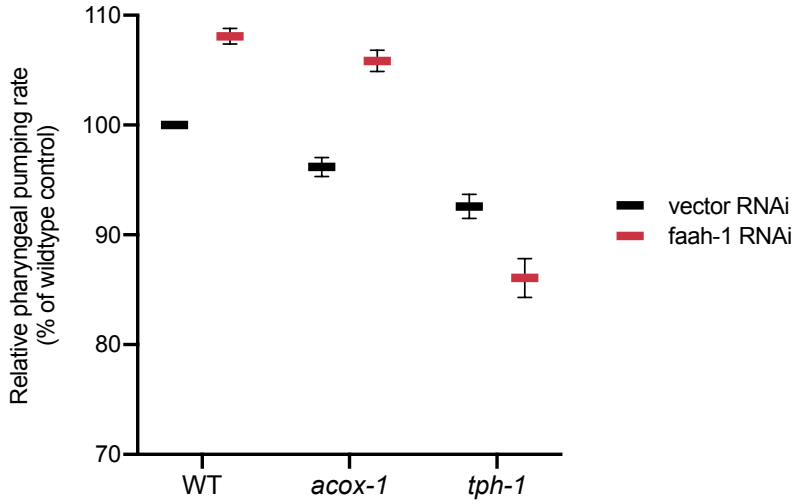
Relative pharyngeal pumping rate
(% of wildtype control)
110
100
90
80
70
vector RNAi
faah-1 RNAi
WT
acox-1
tph-1

Figure 4.5 RNAi inactivation of fatty acid amide hydrolase (*faah-1*) stimulates feeding responses in a serotonin dependent manner

(A) Pharyngeal pumping rates of wildtype and *aak-2;acox-1* animals treated with vector or *faah-1* RNAi. Error bars indicate +/- SEM from mean, n=8 animals per condition. (B) Pharyngeal pumping rates of wildtype, *acox-1* and *tph-1* animals treated with vector or *faah-1* RNAi. Error bars indicate +/- SEM from mean, n=10 animals per condition. *** $p < 0.001$, ANOVA (Tukey).

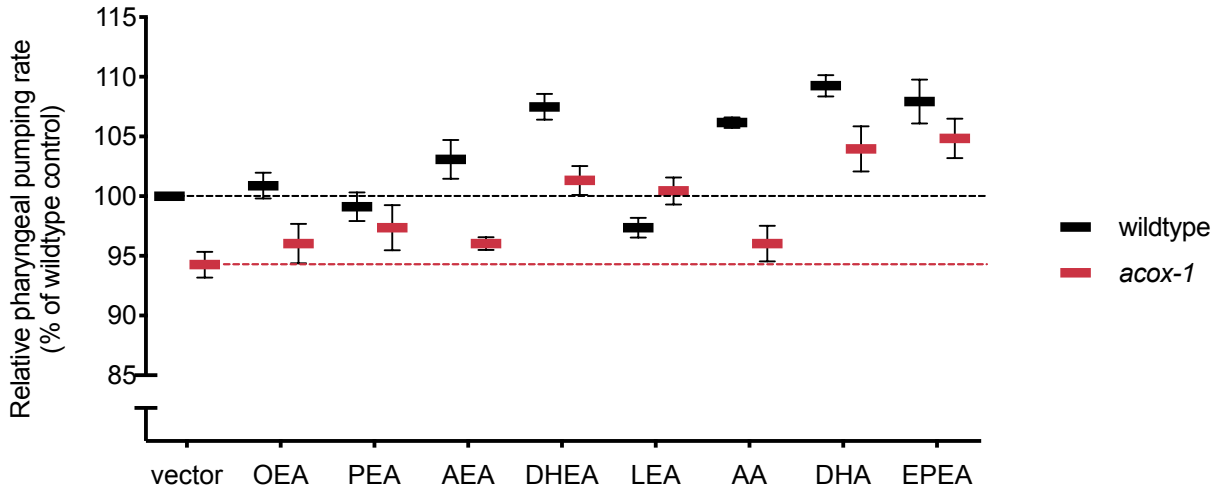

Figure 4.6 Exogenous omega-3 fatty acid derivatives elevate feeding rates of wildtype and *acox-1* mutants

(A) Animals were grown from L1s on plates containing 200μM of each fatty acid before assessing pharyngeal pumping rates of day 1 adults. Error bars indicate +/- SEM from mean, n=5 animals per condition. Oleoylethanolamine (OEA), palmitoylethanolamine (PEA), arachidonoyl ethanolamine (AEA), docosahexaenoyl ethanolamine (DHEA), linoleoyl ethanolamine (LEA), arachidonic acid (AA), docosahexaenoic acid (DHA), eicosapentaenoyl ethanolamine (EPEA).

References:

1. Riekeberg E, Powers R. New frontiers in metabolomics: from measurement to insight. F1000Research. Faculty of 1000 Ltd; 2017;6: 1148. doi:10.12688/F1000RESEARCH.11495.1
2. You Y, Kim J, Raizen DM, Avery L. Insulin, cGMP, and TGF-β Signals Regulate Food Intake and Quiescence in C. elegans: A Model for Satiety. Cell Metab. 2008;7: 249–257. doi:10.1016/j.cmet.2008.01.005
3. Pool A-H, Scott K. Feeding Regulation in Drosophila. Curr Opin Neurobiol. 2014;29: 57–63. doi:10.1016/j.conb.2014.05.008
4. Lemieux GA, Cunningham KA, Lin L, Mayer F, Werb Z, Ashrafi K. Kynurenic Acid Is a Nutritional Cue that Enables Behavioral Plasticity. Cell. 2015;160: 119–131. doi:10.1016/j.cell.2014.12.028
5. Tremblay A, Bellisle F. Nutrients, Satiety, and Control of Energy Intake. Appl Physiol Nutr Metab. NRC Research Press; 2015;40: 971–979. doi:10.1139/apnm-2014-0549
6. Corrales-Carvajal VM, Faisal AA, Ribeiro C. Internal States Drive Nutrient Homeostasis by Modulating Exploration-Exploitation Trade-Off. Elife. 2016;5. doi:10.7554/eLife.19920
7. Heeley N, Blouet C. Central Amino Acid Sensing in the Control of Feeding Behavior. Front Endocrinol (Lausanne). Frontiers Media SA; 2016;7: 148. doi:10.3389/fendo.2016.00148
8. Augustine V, Gokce SK, Oka Y. Peripheral and Central Nutrient Sensing Underlying Appetite Regulation. Trends Neurosci. Elsevier; 2018;41: 526–539.

doi:10.1016/j.tins.2018.05.003

9. Templeman NM, Murphy CT. Regulation of Reproduction and Longevity by Nutrient-Sensing Pathways. J Cell Biol. 2018;217: 93–106. doi:10.1083/jcb.201707168

10. Blouet C, Schwartz GJ. Hypothalamic Nutrient Sensing in the Control of Energy Homeostasis. Behav Brain Res. Elsevier; 2010;209: 1–12. doi:10.1016/J.BBR.2009.12.024

11. Myers MG, Olson DP. Central Nervous System Control of Metabolism. Nature. Nature Publishing Group; 2012;491: 357–363. doi:10.1038/nature11705

12. Obici S, Feng Z, Morgan K, Stein D, Karkanias G, Rossetti L. Central Administration of Oleic Acid Inhibits Glucose Production and Food Intake. Diabetes. American Diabetes Association; 2002;51: 271–5. doi:10.2337/DIABETES.51.2.271

13. Hotamisligil GS, Erbay E. Nutrient Sensing and Inflammation in Metabolic Diseases. Nat Rev Immunol. NIH Public Access; 2008;8: 923–34. doi:10.1038/nri2449

14. Efeyan A, Comb WC, Sabatini DM. Nutrient-Sensing Mechanisms and Pathways. Nature. Nature Publishing Group; 2015;517: 302–310. doi:10.1038/nature14190

15. McCloskey RJ, Fouad AD, Churgin MA, Fang-Yen C. Food Responsiveness Regulates Episodic Behavioral States in Caenorhabditis elegans. J Neurophysiol. 2017;117: 1911–1934. doi:10.1152/jn.00555.2016

16. Horvitz HR, Chalfie M, Trent C, Sulston JE, Evans PD. Serotonin and Octopamine in the Nematode Caenorhabditis elegans. Science (80-). 1982;216: 1012–4.

Available: http://www.ncbi.nlm.nih.gov/pubmed/6805073

17. Segalat L, Elkes D, Kaplan J. Modulation of Serotonin-Controlled Behaviors by Go in Caenorhabditis elegans. Science (80-). 1995;267: 1648–1651. doi:10.1126/science.7886454

18. Waggoner LE, Zhou GTT, Schafer RW, Schafer WR. Control of Alternative Behavioral States by Serotonin in Caenorhabditis elegans. Neuron. Cell Press; 1998;21: 203–214. doi:10.1016/S0896-6273(00)80527-9

19. Srinivasan S, Sadegh L, Elle IC, Christensen AGL, Faergeman NJ, Ashrafi K. Serotonin Regulates C. elegans Fat and Feeding through Independent Molecular Mechanisms. Cell Metab. NIH Public Access; 2008;7: 533–44. doi:10.1016/j.cmet.2008.04.012

20. Entchev E V, Patel DS, Zhan M, Steele AJ, Lu H, Ch'ng Q. A Gene Expression Based Neural Code for Food Abundance that Modulates Lifespan. Elife. eLife Sciences Publications, Ltd; 2015;4: e06259. doi:10.7554/eLife.06259

21. Churgin MA, Mccloskey RJ, Peters E, Fang-Yen C, Horvitz R, Sze JY, et al. Antagonistic Serotonergic and Octopaminergic Neural Circuits Mediate Food-Dependent Locomotory Behavior in Caenorhabditis elegans. J Neurosci. 2017;37: 7811–7823. doi:10.1523/JNEUROSCI.2636-16.2017

22. Sze JY, Victor M, Loer C, Shi Y, Ruvkun G. Food and Metabolic Signalling Defects in a Caenorhabditis elegans Serotonin-Synthesis Mutant. Nature. Nature Publishing Group; 2000;403: 560–564. doi:10.1038/35000609

23. Song B, Avery L. Serotonin Activates Overall Feeding by Activating Two Separate Neural Pathways in Caenorhabditis elegans. J Neurosci. Society for

Neuroscience; 2012;32: 1920–31. doi:10.1523/JNEUROSCI.2064-11.2012

24. Cunningham KA, Bouagnon AD, Barros AG, Lin L, Malard L, Romano-Silva MA, et al. Loss of a Neural AMP-Activated Kinase Mimics the Effects of Elevated Serotonin on Fat, Movement, and Hormonal Secretions. PLoS Genet. 2014;10. doi:10.1371/journal.pgen.1004394

25. Zhang Y, Lu H, Bargmann CI. Pathogenic Bacteria Induce Aversive Olfactory Learning in Caenorhabditis elegans. Nature. Nature Publishing Group; 2005;438: 179–184. doi:10.1038/nature04216

26. Sawin ER, Ranganathan R, Horvitz HR. C. elegans Locomotory Rate Is Modulated by the Environment through a Dopaminergic Pathway and by Experience through a Serotonergic Pathway. Neuron. Cell Press; 2000;26: 619–631. doi:10.1016/S0896-6273(00)81199-X

27. Avery L. The Genetics of Feeding in Caenorhabditis elegans. Genetics. 1993;133: 897–917.

28. Avery L, Shtonda BB. Food Transport in the C. elegans Pharynx. J Exp Biol. 2003;206: 2441–2457. Available: http://www.ncbi.nlm.nih.gov/pubmed/12796460

29. You Y, Kim J, Cobb M, Avery L. Starvation Activates MAP Kinase through the Muscarinic Acetylcholine Pathway in Caenorhabditis elegans Pharynx. Cell Metab. NIH Public Access; 2006;3: 237–45. doi:10.1016/j.cmet.2006.02.012

30. Cunningham KA, Hua Z, Srinivasan S, Liu J, Lee BH, Edwards RH, et al. AMP-activated Kinase Links Serotonergic Signaling to Glutamate Release for Regulation of Feeding Behavior in C. elegans. Cell Metab. NIH Public Access; 2012;16: 113–21. doi:10.1016/j.cmet.2012.05.014

31. Lam DD, Heisler LK. Serotonin and Energy Balance: Molecular Mechanisms and Implications for Type 2 Diabetes. Expert Rev Mol Med. Cambridge University Press; 2007;9: 1–24. doi:10.1017/S1462399407000245

32. Noble T, Stieglitz J, Srinivasan S. An Integrated Serotonin and Octopamine Neuronal Circuit Directs the Release of an Endocrine Signal to Control C. elegans Body Fat. Cell Metab. 2013;18: 672–684. Available: https://www.sciencedirect.com/science/article/pii/S1550413113003768?via%3Dihub

33. Palamiuc L, Noble T, Witham E, Ratanpal H, Vaughan M, Srinivasan S. A Tachykinin-like Neuroendocrine Signalling Axis Couples Central Serotonin Action and Nutrient Sensing with Peripheral Lipid Metabolism. Nat Commun. Nature Publishing Group; 2017;8: 14237. doi:10.1038/ncomms14237

34. Goldstein DJ, Rampey AH, Dornseif BE, Levine LR, Potvin JH, Fludzinski LA. Fluoxetine: a Randomized Clinical Trial in the Maintenance of Weight Loss. Obes Res. 1993;1: 92–8. Available: http://www.ncbi.nlm.nih.gov/pubmed/16350565

35. Chan EW, He Y, Chui CSL, Wong AYS, Lau WCY, Wong ICK. Efficacy and safety of lorcaserin in obese adults: a meta-analysis of 1-year randomized controlled trials (RCTs) and narrative review on short-term RCTs. Obes Rev. 2013;14: 383–392. doi:10.1111/obr.12015

36. Hobson R, Hapiak V, Xiao H, … KB-, 2006 U. SER-7, a Caenorhabditis elegans 5-HT7-like Receptor, is Essential for the 5-HT Stimulation of Pharyngeal Pumping and Egg Laying. Genetics. 2005;172: 159–169. Available: http://www.genetics.org/content/172/1/159.short

37. Salway JG. Metabolism at a Glance [Internet]. 3rd. Wiley-Blackwell; 2004. Available: https://www.wiley.com/en-us/Metabolism+at+a+Glance%2C+3rd+Edition-p-9781118682074

38. Hardie DG, Ross FA, Hawley SA. AMPK: a Nutrient and Energy Sensor that Maintains Energy Homeostasis. Nat Rev Mol Cell Biol. Nature Publishing Group; 2012;13: 251–262. doi:10.1038/nrm3311

39. Pocock R, Hobert O. Hypoxia Activates a Latent Circuit for Processing Gustatory Information in C. elegans. Nat Neurosci. Nature Publishing Group; 2010;13: 610–614. doi:10.1038/nn.2537

40. Lee H, Crane MM, Zhang Y, Lu H. Quantitative screening of genes regulating tryptophan hydroxylase transcription in Caenorhabditis elegans using microfluidics and an adaptive algorithm. Integr Biol (Camb). NIH Public Access; 2013;5: 372–80. doi:10.1039/c2ib20078c

41. Qin Y, Zhang X, Zhang Y. A Neuronal Signaling Pathway of CaMKII and Gqα Regulates Experience-Dependent Transcription of tph-1. J Neurosci. NIH Public Access; 2013;33: 925–35. doi:10.1523/JNEUROSCI.2355-12.2013

42. Fitzpatrick PF. Tetrahydropterin-Dependent Amino Acid Hydroxylases. Annu Rev Biochem. Annual Reviews 4139 El Camino Way, P.O. Box 10139, Palo Alto, CA 94303-0139, USA ; 1999;68: 355–381. doi:10.1146/annurev.biochem.68.1.355

43. Wanders RJA. Metabolic Functions of Peroxisomes in Health and Disease. Biochimie. Elsevier; 2014;98: 36–44. doi:10.1016/J.BIOCHI.2013.08.022

44. Joo H-J, Kim K-Y, Yim Y-H, Jin Y-X, Kim H, Kim M-Y, et al. Contribution of the Peroxisomal Acox Gene to the Dynamic Balance of Daumone Production in

Caenorhabditis elegans. J Biol Chem. American Society for Biochemistry and Molecular Biology; 2010;285: 29319–25. doi:10.1074/jbc.M110.122663

45. Wanders RJA, Waterham HR. Biochemistry of Mammalian Peroxisomes Revisited. Annu Rev Biochem. Annual Reviews ; 2006;75: 295–332. doi:10.1146/annurev.biochem.74.082803.133329

46. Hellerer T, Axäng C, Brackmann C, Hillertz P, Pilon M, Enejder A. Monitoring of Lipid Storage in Caenorhabditis elegans using Coherent anti-Stokes Raman Scattering (CARS) Microscopy. Proc Natl Acad Sci U S A. National Academy of Sciences; 2007;104: 14658–63. doi:10.1073/pnas.0703594104

47. Wang MC, Min W, Freudiger CW, Ruvkun G, Xie XS. RNAi Screening for Fat Regulatory Genes with SRS Microscopy. Nat Methods. Nature Publishing Group; 2011;8: 135–138. doi:10.1038/nmeth.1556

48. Van Gilst MR, Hadjivassiliou H, Yamamoto KR. A Caenorhabditis elegans Nutrient Response System Partially Dependent on Nuclear Receptor NHR-49. Proc Natl Acad Sci U S A. National Academy of Sciences; 2005;102: 13496–501. doi:10.1073/pnas.0506234102

49. Harvald EB, Sprenger RR, Braendgaard K, Gartner A, Lamond AI, Faergeman Correspondence NJ. Multi-omics Analyses of Starvation Responses Reveal a Central Role for Lipoprotein Metabolism in Acute Starvation Survival in C. elegans. Cell Syst. 2017;5: 38-52.e4. doi:10.1016/j.cels.2017.06.004

50. McGhee J. The C. elegans Intestine. WormBook. 2007; 1–36. doi:10.1895/wormbook.1.133.1

51. Zhang X, Li K, Jones RA, Bruner SD, Butcher RA. Structural Characterization of

Acyl-CoA Oxidases Reveals a Direct Link Between Pheromone Biosynthesis and Metabolic State in Caenorhabditis elegans. Proc Natl Acad Sci U S A. National Academy of Sciences; 2016;113: 10055–60. doi:10.1073/pnas.1608262113

52. Poirier Y, Antonenkov VD, Glumoff T, Hiltunen JK. Peroxisomal β-oxidation—A Metabolic Pathway with Multiple Functions. Biochim Biophys Acta - Mol Cell Res. Elsevier; 2006;1763: 1413–1426. doi:10.1016/J.BBAMCR.2006.08.034

53. Tokuoka K, Nakajima Y, Hirotsu K, Miyahara I, Nishina Y, Shiga K, et al. Three-Dimensional Structure of Rat-Liver Acyl-CoA Oxidase in Complex with a Fatty Acid: Insights into Substrate-Recognition and Reactivity toward Molecular Oxygen. J Biochem. Oxford University Press; 2006;139: 789–795. doi:10.1093/jb/mvj088

54. Zhang X, Feng L, Chinta S, Singh P, Wang Y, Nunnery JK, et al. Acyl-CoA Oxidase Complexes Control the Chemical Message Produced by Caenorhabditis elegans. Proc Natl Acad Sci U S A. National Academy of Sciences; 2015;112: 3955–60. doi:10.1073/pnas.1423951112

55. Zhang X, Wang Y, Perez DH, Jones Lipinski RA, Butcher RA, Lipinski RAJ, et al. Acyl-CoA Oxidases Fine-Tune the Production of Ascaroside Pheromones with Specific Side Chain Lengths. ACS Chem Biol. American Chemical Society; 2018; acschembio.7b01021. doi:10.1021/acschembio.7b01021

56. von Reuss SH, Bose N, Srinivasan J, Yim JJ, Judkins JC, Sternberg PW, et al. Comparative metabolomics reveals biogenesis of ascarosides, a modular library of small-molecule signals in C. elegans. J Am Chem Soc. 2012;134: 1817–24. doi:10.1021/ja210202y

57. Izrayelit Y, Robinette SL, Bose N, von Reuss SH, Schroeder FC. 2D NMR-Based Metabolomics Uncovers Interactions between Conserved Biochemical Pathways in the Model Organism *Caenorhabditis elegans*. ACS Chem Biol. 2013;8: 314–319. doi:10.1021/cb3004644

58. Neess D, Bek S, Engelsby H, Gallego SF, Færgeman NJ. Long-Chain Acyl-CoA Esters in Metabolism and Signaling: Role of Acyl-CoA Binding Proteins. Prog Lipid Res. Elsevier Ltd; 2015;59: 1–25. doi:10.1016/j.plipres.2015.04.001

59. Li LO, Klett EL, Coleman RA. Acyl-CoA Synthesis, Lipid Metabolism and Lipotoxicity. Biochim Biophys Acta - Mol Cell Biol Lipids. Elsevier; 2010;1801: 246–251. doi:10.1016/J.BBALIP.2009.09.024

60. Hiroshi T, Kazuaki I, Satoshi O. Inhibition of Acyl-CoA Synthetase by Triacsins. Biochim Biophys Acta - Lipids Lipid Metab. Elsevier; 1987;921: 595–598. doi:10.1016/0005-2760(87)90088-9

61. Constantinides PP, Steim JM. Physical Properties of Fatty Acyl-CaA. J Biol Chem. 1985;260: 7573–7580. doi:10.1016/B978-0-12-375083-9.00103-3

62. Larson TR, Graham IA. Technical Advance: A Novel Technique for the Sensitive Quantification of Acyl CoA Esters from Plant Tissues. Plant J. Wiley/Blackwell (10.1111); 2008;25: 115–125. doi:10.1111/j.1365-313X.2001.00929.x

63. Cooper DE, Young PA, Klett EL, Coleman RA. Physiological Consequences of Compartmentalized Acyl-CoA Metabolism. J Biol Chem. American Society for Biochemistry and Molecular Biology; 2015;290: 20023–31. doi:10.1074/jbc.R115.663260

64. Grevengoed TJ, Klett EL, Coleman RA. Acyl-CoA Metabolism and Partitioning.

Annu Rev Nutr. NIH Public Access; 2014;34: 1–30. doi:10.1146/annurev-nutr-071813-105541

65. Waku K. Origins and Fates of Fatty Acyl-CoA Esters. Biochim Biophys Acta - Lipids Lipid Metab. Elsevier; 1992;1124: 101–111. doi:10.1016/0005-2760(92)90085-A

66. Tautenhahn R, Patti GJ, Rinehart D, Siuzdak G. XCMS Online: A Web-Based Platform to Process Untargeted Metabolomic Data. Anal Chem. American Chemical Society; 2012;84: 5035–5039. doi:10.1021/ac300698c

67. Artyukhin AB, Yim JJ, Srinivasan J, Izrayelit Y, Bose N, von Reuss SH, et al. Succinylated octopamine ascarosides and a new pathway of biogenic amine metabolism in Caenorhabditis elegans. J Biol Chem. 2013;288: 18778–83. doi:10.1074/jbc.C113.477000

68. Garg N, Kapono CA, Lim YW, Koyama N, Vermeij MJA, Conrad D, et al. Mass Spectral Similarity for Untargeted Metabolomics Data Analysis of Complex Mixtures. Int J Mass Spectrom. 2015;377: 719–727. doi:10.1016/j.ijms.2014.06.005

69. Wang M, Carver JJ, Phelan V V, Sanchez LM, Garg N, Peng Y, et al. Sharing and community curation of mass spectrometry data with Global Natural Products Social Molecular Networking. Nat Biotechnol. 2016;34: 828–837. doi:10.1038/nbt.3597

70. Butcher RA, Fujita M, Schroeder FC, Clardy J. Small-molecule pheromones that control dauer development in Caenorhabditis elegans. Nat Chem Biol. 2007;3: 420–2. doi:10.1038/nchembio.2007.3

71. Kaplan F, Srinivasan J, Mahanti P, Ajredini R, Durak O, Nimalendran R, et al. Ascaroside Expression in Caenorhabditis elegans is Strongly Dependent on Diet and Developmental Stage. PLoS One. 2011;6: e17804. doi:10.1371/journal.pone.0017804

72. Srinivasan J, von Reuss SH, Bose N, Zaslaver A, Mahanti P, Ho MC, et al. A modular library of small molecule signals regulates social behaviors in Caenorhabditis elegans. PLoS Biol. 2012;10: e1001237. doi:10.1371/journal.pbio.1001237

73. Butcher RA, Ragains JR, Li W, Ruvkun G, Clardy J, Mak HY. Biosynthesis of the Caenorhabditis elegans dauer pheromone. Proc Natl Acad Sci U S A. 2009;106: 1875–9. doi:10.1073/pnas.0810338106

74. de Jong L, Meng Y, Dent J, Hekimi S. Thiamine Pyrophosphate Biosynthesis and Transport in the Nematode Caenorhabditis elegans. Genetics. Genetics Society of America; 2004;168: 845–54. doi:10.1534/genetics.104.028605

75. Gibellini F, Smith TK. The Kennedy Pathway- de novo Synthesis of Phosphatidylethanolamine and Phosphatidylcholine. IUBMB Life. John Wiley & Sons, Ltd; 2010;62: n/a-n/a. doi:10.1002/iub.337

76. Simon GM, Cravatt BF. Endocannabinoid Biosynthesis Proceeding through Glycerophospho-N-acyl Ethanolamine and a Role for Alpha/Beta-Hydrolase 4 in this Pathway. J Biol Chem. American Society for Biochemistry and Molecular Biology; 2006;281: 26465–72. doi:10.1074/jbc.M604660200

77. Calignano A, Rana G La, Giuffrida A, Piomelli D. Control of Pain Initiation by Endogenous Cannabinoids. Nature. Nature Publishing Group; 1998;394: 277–

281. doi:10.1038/28393

78. Rodríguez de Fonseca F, Navarro M, Gómez R, Escuredo L, Nava F, Fu J, et al. An Anorexic Lipid Mediator Regulated by Feeding. Nature. Nature Publishing Group; 2001;414: 209–212. doi:10.1038/35102582

79. Di Marzo V, Matias I. Endocannabinoid Control of Food Intake and Energy Balance. Nat Neurosci. Nature Publishing Group; 2005;8: 585–589. doi:10.1038/nn1457

80. Naughton SS, Mathai ML, Hryciw DH, McAinch AJ. Fatty Acid Modulation of the Endocannabinoid System and the Effect on Food Intake and Metabolism. Int J Endocrinol. Hindawi; 2013;2013: 361895. doi:10.1155/2013/361895

81. Lucanic M, Held JM, Vantipalli MC, Klang IM, Graham JB, Gibson BW, et al. N-acylethanolamine Signalling Mediates the Effect of Diet on Lifespan in Caenorhabditis elegans. Nature. Nature Publishing Group; 2011;473: 226–229. doi:10.1038/nature10007

82. Trent C, Tsuing N, Horvitz HR. Egg-laying Defective Mutants of the Nematode Caenorhabditis elegans. Genetics. 1983;104: 619–47. Available: http://www.ncbi.nlm.nih.gov/pubmed/11813735

83. Banerjee N, Bhattacharya R, Gorczyca M, Collins KM, Francis MM. Local Neuropeptide Signaling Modulates Serotonergic Transmission to Shape the Temporal Organization of C. elegans Egg-Laying Behavior. PLoS Genet. 2017;13: e1006697. doi:10.1371/journal.pgen.1006697

84. Bastiani CA, Gharib S, Simon MI, Sternberg PW. Caenorhabditis elegans Gαq Regulates Egg-Laying Behavior via a PLCβ-Independent and Serotonin-

Dependent Signaling Pathway and Likely Functions Both in the Nervous System and in Muscle. Genetics. 2003;165: 1805–1822. Available: https://www.ncbi.nlm.nih.gov/pmc/articles/PMC1462877/pdf/14704167.pdf

85. Hardaker LA, Singer E, Kerr R, Zhou G, Schafer WR. Serotonin Modulates Locomotory Behavior and Coordinates Egg-Laying and Movement in Caenorhabditis elegans. J Neurobiol. 2001;49: 303–13. Available: http://www.ncbi.nlm.nih.gov/pubmed/11745666

86. Shyn SI, Kerr R, Schafer WR. Serotonin and Go Modulate Functional States of Neurons and Muscles Controlling C. elegans Egg-Laying Behavior. Curr Biol. 2003;13: 1910–1915. doi:10.1016/J.CUB.2003.10.025

87. Zhang M, Chung SH, Fang-Yen C, Craig C, Kerr RA, Suzuki H, et al. A Self-Regulating Feed-Forward Circuit Controlling C. elegans Egg-Laying Behavior. Curr Biol. 2008;18: 1445–1455. doi:10.1016/j.cub.2008.08.047

88. Collins KM, Bode A, Fernandez RW, Tanis JE, Brewer JC, Creamer MS, et al. Activity of the C. elegans Egg-Laying Behavior Circuit is Controlled by Competing Activation and Feedback Inhibition. Elife. eLife Sciences Publications, Ltd; 2016;5: e21126. doi:10.7554/eLife.21126

89. Schafer WR. Genetics of Egg-Laying in Worms. Annu Rev Genet. 2006;40: 487–509. doi:10.1146/annurev.genet.40.110405.090527

90. Bargmann CI. Neurobiology of the Caenorhabditis elegans Genome. Science (80-). 1998;282: 2028–33. Available: http://www.ncbi.nlm.nih.gov/pubmed/9851919

91. González C, Baez-Nieto D, Valencia I, Oyarzún I, Rojas P, Naranjo D, et al. K^+ Channels: Function-Structural Overview. Comprehensive Physiology. Hoboken,

NJ, USA: John Wiley & Sons, Inc.; 2012. pp. 2087–2149. doi:10.1002/cphy.c110047

92. Johnstone DB, Wei A, Butler A, Salkoff L, Thomas JH. Behavioral Defects in C. elegans egl-36 Mutants Result from Potassium Channels Shifted in Voltage-Dependence of Activation. Neuron. Cell Press; 1997;19: 151–164. doi:10.1016/S0896-6273(00)80355-4

93. Elkes DA, Cardozo DL, Madison J, Kaplan JM. EGL-36 Shaw Channels Regulate C. elegans Egg-Laying Muscle Activity. Neuron. 1997;19: 165–74. Available: http://www.ncbi.nlm.nih.gov/pubmed/9247272

94. Salkoff L. Potassium channels in C. elegans. WormBook. 2006; doi:10.1895/wormbook.1.42.1

95. Reiner DJ, Weinshenker D, Thomas JH. Analysis of Dominant Mutations Affecting Muscle Excitation in Caenorhabditis elegans [Internet]. 1995. Available: http://www.genetics.org/content/genetics/141/3/961.full.pdf

96. LeBoeuf B, Gruninger TR, Garcia LR. Food Deprivation Attenuates Seizures through CaMKII and EAG K+ Channels. PLoS Genet. Public Library of Science; 2007;3: e156. doi:10.1371/journal.pgen.0030156

97. LeBoeuf B, Guo X, García LR. The Effects of Transient Starvation Persist through Direct Interactions between CaMKII and Ether-a-Go-Go K+ Channels in C. elegans Males. Neuroscience. Pergamon; 2011;175: 1–17. doi:10.1016/J.NEUROSCIENCE.2010.12.002

98. Guo X, Navetta A, Gualberto DG, García LR. Behavioral Decay in Aging Male C. elegans Correlates with Increased Cell Excitability. Neurobiol Aging. Elsevier;

2012;33: 5–23. doi:10.1016/J.NEUROBIOLAGING.2011.12.016

99. Weinshenker D, Wei A, Salkoff L, Thomas JH. Block of an Ether-a-Go-Go-like K(+) Channel by Imipramine Rescues egl-2 Excitation Defects in Caenorhabditis elegans. J Neurosci. Society for Neuroscience; 1999;19: 9831–40. doi:10.1523/JNEUROSCI.19-22-09831.1999

100. Brüggemann A, Pardo LA, Stühmer W, Pongs O. Ether-à-go-go Encodes a Voltage-Gated Channel Permeable to K+ and Ca2+ and Modulated by cAMP. Nature. Nature Publishing Group; 1993;365: 445–448. doi:10.1038/365445a0

101. Weinshenker D, Garriga G, Thomas JH. Genetic and Pharmacological Analysis of Neurotransmitters Controlling Egg Laying in C. elegans. J Neurosci. 1995;15: 6975–85. Available: http://www.ncbi.nlm.nih.gov/pubmed/7472454

102. White JG, Southgate E, Thomson JN, Brenner S. The Structure of the Nervous System of the Nematode Caenorhabditis elegans. Philos Trans R Soc B Biol Sci. 1986;314: 1–340. doi:10.1098/rstb.1986.0056

103. Witham E, Comunian C, Ratanpal H, Skora S, Zimmer M, Srinivasan S. C. elegans Body Cavity Neurons Are Homeostatic Sensors that Integrate Fluctuations in Oxygen Availability and Internal Nutrient Reserves. Cell Rep. NIH Public Access; 2016;14: 1641–1654. doi:10.1016/j.celrep.2016.01.052

104. Sieburth D, Madison JM, Kaplan JM. PKC-1 regulates secretion of neuropeptides. Nat Neurosci. 2007;10: 49–57. doi:10.1038/nn1810

105. Akerboom J, Chen T-W, Wardill TJ, Tian L, Marvin JS, Mutlu S, et al. Optimization of a GCaMP Calcium Indicator for Neural Activity Imaging. J Neurosci. 2012;32: 13819–13840. doi:10.1523/JNEUROSCI.2601-12.2012

106. Zimmer M, Gray JM, Pokala N, Chang AJ, Karow DS, Marletta MA, et al. Neurons Detect Increases and Decreases in Oxygen Levels Using Distinct Guanylate Cyclases. Neuron. 2009;61. Available: http://www.ncbi.nlm.nih.gov/pubmed/19323996

107. Busch KE, Laurent P, Soltesz Z, Murphy RJ, Faivre O, Hedwig B, et al. Tonic Signaling from O2 Sensors Sets Neural Circuit Activity and Behavioral State. Nat Neurosci. 2012;15: 581–591. doi:10.1038/nn.3061

108. Schrödel T, Prevedel R, Aumayr K, Zimmer M, Vaziri A. Brain-wide 3D imaging of Neuronal Activity in Caenorhabditis elegans with Sculpted Light. Nat Methods. Nature Publishing Group; 2013;10: 1013–1020. doi:10.1038/nmeth.2637

109. Gray JM, Karow DS, Lu H, Chang AJ, Chang JS, Ellis RE, et al. Oxygen Sensation and Social Feeding Mediated by a C. elegans Guanylate Cyclase Homologue. Nature. 2004;430: 317–322. doi:10.1038/nature02714

110. Cheung BHH, Cohen M, Rogers C, Albayram O, de Bono M. Experience-Dependent Modulation of C. elegans Behavior by Ambient Oxygen. Curr Biol. 2005;15: 905–917. doi:10.1016/j.cub.2005.04.017

111. Chang AJ, Chronis N, Karow DS, Marletta MA, Bargmann CI. A Distributed Chemosensory Circuit for Oxygen Preference in C. elegans. Ahringer J, editor. PLoS Biol. Public Library of Science; 2006;4: e274. doi:10.1371/journal.pbio.0040274

112. Lam TKT, Schwartz GJ, Rossetti L. Hypothalamic Sensing of Fatty Acids. Nat Neurosci. Nature Publishing Group; 2005;8: 579–584. doi:10.1038/nn1456

113. Obici S, Feng Z, Arduini A, Conti R, Rossetti L. Inhibition of Hypothalamic

Carnitine Palmitoyltransferase-1 decreases Food Intake and Glucose Production. Nat Med. Nature Publishing Group; 2003;9: 756–761. doi:10.1038/nm873

114. Faergeman NJ, Knudsen J. Role of long-chain fatty acyl-CoA esters in the regulation of metabolism and in cell signalling. Biochem J. 1997;323 (Pt 1: 1–12. doi:10.1042/bj3230001

115. Hill M, Gorzalka B. The Endocannabinoid System and the Treatment of Mood and Anxiety Disorders. CNS Neurol Disord - Drug Targets. 2009;8: 451–458. doi:10.2174/187152709789824624

116. Valenti M, Cottone E, Martinez R, De Pedro N, Rubio M, Viveros MP, et al. The Endocannabinoid System in the Brain of Carassius auratus and its Possible Role in the Control of Food Intake. J Neurochem. 2005;95: 662–672. doi:10.1111/j.1471-4159.2005.03406.x

117. Kirkham TC, Williams CM, Fezza F, Marzo V Di. Endocannabinoid levels in rat limbic forebrain and hypothalamus in relation to fasting, feeding and satiation: stimulation of eating by 2-arachidonoyl glycerol. Br J Pharmacol. 2002;136: 550–557. doi:10.1038/sj.bjp.0704767

118. Lutz B. Endocannabinoid Signals in the Control of Emotion. Curr Opin Pharmacol. Elsevier; 2009;9: 46–52. doi:10.1016/J.COPH.2008.12.001

119. Coates JC, de Bono M. Antagonistic pathways in neurons exposed to body fluid regulate social feeding in Caenorhabditis elegans. Nature. Nature Publishing Group; 2002;419: 925–929. doi:10.1038/nature01170

120. Macosko EZ, Pokala N, Feinberg EH, Chalasani SH, Butcher RA, Clardy J, et al. A Hub-and-Spoke Circuit Drives Pheromone Attraction and Social Behaviour in C.

elegans. Nature. 2009;458: 1171–1175. doi:10.1038/nature07886

121. Mok CA, Healey MP, Shekhar T, Leroux MR, Héon E, Zhen M. Mutations in a Guanylate Cyclase GCY-35/GCY-36 Modify Bardet-Biedl Syndrome–Associated Phenotypes in Caenorhabditis elegans. Katsanis N, editor. PLoS Genet. Public Library of Science; 2011;7: e1002335. doi:10.1371/journal.pgen.1002335

122. Liu T, Cai D. Counterbalance between BAG and URX Neurons via Guanylate Cyclases Controls Lifespan Homeostasis in C. elegans. EMBO J. 2013;32: 1529–1542. doi:10.1038/emboj.2013.75

123. Skora S, Mende F, Zimmer M. Energy Scarcity Promotes a Brain-wide Sleep State Modulated by Insulin Signaling in C. elegans. Cell Rep. Elsevier; 2018;22: 953–966. doi:10.1016/j.celrep.2017.12.091

124. Ganetzky B, Robertson GA, Wilson GF, Trudeau MC, Titus SA. The EAG Family of K+ Channels in Drosophila and Mammals. Ann N Y Acad Sci. 1999;868: 356–69. Available: http://www.ncbi.nlm.nih.gov/pubmed/10414305

125. Miki T, Liss B, Minami K, Shiuchi T, Saraya A, Kashima Y, et al. ATP-sensitive K+ channels in the Hypothalamus are Essential for the Maintenance of Glucose Homeostasis. Nat Neurosci. Nature Publishing Group; 2001;4: 507–512. doi:10.1038/87455

126. Park YB, Choi YJ, Park SY, Kim JY, Kim SH, Song DK, et al. ATP-Sensitive Potassium Channel-Deficient Mice Show Hyperphagia but Are Resistant to Obesity. Korean Diabetes Association; 2011;35. doi:10.4093/dmj.2011.35.3.219

127. Sohn J-W. Ion Channels in the Central Regulation of Energy and Glucose Homeostasis. Front Neurosci. 2013;7: 85. doi:10.3389/fnins.2013.00085

128. Ma W, Berg J, Yellen G. Ketogenic Diet Metabolites Reduce Firing in Central Neurons by Opening KATP Channels. J Neurosci. 2007;27: 3618–3625. doi:10.1523/JNEUROSCI.0132-07.2007

129. Lutas A, Yellen G. The Ketogenic Diet: Metabolic Influences on Brain Excitability and Epilepsy. Trends Neurosci. NIH Public Access; 2013;36: 32–40. doi:10.1016/j.tins.2012.11.005

130. Lund TM, Ploug KB, Iversen A, Jensen AA, Jansen-Olesen I. The Metabolic Impact of β-hydroxybutyrate on Neurotransmission: Reduced Glycolysis Mediates Changes in Calcium Responses and K ATP Channel Receptor Sensitivity. J Neurochem. John Wiley & Sons, Ltd (10.1111); 2015;132: 520–531. doi:10.1111/jnc.12975

131. Huang C-L, Feng S, Hilgemann DW. Direct Activation of Inward Rectifier Potassium Channels by PIP2 and its Stabilization by Gβγ. Nature. 1998;391: 803–806. doi:10.1038/35882

132. Tang XD, Santarelli LC, H. Heinemann S, Hoshi T. Metabolic Regulation of Potassium Channels. Annu Rev Physiol. 2004;66: 131–159. doi:10.1146/annurev.physiol.66.041002.142720

133. Hille B, Dickson E, Kruse M, Falkenburger B. Dynamic Metabolic Control of an Ion Channel. Progress in molecular biology and translational science. 2014. pp. 219–247. doi:10.1016/B978-0-12-397897-4.00008-5

134. Jonas EA, Kaczmarek LK. Regulation of Potassium Channels by Protein Kinases. Curr Opin Neurobiol. Elsevier Current Trends; 1996;6: 318–323. doi:10.1016/S0959-4388(96)80114-0

135. Manville RW, Papanikolaou M, Abbott GW. Direct Neurotransmitter Activation of Voltage-gated Potassium Channels. Nat Commun. Nature Publishing Group; 2018;9: 1847. doi:10.1038/s41467-018-04266-w

136. Wise SD. Clinical Studies with Fluoxetine in Obesity. Am J Clin Nutr. 1992;55: 181S-184S. doi:10.1093/ajcn/55.1.181s

137. Even P, Nicolaidis S. Dextrofenfluramine Increases Energy Cost of Muscular Effort. Pharmacol Biochem Behav. 1986;24: 647–655. Available: https://www.sciencedirect.com/science/article/pii/0091305786905708

138. Rothwell N, Stock M. Effect of Diet and Fenfluramine on Thermogenesis in the Rat: Possible Involvement of Serotonergic Mechanisms. Int J Obes. 1987;11: 319–324. Available: https://europepmc.org/abstract/med/3667065

139. Choi S, Jonak EM, Simpson L, Patil V, Fernstrom JD. Intermittent, Chronic Fenfluramine Administration to Rats Repeatedly Suppresses Food Intake Despite Substantial Brain Serotonin Reductions. Brain Res. Elsevier; 2002;928: 30–39. doi:10.1016/S0006-8993(01)03330-3

140. Brenner S. The Genetics of Caenorhabditis elegans. Genetics. 1974;77: 71–94. Available: http://www.ncbi.nlm.nih.gov/pubmed/4366476

141. Afgan E, Baker D, Batut B, van den Beek M, Bouvier D, Cech M, et al. The Galaxy Platform for Accessible, Reproducible and Collaborative Biomedical Analyses: 2018 update. Nucleic Acids Res. Oxford University Press; 2018;46: W537–W544. doi:10.1093/nar/gky379

142. Kim D, Pertea G, Trapnell C, Pimentel H, Kelley R, Salzberg SL. TopHat2: Accurate Alignment of Transcriptomes in the Presence of Insertions, Deletions

and Gene Fusions. Genome Biol. BioMed Central; 2013;14: R36. doi:10.1186/gb-2013-14-4-r36

143. Anders S, Pyl PT, Huber W. HTSeq--a Python Framework to Work with High-Throughput Sequencing Data. Bioinformatics. Oxford University Press; 2015;31: 166–9. doi:10.1093/bioinformatics/btu638

144. Love MI, Huber W, Anders S. Moderated Estimation of Fold Change and Dispersion for RNA-seq Data with DESeq2. Genome Biol. BioMed Central; 2014;15: 550. doi:10.1186/s13059-014-0550-8

145. Forsberg EM, Huan T, Rinehart D, Benton HP, Warth B, Hilmers B, et al. Data Processing, Multi-omic Pathway Mapping, and Metabolite Activity Analysis sing XCMS Online. Nat Protoc. 2018;13: 633–651. doi:10.1038/nprot.2017.151

146. Wolfgang MJ, Kurama T, Dai Y, Suwa A, Asaumi M, Matsumoto S -i., et al. The brain-specific carnitine palmitoyltransferase-1c regulates energy homeostasis. Proc Natl Acad Sci. 2006;103: 7282–7287. doi:10.1073/pnas.0602205103

147. Ramirez S, Martins L, Jacas J, Carrasco P, Pozo M, Clotet J, et al. Hypothalamic Ceramide Levels Regulated by CPT1C Mediate the Orexigenic Effect of Ghrelin. Diabetes. 2013;62: 2329–2337. doi:10.2337/db12-1451

148. Gao S, Zhu G, Gao X, Wu D, Carrasco P, Casals N, et al. Important roles of brain-specific carnitine palmitoyltransferase and ceramide metabolism in leptin hypothalamic control of feeding. Proc Natl Acad Sci U S A. National Academy of Sciences; 2011;108: 9691–6. doi:10.1073/pnas.1103267108

149. Rodríguez-Rodríguez R, Miralpeix C, Fosch A, Pozo M, Calderón-Domínguez M, Perpinyà X, et al. CPT1C in the ventromedial nucleus of the hypothalamus is

necessary for brown fat thermogenesis activation in obesity. Mol Metab. Elsevier; 2019;19: 75–85. doi:10.1016/J.MOLMET.2018.10.010

150. Sierra AY, Gratacós E, Carrasco P, Clotet J, Ureña J, Serra D, et al. CPT1c is localized in endoplasmic reticulum of neurons and has carnitine palmitoyltransferase activity. J Biol Chem. American Society for Biochemistry and Molecular Biology; 2008;283: 6878–85. doi:10.1074/jbc.M707965200

151. Lee J, Wolfgang MJ. Metabolomic profiling reveals a role for CPT1c in neuronal oxidative metabolism. BMC Biochem. BioMed Central; 2012;13: 23. doi:10.1186/1471-2091-13-23

152. Chen X, Xu F, Zhu C, Ji J, Zhou X, Feng X, et al. Dual sgRNA-directed gene knockout using CRISPR/Cas9 technology in Caenorhabditis elegans. Sci Rep. 2015;4: 7581. doi:10.1038/srep07581

153. Cansell C, Luquet S. Mesolimbic lipid sensing and the regulation of feeding behaviour. 2015;22. doi:10.1051/ocl/2015013

154. Waggoner LE, Hardaker LA, Golik S, Schafer WR. Effect of a neuropeptide gene on behavioral states in Caenorhabditis elegans egg-laying. Genetics. 2000;154: 1181–92. Available: http://www.ncbi.nlm.nih.gov/pubmed/10757762

155. Kyuhyung K, Li C. Expression and Regulation of an FMRFamide-Related Neuropeptide Gene Family in Caenorhabditis elegans. J Comp Neurol. 2004;475: 540–550. doi:10.1002/cne.20189

156. Buntschuh I, Raps DA, Joseph I, Reid C, Chait A, Totanes R, et al. FLP-1 neuropeptides modulate sensory and motor circuits in the nematode Caenorhabditis elegans. PLoS One. Public Library of Science; 2018;13:

e0189320. doi:10.1371/journal.pone.0189320

157. Sasidharan N, Sumakovic M, Hannemann M, Hegermann J, Liewald JF, Olendrowitz C, et al. RAB-5 and RAB-10 cooperate to regulate neuropeptide release in Caenorhabditis elegans. Proc Natl Acad Sci. 2012;109: 18944–18949. doi:10.1073/pnas.1203306109

158. Bany IA, Dong M-Q, Koelle MR. Genetic and cellular basis for acetylcholine inhibition of Caenorhabditis elegans egg-laying behavior. J Neurosci. 2003;23: 8060–9. Available: http://www.ncbi.nlm.nih.gov/pubmed/12954868

159. McKay JP, Raizen DM, Gottschalk A, Schafer WR, Avery L. eat-2 and eat-18 are required for nicotinic neurotransmission in the Caenorhabditis elegans pharynx. Genetics. 2004;166: 161–9. Available: http://www.ncbi.nlm.nih.gov/pubmed/15020415

160. Avery L, Horvitz HR. Pharyngeal pumping continues after laser killing of the pharyngeal nervous system of C. elegans. Neuron. 1989;3: 473–85. Available: http://www.ncbi.nlm.nih.gov/pubmed/2642006

161. Kim J, Poole DS, Waggoner LE, Kempf A, Ramirez DS, Treschow PA, et al. Genes affecting the activity of nicotinic receptors involved in Caenorhabditis elegans egg-laying behavior. Genetics. 2001;157: 1599–610. Available: http://www.ncbi.nlm.nih.gov/pubmed/11290716

162. Dallière N, Bhatla N, Luedtke Z, Ma DK, Woolman J, Walker RJ, et al. Multiple excitatory and inhibitory neural signals converge to fine-tune Caenorhabditis elegans feeding to food availability. FASEB J. 2016;30: 836–848. doi:10.1096/fj.15-279257

163. Avery L, Horvitz HR. Effects of Starvation and Neuroactive Drugs on Feeding in Caenorhabditis elegans. J Exp Zool. John Wiley & Sons, Ltd; 1990;253: 263–270. doi:10.1002/jez.1402530305

164. Picciotto MR, Higley MJ, Mineur YS. Acetylcholine as a Neuromodulator: Cholinergic Signaling Shapes Nervous System Function and Behavior. Neuron. Elsevier Inc.; 2012;76: 116–129. doi:10.1016/j.neuron.2012.08.036

165. Kim J, Poole DS, Waggoner LE, Kempf A, Ramirez DS, Treschow PA, et al. Genes affecting the activity of nicotinic receptors involved in Caenorhabditis elegans egg-laying behavior. Genetics. 2001;157: 1599–610. Available: http://www.ncbi.nlm.nih.gov/pubmed/11290716

166. Niacaris T, Avery L. Serotonin regulates repolarization of the C. elegans pharyngeal muscle. J Exp Biol. 2003;206: 223–31. Available: http://www.ncbi.nlm.nih.gov/pubmed/12477893

167. Raizen DM, Lee RY, Avery L. Interacting genes required for pharyngeal excitation by motor neuron MC in Caenorhabditis elegans. Genetics. Genetics Society of America; 1995;141: 1365–82. Available: http://www.ncbi.nlm.nih.gov/pubmed/8601480

168. Matta SG, Balfour DJ, Benowitz NL, Boyd RT, Buccafusco JJ, Caggiula AR, et al. Guidelines on nicotine dose selection for in vivo research. Psychopharmacology (Berl). Springer-Verlag; 2007;190: 269–319. doi:10.1007/s00213-006-0441-0

169. Haj-Dahmane S, Shen R-Y. Modulation of the serotonin system by endocannabinoid signaling. Neuropharmacology. NIH Public Access; 2011;61: 414–20. doi:10.1016/j.neuropharm.2011.02.016

170. Egashira N, Mishima K, Iwasaki K, Fujiwara M. Intracerebral microinjections of delta 9-tetrahydrocannabinol: search for the impairment of spatial memory in the eight-arm radial maze in rats. Brain Res. 2002;952: 239–45. Available: http://www.ncbi.nlm.nih.gov/pubmed/12376185

171. Sagredo O, Ramos JA, Fernández-Ruiz J, Rodríguez MLL, de Miguel R. Chronic Δ9-tetrahydrocannabinol administration affects serotonin levels in the rat frontal cortex. Naunyn Schmiedebergs Arch Pharmacol. 2006;372: 313–317. doi:10.1007/s00210-005-0026-1

172. Mackie K. Signaling via CNS cannabinoid receptors. Mol Cell Endocrinol. 2008;286: S60–S65. doi:10.1016/j.mce.2008.01.022

173. Lehtonen M, Storvik M, Malinen H, Hyytiä P, Lakso M, Auriola S, et al. Determination of endocannabinoids in nematodes and human brain tissue by liquid chromatography electrospray ionization tandem mass spectrometry. J Chromatogr B. 2011;879: 677–694. doi:10.1016/j.jchromb.2011.02.004

174. McPartland J, Di Marzo V, De Petrocellis L, Mercer A, Glass M. Cannabinoid receptors are absent in insects. J Comp Neurol. 2001;436: 423–9. Available: http://www.ncbi.nlm.nih.gov/pubmed/11447587

175. Pastuhov SI, Matsumoto K, Hisamoto N. Endocannabinoid signaling regulates regenerative axon navigation in *Caenorhabditis elegans* via the GPCRs NPR-19 and NPR-32. Genes to Cells. 2016;21: 696–705. doi:10.1111/gtc.12377

176. Oakes MD, Law WJ, Clark T, Bamber BA, Komuniecki R. Cannabinoids Activate Monoaminergic Signaling to Modulate Key *C. elegans* Behaviors. J Neurosci. 2017;37: 2859–2869. doi:10.1523/JNEUROSCI.3151-16.2017

177. Schmid HHO, Berdyshev EV. Cannabinoid receptor-inactive N - acylethanolamines and other fatty acid amides: metabolism and function. Prostaglandins, Leukot Essent Fat Acids. 2002;66: 363–376. doi:10.1054/plef.2001.0348

178. Balvers MGJ, Verhoeckx KCM, Plastina P, Wortelboer HM, Meijerink J, Witkamp RF. Docosahexaenoic acid and eicosapentaenoic acid are converted by 3T3-L1 adipocytes to N-acyl ethanolamines with anti-inflammatory properties. Biochim Biophys Acta - Mol Cell Biol Lipids. Elsevier; 2010;1801: 1107–1114. doi:10.1016/J.BBALIP.2010.06.006

179. Fezza F, Bari M, Florio R, Talamonti E, Feole M, Maccarrone M, et al. Endocannabinoids, Related Compounds and Their Metabolic Routes. Molecules. Multidisciplinary Digital Publishing Institute; 2014;19: 17078–17106. doi:10.3390/molecules191117078

180. Yang R, Fredman G, Krishnamoorthy S, Agrawal N, Irimia D, Piomelli D, et al. Decoding functional metabolomics with docosahexaenoyl ethanolamide (DHEA) identifies novel bioactive signals. J Biol Chem. American Society for Biochemistry and Molecular Biology; 2011;286: 31532–41. doi:10.1074/jbc.M111.237990

181. Dyall SC. Long-chain omega-3 fatty acids and the brain: a review of the independent and shared effects of EPA, DPA and DHA. Front Aging Neurosci. Frontiers Media SA; 2015;7: 52. doi:10.3389/fnagi.2015.00052

182. Watts JL, Browse J. Genetic dissection of polyunsaturated fatty acid synthesis in Caenorhabditis elegans. Proc Natl Acad Sci. 2002;99: 5854–5859. doi:10.1073/pnas.092064799

183. Zhu G, Chen H, Wu X, Zhou Y, Lu J, Chen H, et al. A modified n–3 fatty acid desaturase gene from Caenorhabditis briggsae produced high proportion of DHA and DPA in transgenic mice. Transgenic Res. 2008;17: 717–725. doi:10.1007/s11248-008-9171-x

184. Simopoulos AP. The Importance of the Omega-6/Omega-3 Fatty Acid Ratio in Cardiovascular Disease and Other Chronic Diseases. Exp Biol Med. 2008;233: 674–688. doi:10.3181/0711-MR-311

185. Lesa GM, Palfreyman M, Hall DH, Clandinin MT, Rudolph C, Jorgensen EM, et al. Long Chain Polyunsaturated Fatty Acids are Required for Efficient Neurotransmission in C. elegans. J Cell Sci. 2003;116: 4965–4975. doi:10.1242/jcs.00918

Publishing Agreement

It is the policy of the University to encourage the distribution of all theses, dissertations, and manuscripts. Copies of all UCSF theses, dissertations, and manuscripts will be routed to the library via the Graduate Division. The library will make all theses, dissertations, and manuscripts accessible to the public and will preserve these to the best of their abilities, in perpetuity.

Please sign the following statement:

I hereby grant permission to the Graduate Division of the University of California, San Francisco to release copies of my thesis, dissertation, or manuscript to the Campus Library to provide access and preservation, in whole or in part, in perpetuity.

Author Signature

June 13th, 2019
Date